Department of Biotechnology and Biosciences

PhD program in Converging Technologies for Biomolecular Systems
Cycle 34

Differentiation of a dorsal root ganglion neuron model induced by a novel approach of thermal stimulation: a morphological and functional investigation

Blasa Stefania

Registration number   780185

Tutor: Rocchetti Marcella

Supervisor: Lecchi Marzia Maria

Coordinator: Branduardi Paola

ACADEMIC YEAR   2020/2021

To Leela

CONTENTS

CHAPTER 4: Neuronal differentiation induced by scalable thermal stimulation **108**

ABSTRACT

Thermal stimulation with different temperatures (from 38°C to 50°C) and durations (from milliseconds to several days) promotes the differentiation of various cell types like *Xenopus laevis* oocytes, cultured mammalian cells, stem cells and cancer cells. Moreover, in neurons, heating represents a promising approach to elicit depolarizing currents, to induce neurite outgrowth and the expression of neuronal markers, and for functional recovery. These effects have been associated to changes in cell membrane capacitance and in ion channel properties, and to the activation of differentiation pathways, but the underlying mechanisms remain so far unknown.

The present project was aimed to investigate the eventual modifications, induced by two approaches of thermal stimulation, on the behavior of a model of dorsal root ganglion (DRG) neurons, the F-11 cell line, previously characterized in our laboratory. These cells express ion channels and cell membrane receptors consistent with those of sensory neurons and represent a good model to study neuronal proliferation and differentiation mechanisms.

Initially, we performed experiments of bulk stimulation: cells were placed in an incubator in which different temperatures were imposed for variable time intervals. This procedure was repeated for two consecutive days. Thus, morphological and functional analysis were performed until 8 days in culture. Results showed a significant difference in neurite elongation and in electrophysiological properties (resting membrane potential, Na^+ and K^+ current density and action potential frequency) in samples heated at 41,5°C for 30 minutes versus 37°C samples. The analysis of intracellular Ca^{2+} signals evoked by Capsaicin was performed to verify the involvement of TRPV1 (Transient Receptor Potential Vanilloid) channels in the effects of heating. Preliminary results showed that Ca^{2+} transients were higher in heated cells compared to control, suggesting that the treatment could increase the expression and/or modify the properties of TRPV1 channels, which are permeable to Ca^{2+}. Considering these results, we investigated the effects of a scalable

6

thermal stimulation method, established by irradiating Prussian Blue nanoparticles (PBNPs) with a near infrared laser. A disc of PBNPs, dispersed in poly vinyl alcohol (PVA), was placed on the outer surface of the petri dish in which the cells were seeded, avoiding a direct contact between the material and the cells, and it was irradiated by a near infrared laser to increase culture medium temperature to 41,5°C. Neurite elongation was significantly increased in irradiated cells compared to non-irradiated control cells and significant differences were also recorded during the functional analysis by the patch-clamp technique. To verify if the effects on cellular properties could be maintained for a longer period, we performed a functional investigation also on cells maintained in culture for more than 8 days, and we observed that F-11 cells could maintain a differentiated phenotype also after 12 days.

In conclusion, here we present a novel method to induce neuronal differentiation by using a combination of light sensitive nanoparticles and NIR laser, that was applied with success on a neuroblastoma cell line, maintained in culture without chemical differentiating agents or genetic techniques and without any contamination with the photothermal material. Our results suggest that targeted heating could be a promising approach for *in vivo* therapy to induce neurite outgrowth and neuronal behavior modifications.

CHAPTER 1: Introduction

PART I

1. OVERVIEW OF THE NERVOUS SYSTEM

1.1. Cell anatomy and behavior

1.1.1. Neurons and glial cells

The nervous system is a complex structure that controls the interactions between the organisms and the environment, and it is responsible of the control of behavior, cognitive functions and psychical and mental processes. For these reasons, it is considered one of the most difficult and fascinating systems to explore. It is divided in two components: the central nervous system (CNS), which includes the brain and the spinal cord; and the peripheral nervous system (PNS), which is composed by ganglia and peripheral nerves outside the brain and the spinal cord. These two systems are anatomically separated but are highly interconnected for the correct functioning of the whole nervous system. Regardless of the component studied, the nervous system has two principal types of cells: nerve cells (or neurons) and glial cells (or glia).

The neuron represents the functional unit of the nervous system and it is composed by four regions. The cell body (or soma) contains the nucleus, the organelles and the perykarion (the cell soma cytoplasm) and gives rise to dendrites and axon. The dendrites are often multiple, could assume a tree-shape form and receive information from other nervous cells. The axon is the principal conducting unit of the nervous cell, emerges from a structure on the soma called axon hillock and converges information for long distances in the form of transient electrical signals called action potentials. Lastly, the presynaptic terminals are situated at the end of the axons and represent the transmitting units of the neuron.

The communication among neurons can occur through specialized structures called synapses, which are constituted by the presynaptic terminal, that brings contacts (directly

or indirectly) with the cell that receives the information, which is called post-synaptic cell. There are two types of synapses: electrical and chemical. In the electrical synapses, the presynaptic terminal is in direct contact with the postsynaptic membrane through gap-junctions. When an action potential reaches the presynaptic terminal, the flux of positive charges passes through high-conductance channels to the postsynaptic membrane, depolarizing it, and if this leads to a threshold, an action potential is generated in the membrane of the postsynaptic cell. In the chemical synapses there is no continuity between presynaptic and postsynaptic cells and between their membranes there is an extracellular space called synaptic cleft. When a stimulus reaches the presynaptic terminal, the vesicles containing the neurotransmitters fuse with the presynaptic membrane and the neurotransmitters are released in the synaptic cleft. Thus, they reach the post-synaptic membrane and interact directly or indirectly with specific receptors. This binding leads to the opening of channels that modify the membrane potential of the postsynaptic cell, by establishing an influx of ions (cations or anions) and a consequent depolarization or hyperpolarization at this site.

Based on cell shape and, in particular, on their processes, neurons can be distinguished morphologically in three groups: unipolar, bipolar and multipolar cells (Fig. 1). Unipolar neurons have an axon and receiving processes that function as a dendrite. Bipolar neurons have usually one axon and one dendrite, and represent the majority of sensory cells. Some of these, such as dorsal root ganglion neurons, that carry information about touch, pain, thermal perception etc. are called pseudo-unipolar because the two processes fuse and, after emerging from the soma, they split in two branches. Multipolar neurons represent the majority of neurons in the central nervous system and have an axon and multiple dendrites, which innervate different cell regions (soma, axons or dendrites).
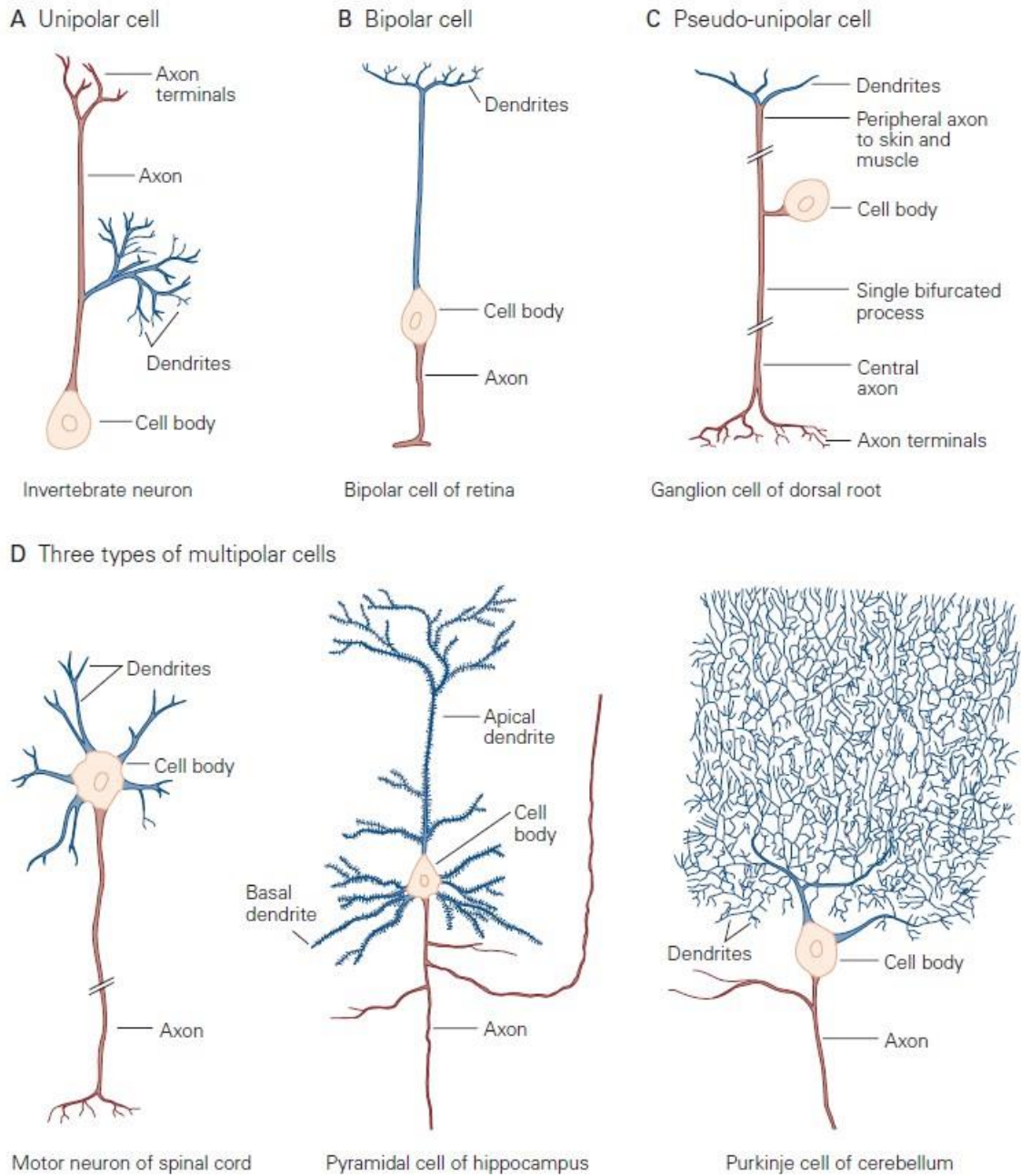
Figure 1. Morphological neuronal classification. According to the number of processes generated from the cell body, neurons can be classified as unipolar, bipolar or multipolar (Kandel et al., 2013).

As all other cell types, neuronal precursors can go through two distinct processes during their life: proliferation or differentiation. Most cells tend to proliferate to increase their number and simultaneously follow a gradual process called differentiation (Fig. 2), in which they acquire specialized morphology and function. When they reach a complete differentiation, the process of proliferation arrests and they permanently exit the cell

division cycle (Ruijtenberg et al., 2016). The differentiation process involves a complex interaction between several molecules and chemicals. This induces the activation of transductional pathways, changes in gene expression and modifications in ionic concentrations, especially in the intracellular Ca^{2+} level, that is able to induce differentiation probably through modifications of proteins in local regions (Spitzer et al., 2000), and changes in intracellular and extracellular composition, leading to a mature neuron with specific morphology and electrical activity.
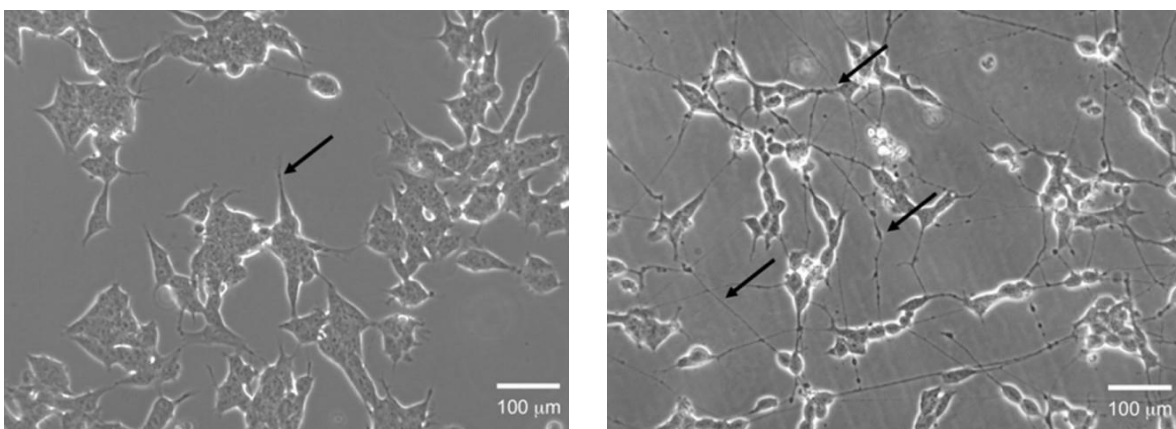
Figure 2. Undifferentiated (left) and differentiated (right) human SH-SY5Y cells. Arrows show extension and connection of neurites and vesicular transport along them (modified from Murillo et al., 2017).

Based on their functions, neurons can also be classified into three different types: sensory neurons are responsible to carry the information from the periphery to the central nervous system; motor neurons control muscles and glands, and interneurons process and conduct information at the level of local circuits.

Glial cells surround neurons and have several functions, such as structural and nutritional support, buffering of extracellular K^+ concentration, guidance for outgrowth of neurites and axons, myelin formation around axons and scavenger action after injury or cell death. They include astrocytes, which provide nutritive, buffering and structural

support, microglia, with immunoprotective activity, and oligodendrocytes (in the central nervous system) or Schwann cells (in the peripheral nervous system), which are responsible for the myelination of axons in these sites.

1.1.2. Electrical activity of neurons

As other cell types, neurons are excitable cells that use the alteration of their membrane potential to generate electrical signals to communicate with other cells. The membrane potential of a neuron is also called resting membrane potential (V_r) and results from an unequal distribution of positive and negative ions on the two sides of the membrane, maintained by the Na^+/K^+ ATPase (Na^+/K^+ pump). Ions can pass through the membrane following a concentration gradient, from a more concentrate compartment to a less concentrate one, or following an electrical gradient, when the charge present on one side of the membrane attracts the ions of the opposite charge from the opposite side of the membrane itself. Together, these two components give the electrochemical gradient, which is fundamental for the maintenance of the membrane potential. A neuron has a resting membrane potential of about -65 mV (the negative sign is due to the fact that the outside of the membrane is arbitrarily defined as zero), and an alteration of this potential could lead to the generation of an action potential. When a neuron receives a stimulus, the membrane tends to depolarize, becoming less negative thanks to the opening of voltage-gated ion channels that bring cations into the cell. This depolarization opens other voltage-dependent channels permeable to Na^+. Thus, cations enter the cell and the depolarization reaches a value called the threshold, from which the action potential is generated. During this process, Na^+-channels gradually inactivate; simultaneously, there is an activation of voltage-dependent K^+ channels that allow the potassium efflux across the plasma membrane, causing a repolarization that leads the membrane potential back to its resting value. After the action potential, there is a short phase called afterhyperpolarization. This phase is due to the K^+ channels, which close a few milliseconds after the reaching of the

resting membrane potential, leading to a more negative membrane potential. The action potential is also followed by a refractory period, which is divided in two steps: the absolute refractory period, during which the cell is not excitable, and the relative refractory period, in which the cell can be excited only by a larger stimulus.

This process can occur thanks to the presence of several ion channels on the neuronal cell membrane. The structure of the ion channels consists in a water-filled pore that passes through the membrane, formed by a protein with repeated structure or by several subunits, with a mass between 10 and 250 kDa. The pore region is included into the transmembrane domains, that in the case of voltage-gated ion channels are similar in different families: the K_v channels are composed by 4 subunits, each one with 6 transmembrane domains (S1-S6) and a P-loop between S5 and S6. The tetramer is either homomeric and heteromeric and has a domain T1 in the N-terminus that is responsible for a functional K_v channel. The structure of Ca_v and Na_v channels differs from the structure of K_v channels because the 24 transmembrane tetramer has homologous repeated domains (I, II, III and IV), each of them is equal to a single K_v subunit. On the contrary, inwardly rectifying K^+ channels are not gated by voltage and have the simplest structure for an ion channel, with 4 subunits, each with 2 transmembrane segments (M1 and M2) analogous to S5 and S6 of K_v. In the Twin-pore channels, two of these subunits are linked.

In general, the region responsible for the conduction and the selectivity to one specific ion lies in the P-loop and in the S5 and S6 transmembrane domains, while the voltage-sensor lies in the S4 domain. A particular family of channels, the Transient Receptor Potential (TRP) channels, has a weak voltage-dependence that can act in synergy with other stimuli such as vanilloids or temperature. More details on these channels will be discussed in the second part of the introduction.

The electrical properties of neurons can be analyzed by a technique called Patch-Clamp. Many configurations of this technique exist, such as cell-attached, inside-out, outside-out

and perforated patch, but the most common used is the whole-cell configuration, that allows to study the electrical properties of the entire cell membrane. A glass micropipette filled with a standard internal solution, in contact with a microelectrode, is positioned on the surface of the cell and the membrane is pulled into the pipette with the help of a gentle suction until a high resistance (about 1 GΩ) is reached; then the suction causes a rupture in the membrane. Thus, the intracellular solution of the glass pipette and the intracellular environment are in communication and the electrical properties can be recorded. The operator can fix the voltage to study the current flows ("voltage-clamp mode") or fix the current to analyze eventual modifications in the membrane potential ("current-clamp" mode). Voltage steps are imposed to the membrane by the micropipettes and ligands can be administered via the extracellular or the intracellular solution to activate or inactivate channels. The changes in membrane conductance caused by the opening or closing of voltage-dependent ion channels can be calculated by measuring the ionic currents at the imposed membrane potentials (Kew et al., 2010).

1.1.3. The somatosensory system

A nervous circuit can operate properly thanks to two events: the axonal growth and the synaptic connection formation. These processes can occur through the participation of cellular adhesion molecules, extracellular matrix molecules, intracellular signals and growth factors, that allow modifications of the cytoskeleton or changes in gene expression, and that can attract or repulse the growing axon. Moreover, second messengers and molecular receptors could contribute to the intercellular communication and transductional pathway activation for the maturation of synapses, in order to give rise to organized and specialized nervous circuits.

One of the most important nervous circuits is represented by the somatosensory system. The steps that compose the sensory reception are a physical stimulus, the transduction of the stimulus into an electrical impulse and a response. The stimulus is perceived based

on four attributes: the modality by which the stimulus induces the sensation; the intensity; the duration and the location of the stimulus. The stimulus is converted by sensory receptors in an information, represented by a series of action potentials, through a process called neural coding; thus, the information is transmitted to the cerebral cortex and elaborated to formulate a proper response. There are several modalities by which the stimulus can be received: mechanical, proprioceptive, nociceptive and thermal. These modalities are carried by two distinct anatomical pathways: the dorsal column-medial lemniscal system for mechanical and proprioception, and the antero-lateral system for pain and temperature (Fig. 3). In both cases, the information is conveyed by specialized cells called dorsal root ganglion (DRG) neurons, which transduct and transmit the encoded stimulus to the central nervous system thanks to their morphology. In fact, their peripheral terminal consists in a bare nerve ending or an organ with a non-neural capsule surrounding the axon terminal. They have different soma and axon diameters and different sensitivity to stimuli, and their afferent fibers can conduct action potentials at different rates and velocity (Kandel, 1991).
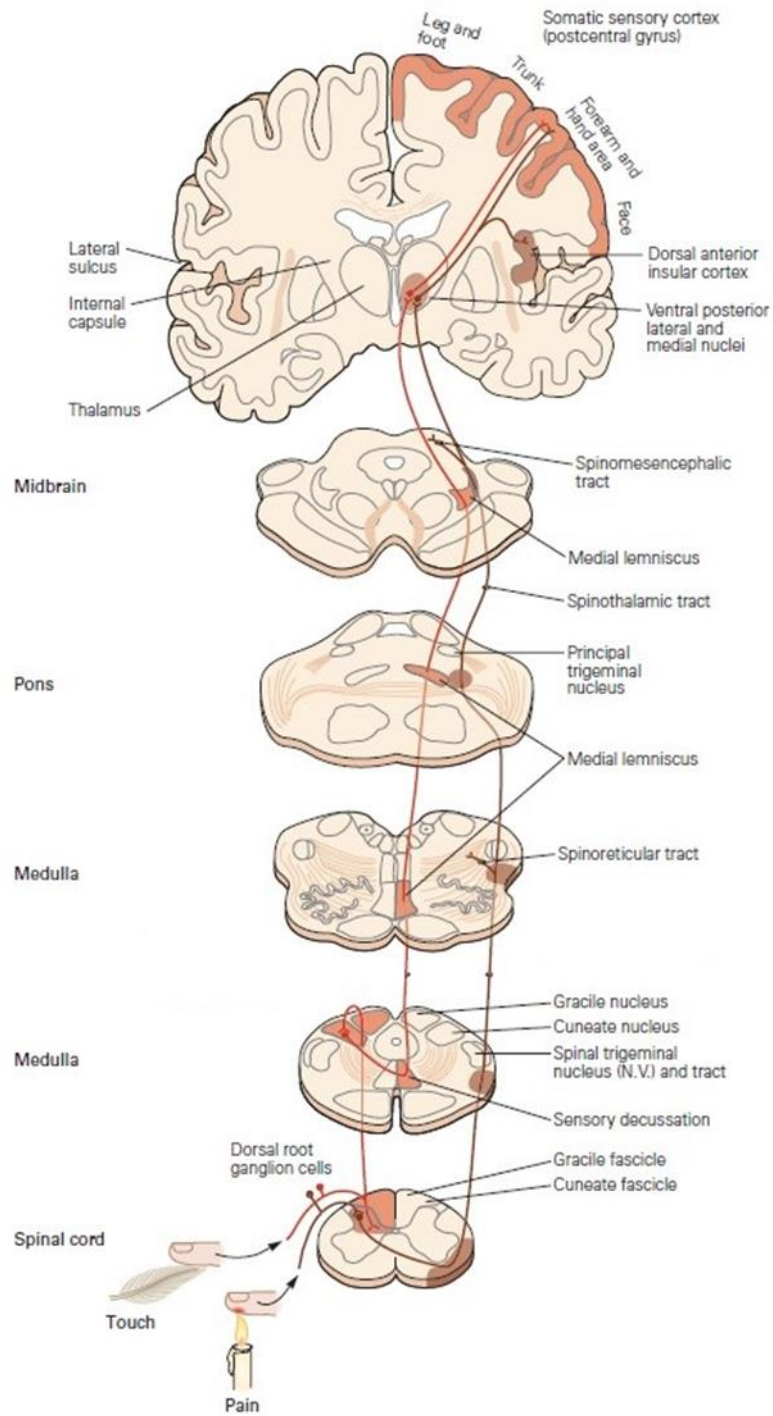
Figure 3. The somatosensory system, composed by the dorsal column-medial lemniscal system (in red) and the antero-lateral system (in brown) (Kandel et al., 2013).

As there are several types of stimuli, there are also several types of sensory receptors. The receptors which respond to pain are called nociceptors. They can respond directly or indirectly to noxious and other stimuli through the communication with chemicals released by damaged cells. They are classified in three types: mechanical nociceptors, activated by a strong mechanical stimulation; thermal nociceptors, activated by heat over 45°C or by cold under 17°C, and polymodal nociceptors, which respond to different types of noxious stimuli, such as temperature and vanilloids, as in the case of TRPV channels (Fig. 4).
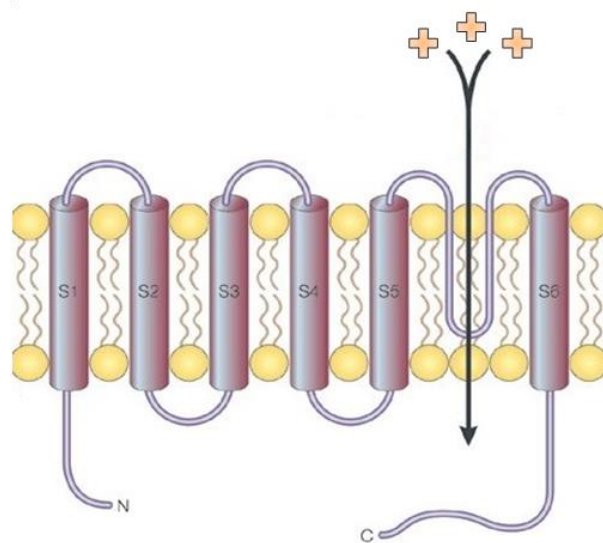
Figure 4. Structure of a typical TRPV channel (Clapham et al., 2001).

In particular, a thermal sensation is induced by warm and cold. Thermal receptors are situated in different spots on skin; cold receptors activate below the physiological temperature, from 1°C to 17°C, while warm receptors activate within a range between 32°C and 45°C. Below 17°C and over 45°C, cold and warm receptors inactivate, and the warm or cold sensation is mediated by the activation of nociceptors.

1.2. *In vitro* cell models for the study of neuronal properties

1.2.1. Primary cells

The human nervous system is one of the most complex systems to investigate. For decades, disciplines as neurophysiology and neurosciences have striven to elucidate its properties and functions, obtaining information using cellular and cognitive approaches, until the development of computational algorithms to understand its behavior (Lisman, 2015). One of the reasons why studying the nervous system is so challenging is that its structures are highly interconnected, and their isolation for analysing the single components is complicated. Thus, for this purpose, it turned out to be very useful the use of cultured cells, that can be divided in primary cells and cell lines. In the first case, cells are isolated directly from the tissue and maintained in particular culture conditions to mimic the properties of the native tissue. These cells are very fragile and have a limited self-renewal and differentiation potential, therefore a continuous preparation of primary cultured cells is needed.

Examples of primary cells are primary embryonic cell cultures such as those derived from Zebrafish, generally used because they can retain cell type-specific key features (Sassen et al., 2017), DRG neuron primary cell cultures or fibroblast cultures (Fig. 5).

DRG neurons represent the most important sensory cells in the whole body. Aside of their morphology and location, they serve as metabolic depot and as a source for different inputs, with receptors that allow subthreshold crosstalk and responsiveness to chemical signals (Devor, 1999). Moreover, they express several types of Ca^{2+} channels and, since their modulators are known to regulate pain sensation in *in vivo* and *in vitro* models, these cells could be used to study the transmission of noxious stimuli (Yusaf et al., 2001).
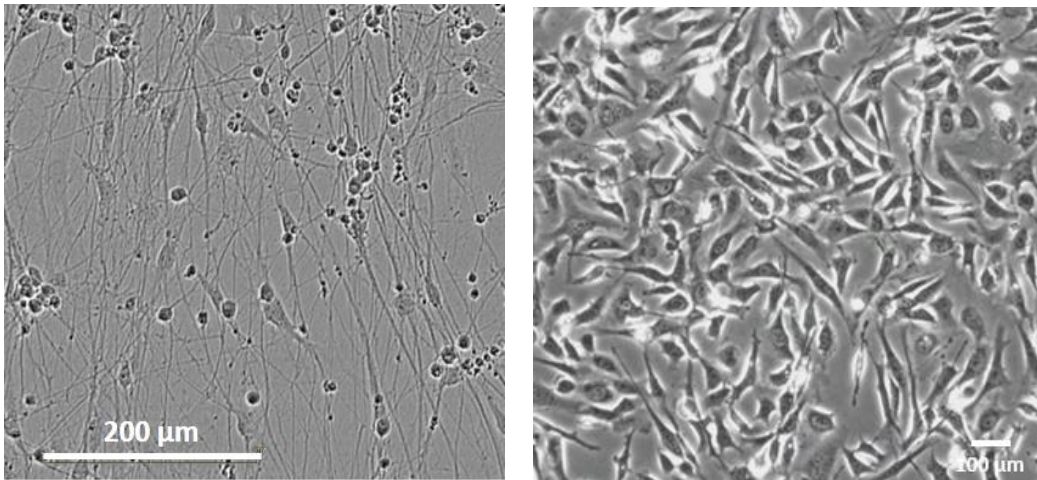
Figure 5. Representative images of rat dorsal root ganglion neurons (on the left) and fibroblasts (on the right) (web sources).

1.2.2. Immortalized cell lines

The second case concerns a cell culture propagated from a primary cell line which can be maintained in culture over a long time period. In this case, the cell line can be defined as finite or continuous. A finite cell line can be maintained for a limited period, after which cells undergo senescence. A continuous cell line is also called immortalized line because its cells can proliferate indefinitely thanks to specific genetic and phenotypic mutations, typical of cancer cells. For their ability to be maintained in culture for a very long period, immortalized cells are frequently preferred instead of primary cultures, because they are less expensive, easy to produce and maintain and do not have any ethical issue to deal with. These cells are used in various fields of scientific research such as vaccine production, drug testing, gene expression and structural and functional behavior studies (Kaur et al., 2012). Examples of these types of cells are PC12 (rat pheochromocytoma cells) (Fig. 6A), SH-SY5Y (human neuroblastoma cells) (Fig. 6B), HEK293 (human embryonic kidney cells) (Fig. 6C), HeLa (human cervical carcinoma line), and F-11 (mouse neuroblastoma x rat DRG hybrid cells) (Fig. 7).

Neuroblastoma cells are widely used in scientific research. Neuroblastoma is a common childhood solid tumor of the autonomic nervous system composed by a small primitive cell surrounded by several mature neurons or ganglia. Cancer cells derive from immature sympathetic ganglion cells and they arrest at different stages of differentiation, some of them showing a spontaneous shift to neuroendocrine cells (Edsjö et al., 2007). Cells that derived from this tumor are used mainly to study the general process of differentiation and neural development, because it was reported that some neuroblastoma cells could spontaneously undergo proliferation and differentiation (Abemayor et al., 1989).

Another cell line highly used in the fields of neuroscience is the immortalized DRG cell line, to study sensory pathways and responses, mechanisms of pain and nociception. Based on the original cells from which they derive, there are several types of immortalized DRG cell cultures. 50B11 cells are generated by transfection of SV40 large antigen with human telomerase reverse transcriptase hTERT into embryonic DRGs. MED17.11 cells represent a mouse embryonic DRG immortalized cell line. HD10.6 cells are human immortalized DRGs. Finally, F-11 cells consist in a hybrid cell line derived from the mouse neuroblastoma cell line N18TG2 and rat DRGs (Haberberger et al., 2020).
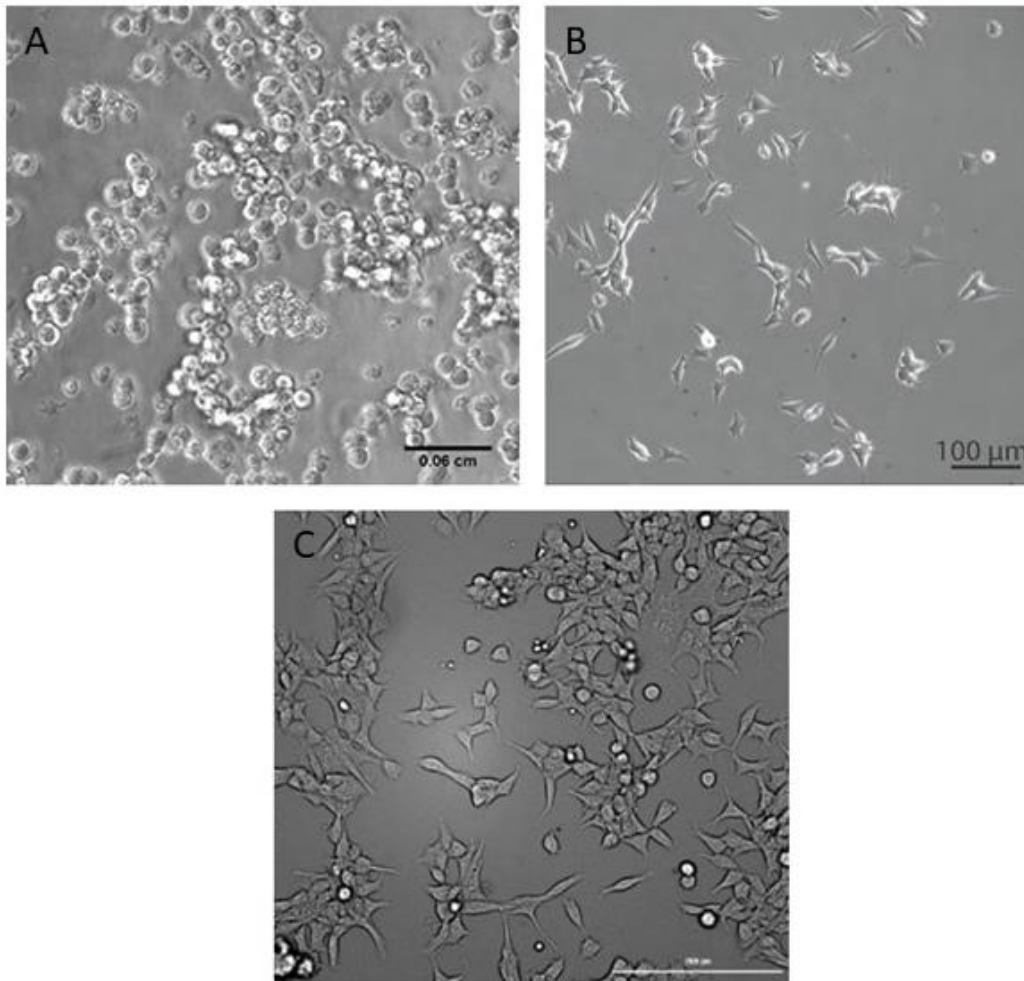
Figure 6. Representative images of PC12 (A), SHSY-5Y (B) and HEK293 (C) cells (web sources).

1.2.3. The F-11 cell line

F-11 cells are somatic hybrids developed by Platika and colleagues from the fusion of rat DRG neurons and mouse neuroblastoma N18TG2 cells deficient in hypoxanthine phosphoribosyltransferase (HPRT). Cells were maintained in a medium containing hypoxantine, aminopterin and thymidine to eliminate neuroblastoma progenitors and with *cis*-hydroxyproline to retard fibroblast outgrowth. 4 out of the derived 17 lines manifested neuronal properties and were selected for cloning.

These hybrid cells showed both rat and mouse chromosomes and isoenzymes and had electrical properties typical of DRG neurons (Platika et al., 1985). When differentiated, they also show specific features consistent with DRG neuron properties, such as the expression

of prostaglandins and bradykinin receptors involved in the transduction pathways of pain, dihydropyridine-sensitive Ca^{2+} channels and $\delta 5$-opioid receptors (Francel et al., 1987). F-11 cells can be differentiated by chemical differentiating agents, small molecules such as cAMP, transcription factors such as Neurogenin I, that with its C-terminus contributes to neurite elongation (Kim et al., 2002), or by using specific scaffolds/supports like neoglucosylated collagen matrices, which could induce differentiation without differentiating agents (Russo et al., 2014). Moreover, we have recently demonstrated that F-11 cells differentiated by serum deprivation express functional ion channels and receptors that are also present in DRG neurons, suggesting that they can be used as an alternative model to primary cells to study the mechanisms involved in the detection and transmission of noxious stimuli (Pastori et al., 2019). The use of this cell line as a suitable *in vitro* model of DRG neurons for different purposes, such as studies on neuronal differentiation, will be discussed in Chapter 4.
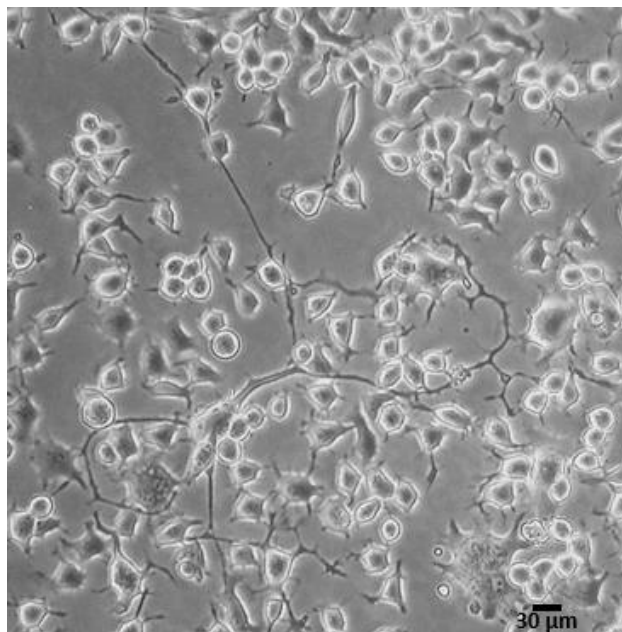
Figure 7. Representative image of F-11 cells grown in serum-deprived medium (from personal archive).

2. NEURONAL CELL LOSS AND NERVE INJURIES

2.1. Neuronal loss and cell death

Neuronal cell loss and peripheral nerve injuries represent an important public health problem and may result in significant disability, impairing the quality of patient's life.

Neuronal death can occur during development and pathology. While cell death during development represents a highly regulated mechanism to generate a functional circuitry within the nervous system, cell death during pathology occurs through an aberrant and uncontrolled mechanism, which is spread in different neurodegenerative diseases.

There are several types of cell death. Apoptosis can be extrinsic, through the death receptor pathway, or intrinsic, controlled by the mitochondrial pathway. Necroptosis is dependent on the Receptor Interacting Kinase 1 and 3 activity and the expression of the pseudokinase Mixed Lineage Kinase Domain-Like. Pathanatos depends on the activity of poly(ADP-ribose) polymerases, while ferroptosis is an iron-dependent necrosis. Autolysis, autosis and autophagy involve lysosomal permeabilization, self-eating and phagocytosis by another cell, respectively. Pyroptosis is mediated by caspase-1, paraptosis is controlled by cytoplasmic vacuolation and oncosis is a type of necrosis present after tissue ischemia. Cell death mediated by mitochondrial permeability transition can also occur (Fig. 8).

In addition to programmed cell death during development, neuronal death can be induced also by loss of connected neurons, by axotomy (transection and degeneration of the axon), by aberrant cell cycle re-entry and by other events such as excitotoxicity (often mediated by glutamate), protein aggregates, reactive oxygen species (ROS) and inflammation (Fricker et al., 2018).

Neuronal cell death represents an important issue because adult neurons have a very limited proliferative and regenerative ability. For this reason, several studies on neuronal differentiation and reprogramming are currently ongoing.

Type of Neuronal Cell Death	Initiators	Mediators	Inhibitors	Outcome
Apoptosis extrinsic	TNF-α, FasL	Caspases 8 + 3,6,7	Bcl-2	Phagocytosis
Apoptosis intrinsic	Multiple	Caspases 9 + 3,6,7	Bcl-2, IAPs	Phagocytosis
Necroptosis	TNF, IAP	RIPK1/3, MLKL	Caspase-8	Necrosis via MLKL
Parthanatos	DNA damage	PARP-1, PAR, AIF	Caspase-3	Necrosis via ATP ↓
Ferroptosis	Iron, glutamate	Fe^{2+}, ROS	GTH, GPX4	Necrosis via ROS
Pyroptosis	Inflammation	Caspase-1, gasdermin		Necrosis Inflam
Oncosis	Ischemia	Calpain I, ATP		Necrosis via ATP ↓
Lysosomal	Calcium, ROS	LMP, cathepsin ↓	HSP	Necrosis inflam
Autophagic	Stress	Beclin, autophagy	Bcl-2	Various
Phagocytic	Inflammation, stress	PS, CRT, opsonins	CD47	Phagocytosis
MitoPore	Calcium, ROS	Cyclophilin, ANT	ATP	Necrosis via ATP ↓

Figure 8. Comparison of different types of neuronal cell death (adapted from Fricker et al., 2018).

2.2. Peripheral nerve traumatic injuries

Traumatic peripheral nerve injuries occur in up to 3% of all patients admitted in trauma centres and represent life-altering injuries that can lead to significant patient morbidity (Houdek et al., 2015). Surgical intervention is the most common therapy, but results showed a poor recovery of peripheral nerves, of about 50%, in patients (Lee et al., 2000, Kuffler et al., 2020). The basic injury types include stretch-related, lacerations and compression injuries, which involve ischemia and mechanical compression.

The anatomy of a peripheral nerve includes three main components (Fig. 9): the epineurium, composed by a connective tissue layer which surrounds the nerve trunk; the perineurium, which surrounds the axon fascicles and is responsible to nerve tensile strength, and the endoneurium, surrounding the single myelinated axon (or groups of unmyelinated axons), composed by a collagenous matrix (Lee et al., 2000; Campbell, 2008). The blood supply lies both on the outer and in the inner surface of the epineurium, where a capillary network extends into the endoneurium and acts as an extension of the blood brain barrier (Houdek et al., 2015).
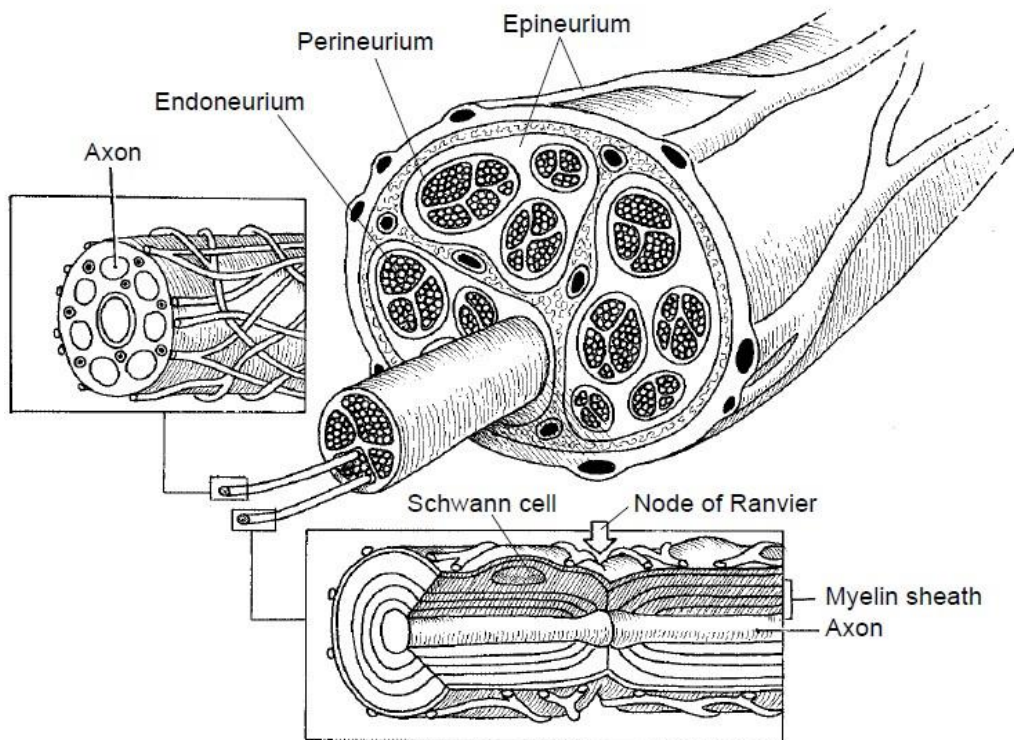
Figure 9. Cross-sectional anatomy of a peripheral nerve with an example of an unmyelinated fiber (left) and a myelinated fiber (bottom) (Lee et al., 2000).

According to severity, there are two classification schemes for peripheral nerve injury, one from Seddon and one from Sunderland (Fig. 10 and Fig. 11). The classification of Seddon divides the injuries in three types: Neurapraxia, Axonotmesis and Neurotmesis. Neurapraxia is the mildest type of injury, characterized by a transient functional damage without loss of nerve continuity. Axonotmesis involves the complete interruption of the axon and the myelin, leading to a complete denervation, but mesenchymal structures are preserved and are able to reinnervate the organ. Neurotmesis includes injuries in which all portions of the nerve are disrupted, and the nerve is completely interrupted (Burnett et al., 2004). The classification of Sunderland divided Axonotmesis in three subcategories (type 2, 3 and 4) based on different degrees of the lesion. The type 2 corresponds to the original Axonotmesis and involves the interruption of the axon, but with mesenchimal

components preserved. The type 3 includes the interruption of the axon and the endoneurium, but perineurium and epineurium remain intact. The type 4 is represented by the loss of axon, endoneurium and perineurium, with the epineurium preserved.

Table 1
Injury Classification

Seddon[2]	Sunderland[1]	Pathophysiologic Features
Neurapraxia	Type 1	Local myelin damage usually secondary to compression
Axonotmesis	Type 2	Loss of continuity of axons; endoneurium, perineurium, and epineurium intact
	Type 3	Loss of continuity of axons and endoneurium; perineurium and epineurium intact
	Type 4	Loss of continuity of axons, endoneurium, and perineurium; epineurium intact
Neurotmesis	Type 5	Complete physiologic disruption of entire nerve trunk

Figure 10. Injury classification of Seddon and Sunderland and their features (Lee et al., 2000).
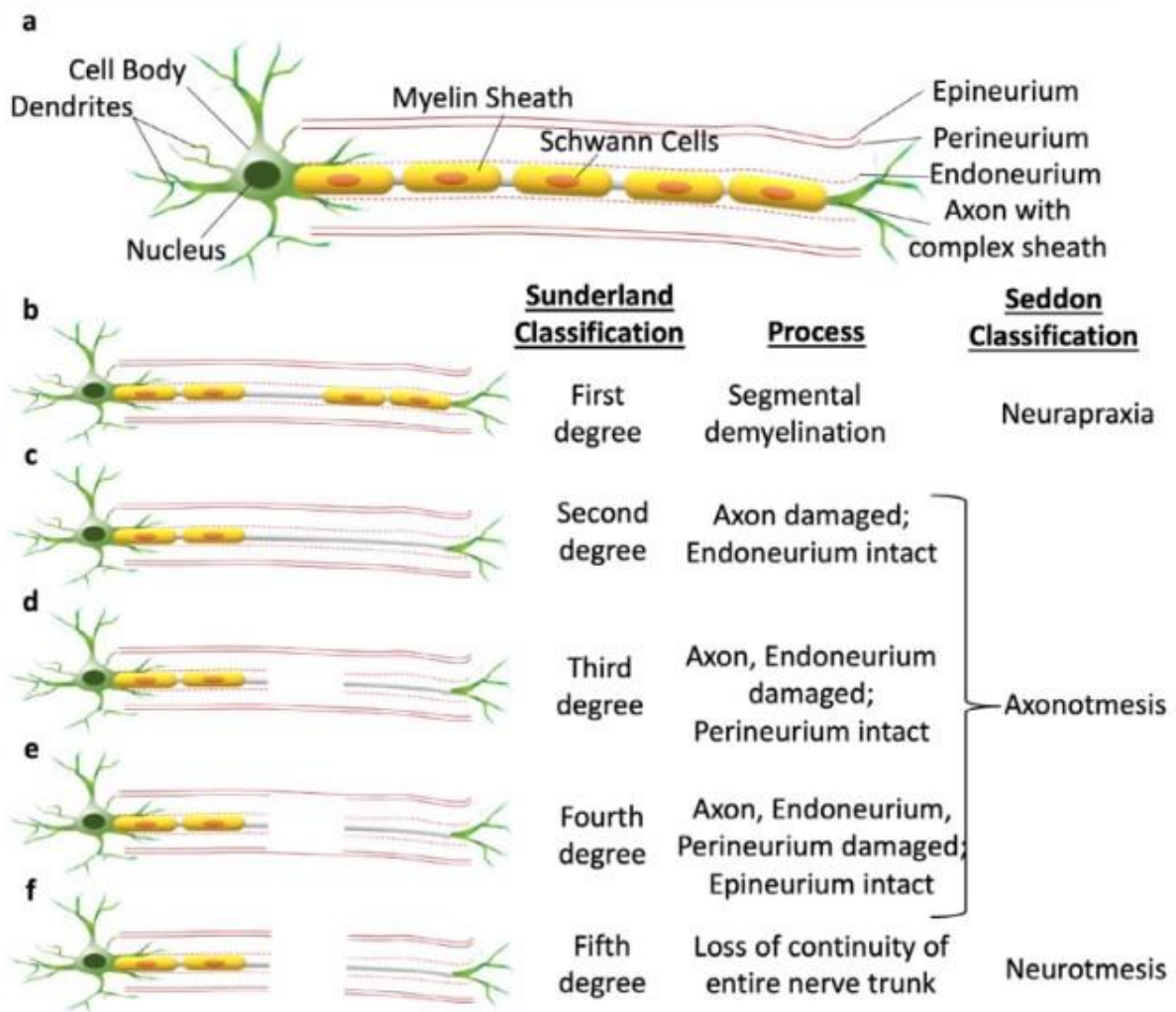
Figure 11. Representation of a peripheral nerve from an intact one (a) to the several types of injuries (b-f) (Vijayavenkataraman, 2020).

A simpler scheme was proposed to divide nerve injures in non-degenerative and degenerative (Thomas and Holdorff, 1993). Non-degenerative injuries did not involve axon loss, while degenerative injuries are classified into those with a complete nerve transection, those with a partial section of the nerve and those in which the endoneurium is preserved (Campbell, 2008). Another simple classification divides the injuries in two types: open or closed. Closed injuries involve nerve continuity and are associated to Neurapraxia and Axonotmesis, whereas open injures are associated to Neurotmesis and require surgery to verify the continuity of the nerve (Dubuisson et al., 1992).

As well as size and diameter axon reduction, after an injury a reduction of synapses and dendritic tree are also evident, due to a loss of dendritic segments. One possible structure

that can form afterwards to contribute to nerve regeneration is the "dendraxon", in proximity of the axotomy. However, it could develop inappropriate connections and impair functional recovery (Navarro et al., 2018).

These classifications are also useful in physical examinations, that are essential in the follow-up of patients, including the Tinel sign, a neurological test commonly used in diagnosing of Carpal Tunnel Syndrome, but which is also performed to verify the presence of nerve regeneration (Kline et al., 2008). With a first degree lesion, there is no axon loss, no atrophy and the Tinel sign remains focal to the site of the lesion. With a second degree lesion, the Tinel sign moves distally, indicating axonal growth, and a weak atrophy develops. With a third degree lesion, atrophy is present and the Tinel sign tends to migrate, but slowly. With fourth and fifth degree lesions, atrophy is rapid, severe and Tinel sign does not migrate. Other examinations that contribute to the evaluation and management of these injuries are electromyography (EMG), magnetic resonance imaging (MRI) and ultrasonography (US). The electromyography measures the compound muscle action potential (CMAP), the nerve action potential (NAP) and the motor unit action potential (MUAP). Action potentials decrease in amplitude in proportion to the severity of the lesion and the time that has passed until the evaluation (Campbell, 2008). MRI gives information on muscle atrophy, tumors and all the features that are not accessible to ultrasounds. Ultrasound examination is commonly used in traumatic injuries, especially for acute injuries with nerve continuity (Houdek et al., 2015).

2.3. Regenerative mechanisms of Peripheral Nervous System

The peripheral nervous system, as opposed to the central nervous system, can at least partially regenerate itself after an injury. In proximity to the lesion site, there is an increase of Ca^{2+} concentration that activates proteolysis which dissolves the cytoskeleton. At the distal level, Schwann cells and fibroblasts start proliferating for a certain period to regenerate the axon, after which Schwann cells die if regeneration does not occur (Hall, 1999). If the perineurium is damaged, fibroblasts and Schwann cells tend to proliferate in a disorganized fashion, leading to neuroma formation (Houdek et al., 2015). DRG neurons cannot regenerate the central part of the axon after a lesion, but can repair their peripheral region. To achieve this, there is an activation of several injury-induced signalling pathways, which regulate gene expression and promote neuronal survival and growth. This signalling includes positive and negative signals, i.e. activation and repression of different molecules and proteins. The positive signals involve the activation of cytokines (LIF, IL-6 and CNTF, leading to activation of JAK-STAT pathway), importin-beta, vimentin and several members of the MAPK family (Erk, JNK and protein kinase G), which together promote the retrograde transport and the growth of injured axons, as well as transcription factors such as c-Jun and JunD, CREB, SOX11 and ATF3. The negative signals include the suppression of the TGF-beta/SMAD2/SMAD3 pathway and of ATF-2, in order to allow proper synaptic development (Abe et al., 2008). Moreover, an injured axon triggers a depolarization that travels back to the soma and leads to a Ca^{2+} influx, which activates voltage-gated Na^+ channels necessary for the regeneration: in fact, it was seen that, in the presence of tetrodotoxin (TTX), the regenerative process is reduced (Mandolesi et al., 2004).

As seen in neuroma, the transported vesicles which accumulate after axotomy include ion channels, especially Na^+ and K^+ channels. In DRG neurons, TTX-sensitive Na^+ channels (Nav1.3) are upregulated after an injury. Since they recover rapidly from inactivation, there is a decrease in the refractory period that contributes, together with a reduction in the expression of K^+ channels, to hyperexcitability and the development of neuropathic pain.

Moreover, specific K$^+$ channels (K$_v$1.1) can accumulate at the periphery of neuroma, probably to stabilize the membrane after the hyperexcitability induced by the overexpression of TTX-sensitive Na$^+$ channels and the downregulation of K$^+$ channels. On the contrary, passive membrane properties remain stable after an injury (Navarro et al., 2018).

Currently, there are no repair techniques that can ensure a complete recovery and regeneration of an impaired nerve as surgical techniques are limited. In humans, a spontaneous recovery by plasticity and reorganization of spinal cord can be obtained in nerve gaps of less than 2 cm, but for gaps longer than 4 cm surgery is required (Reyes et al., 2005). Plasticity can lead to nerve regeneration after injuries, but several factors contribute to a poor functional recovery, including damages on the soma, axonal growth inability and poor specificity of reinnervation. For this reason, several new strategies to potentiate axonal regeneration and promote reinnervation are necessary (Navarro et al., 2007).

3. POSSIBLE MECHANISMS FOR TISSUE REPAIR

There are different techniques involved in nerve tissue repair (Fig. 12). Among these, four are considered as novel applications to investigate, as they currently seem to be the most likely to improve functional recovery in nerve-injured patients: electrical stimulation, tissue engineering, nerve gonduits and optogenetics. Electrical stimulation seems to be one of the most promising approaches in clinical trials. Nerve guidance conduits also represents a potential technique, although they are limited by the diameter and length of the construct. Tissue engineering is used in nerve regeneration and received a great attention in the last few years. Optogenetics technology is a novel therapeutic approach that has gained so much interest after the discovery of its ability to control proteins that regulate axonal regeneration (Mackinnon, 2018).
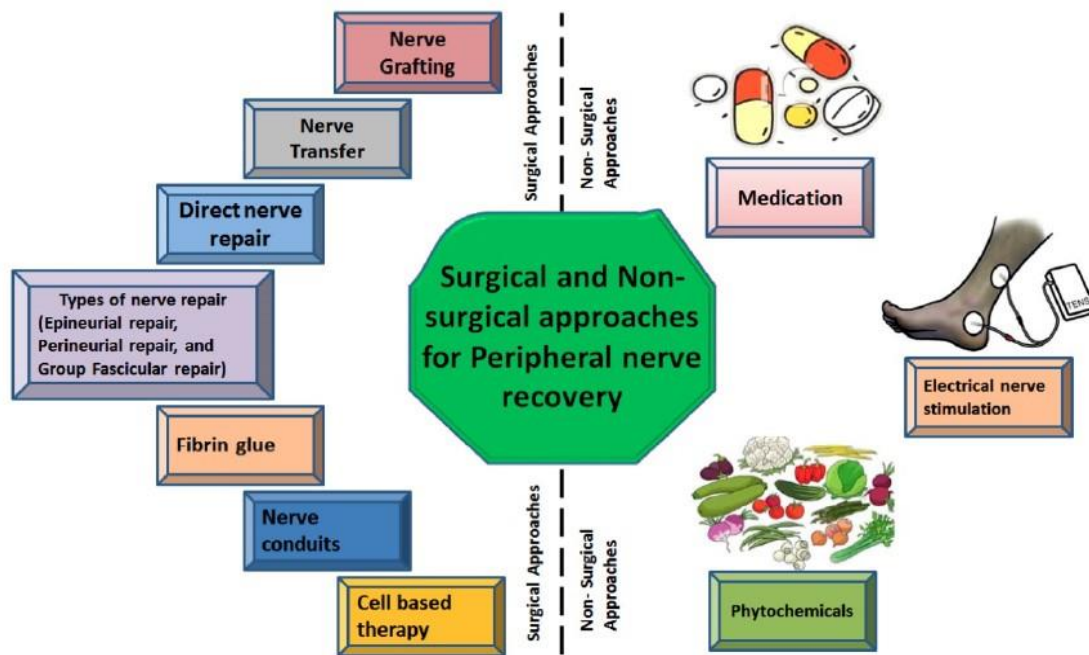
Figure 12. Surgical and non-surgical approaches for peripheral nerve repair (Hussain et al., 2020).

3.1. Surgical intervention and nerve grafts

Surgery is the most common approach used in injured patients, even if the possibility to treat these injuries and improve recovery is limited. The classical treatment involves the resection of the neuroma, neurorrhaphy (or nerve suturing) and implantation into muscles, bones and veins (Yao et al., 2017). Suturing the epineurium is the classical surgical method because it is easy to perform, but the internal structures of the nerve could not match correctly after the suture (Edshage et al., 1964) and this is the major drawback of surgical nerve repair. The development of novel microsurgical techniques could avoid this problem and achieve a better orientation of the internal structures of the nerve (Smith et al., 1964). Perineurial and group fascicular suture techniques are also available and could improve muscle reinnervation in rat sciatic nerve (Brushart et al., 1981-1983). More recently, nerve drafting has been developed as a promising approach to induce axonal regeneration. The graft can be vascularized and serves as a bridge for nerve gaps and as a guide for the axon, providing an optimal microenvironment for Schwann cells that regenerate the fascicles (Lundborg, 1987).

31

There are two types of nerve grafts. Autografts (or autologous) showed good results due to the involvement of Schwann cells, growth factors and adhesion molecules, but have some limitations such as donor-site morbidity, loss of nerve function, scarring, neuroma formation, etc. (Millesi et al., 2007). On the other hand, allografts avoid tissue availability and site morbidity, but are expensive and require a lot of experience (Hess et al., 2005). The use of fibrine glue instead of microsuturing for peripheral nerve repair has gradually increased in the last 20 years due to its ability to decrease inflammation and time of recovery (Sameem et al., 2010). In peripheral nerve injuries and, in particular, in traumatic lesions, surgical timing is usually defined by the "rule of three" (Martins et al., 2013): surgery within 3 days for clean and sharp injuries; surgery within 3 weeks for contusions and surgery within 3 months for closed injuries.

Other types of surgical intervention include:

-nerve transfer, a method in which the nerve is totally reconstructed, very useful in the case of peroneal nerve injury (knee dislocation) treatment together with the removal of hypertrophic epineurium and adjacent tissue, also called neurolysis (Prince et al., 2015);

-biological or synthetic nerve conduits, that are an alternative to autografts and can serve as a bridge between proximal and distal stumps of an injured nerve;

-several cell therapies such as Schwann cell-based therapy or stem cell-based therapy, which involve neural stem cells, bone marrow-derived stem cells, foetal stem cells, adipose stem cells, skin-derived precursor stem cells, hair follicle stem cells and induced pluripotent stem cells (iPSCs) (Hussain et al., 2020).

3.2. Medications and physiotherapy

The use of medications also represents a therapy for peripheral nerve injury treatment (Fig. 13). Medications include opioids, corticosteroids, gels and analgesics. In the central nervous system, it has been seen that N-methyl-D-aspartate (NMDA) antagonists could reduce neuronal degeneration (Tecoma et al., 1989). In treatments of neuropathic pain after traumatic nerve injuries, carbamazepine (a Na^+ channel blocker) was effective in the treatment of painful paresthesias (Rizzo, 1997) and pregabalin (a voltage-dependent Ca^{2+} channel blocker) was effective in the treatment of painful neuromas (Singh et al., 2012). Corticosteroids seem to have good results in the management of pain, but steroids may cause tissue atrophy in the long-term period. Several local anaesthetics are also used in the treatment of nerve injury neuropathic pain with good efficacy, but precautions should be taken in the administration of these medications. Cytological medications include therapies with tumor necrosis factor (TNF) inhibitors, nerve growth factor (NGF) inhibitor, cytotoxin and the alpha smooth muscle actin (Dahl et al., 2008; Kryger et al., 2001; Climent et al., 2013; Weng et al., 2016). However, most of the medications currently available are not useful for peripheral nerve injuries because they calm the pain but cannot accelerate nerve regeneration or functional recovery (Hussain et al., 2020).

ANALGESICS
- Acetaminophen
- Aspirin
- Ibuprofen
- Advil
- Motrin IB etc

OPIOIDS
- Hydomorphene
- Methadone
- Neuropaquell

MEDICATION

TOPICAL TREATMENT
- Pain killing gels/creams (Nervex etc)
- Lidocaine patches

CORTICOSTEROIDS
- Betamethasone
- Prednisone
- Prednisolone
- Triamcinolone
- Methylprednisolone
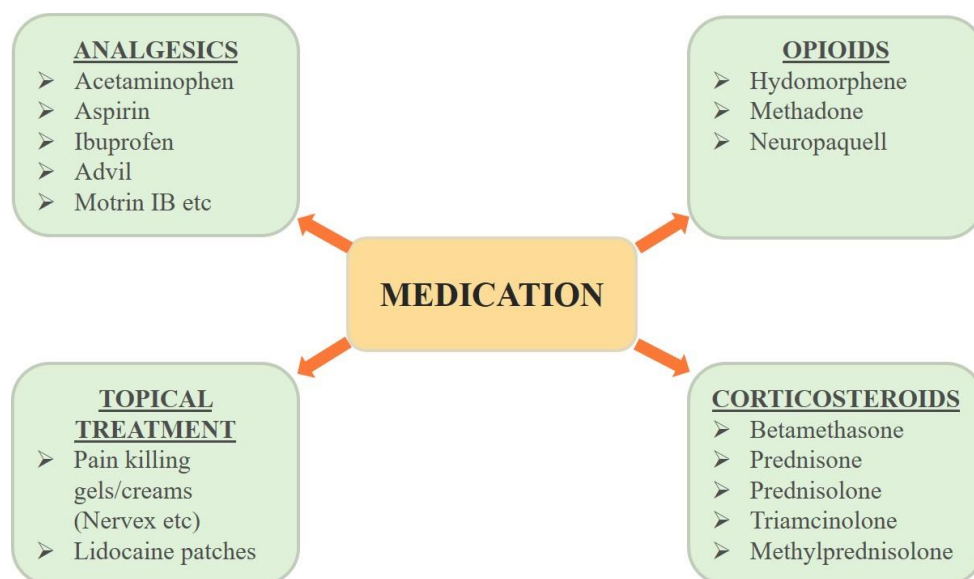
Figure 13. Types of medications available for peripheral nerve pain (modified from Hussain et al., 2020).

After surgery and medications, other treatments for traumatic nerve injuries consist mainly in physiotherapy, as therapeutic massages which could alleviate neuropathic pain (Yao et al., 2017), and electrical stimulation, performed by applying electrical current directly to the skin and the muscle, to induce a contraction to avoid muscle atrophy (Heidland et al., 2013).

3.3. Electrical stimulation

There are several types of electrical stimulation therapy. The brief intraoperative electrical stimulation (BES) has been developed after several studies on electrical stimulation of peripheral nerves in animals, which can accelerate axon regrowth. A stimulation at 20 Hz for 1 hour by a wireless, bioresorbable stimulator (Koo et al., 2018) was effective in accelerating sensorimotor regeneration, probably due to an electrical stimulation-induced production of neurotrophic factors, such as BDNF, NGF and other growth factors (Al-Majed et al., 2000; Geremia et al., 2007). Other types of electrical stimulations include long-term peripheral nerve stimulation (PNS), which improves patient's outcome in painful nerve injuries and seems to be a very promising approach in the treatment of pain (Ransom et al., 2020), and transcutaneous electrical nerve stimulation (TENS), that has become popular in the last decade and it is administrated at high intensities close to the damaged site to achieve pain relief (Johnson et al., 2011). Neuromodulation by using an electrical stimulator implantation is one of the novel electrical stimulation therapies. The overall results reviewed by Mobbs and colleagues are encouraging because, after 35 months from electrical stimulation, 61% of patients experienced a great relief from chronic pain. These patients suffered of peripheral mononeuropathy, plexopathy and other painful syndromes. The treatment is simple, non-traumatic and reversible, while disadvantages include risks of infection, effectiveness loss of the stimulator, and the cost of additional implantations after battery failure (Mobbs et al., 2007).

3.4. Nerve guide conduits

Nerve guide conduits (NGCs) are natural or synthetic, flexible and biodegradable cylindrical structures used for nerve regeneration, which link the nerve endings and provide structural and trophic factors during the regeneration. These systems have several designs, including hollow/non-porous structures, porous structures, grooved and multi-channel pattern and fibrous structures or hydrogel consistency, and different materials, depending on the natural or synthetic origin of the NGC (Vijayavenkataraman, 2020). Natural materials include collagen, gelatin, fibrinogen, chitin, cellulose or chitosan; synthetic materials include poly(ε-caprolactone), poly-lactic acid and poly-glycolic acid (Mogoşanu et al., 2014). To give a good conductivity to the structure, polymers like poly-pyrrole, poly-aniline and poly-thiophene are often blendend with other polymers (Balint et al., 2014), as described below. Fabrication methods can also be distinguished among NGCs, such as solvent casting, gas foaming, phase separation, freeze-drying and electrospinning (Subia, 2003). There are four main properties that NGCs should have to provide a good axonal regeneration: permeability, to allow cell viability via oxygen and nutrients diffusion within the regeneration site; flexibility, to avoid mechanical damages; an appropriate swelling to prevent the block of the tunnel guide during regeneration; and a good rate of degradation (Arslantunali et al., 2014; de Ruiter et al., 2009).

Both *in vitro* and *in vivo* studies were performed to verify the effectiveness of NGCs. The most common cell types used for the *in vitro* studies are PC12, Schwann cells (Kim et al., 2016; Yu et al., 2011), SH-SY5Y, C6 and the mouse neuroblastoma cell line Nb2a (Panahi-Joo et al., 2016; Bryan et al., 2004), and recently the use of stem cells has also started. Regarding the *in vivo* studies, NGCs have been used in clinical practice with significant results, and the combination of tissue, cell and genetic engineering techniques could lead to a better functional recovery in patients with peripheral nerve injuries (Muheremu et al., 2015). Clinical studies showed that short-distance nerve injuries can be treated properly by using NGCs. Since the data collected demonstrated that the regeneration obtained with

NGCs is equivalent to that achieved with autografts, the use of nerve guides could replace these nerve transplantation approaches, which have several disadvantages, such as the number and length of donor nerves, the need of a second surgical procedure and the relatively low recovery rate of motor function of about 40% (Ichihara et al., 2008).

In order to be a good alternative for nerve injury repair, nerve guides should have an excellent electrical conductivity, as mentioned before. Conductive polymeric composites can provide a template for cell growth and allow electrical stimulation to be applied directly on cells (Bettinger et al., 2009), becoming a promising approach in the regenerative medicine. Moreover, the use of conducting polymers permit to focus the stimulation to a specific area, allowing spatial control of the treatment (Schmidt et al., 1997). Their main disadvantage is the low degradability, that could lead to infections and to the need of surgical interventions (Huang et al., 2007), but in the last few years this issue seems to be overcome through the blending of conducting polymers and biodegradable polymers. The most common conductive polymers used in this field are poly-pyrrole and poly-aniline. Poly-pyrrole (Ppy) has been reported to support cell proliferation and adhesion and is largely used for biosensors, drug delivery and coating of neural probes (Sanchvi et al., 2005). Its structure is highly rigid and insoluble and for this reason a biocompatible, optical transparent poly-pyrrole film was synthesized, which could support cell attachment and growth (Wong et al., 1994). Specific combinations of Ppy with other polymers, such as Poly-caprolactone fumarate (PCLF) or Chitosan, increased functional recovery and neurite extension (Marquardt et al., 2013). Poly-aniline (PANI) was explored for tissue engineering more recently, but it can support cell growth as well as Ppy. It can be synthesized in various forms and *in vitro* and *in vivo* studies showed no inflammation at the implant site (Guimarda et al., 2007) and a good biocompatibility (Kamalesh et al., 2000). Other polymers often used in tissue-engineering applications are poly-thiophene (Guimarda et al., 2007), carbon nanotubes and piezoelectric polymeric materials (Ghasemi-Mobarakeh

et al., 2011), or polymeric scaffolds used as extracellular matrix analogues and multichannel scaffolds (Subramanian et al., 2009).

Neural tissue engineering has developed several new techniques such as electrospinning and biofactor immobilization to improve permeability, biodegradability and bioactivity of materials used for nerve conduits. An example is represented by Lumen fillers, composed by micro- and nano-scale features and fibers with specific properties, which facilitate structurally and spatially nerve regeneration (Zhang et al., 2014) and can be filled with stem cells to provide growth guidance (Gaudin wet al., 2016). Moreover, support cells such as Schwann cells and growth factors can be incorporated directly into the nerve guidance conduits to sustain nerve regeneration (Evans, 2001). However, gaps greater than 30 mm and modulation of spatial and temporal cues remain the major challenges for this technique, and the combination of different therapies and the development of new methods that allow a targeted modulation is essential to improve long-term functional recovery (Marquardt et al., 2013).

PART II

1. THE USE OF HEATING ON CELLS

1.1. Cell behavior modifications through heating

Heating has been recently explored as a promising approach for the treatment of oncologic diseases, for the relief of pain and for the induction of cell differentiation or proliferation. Several studies have investigated the effects on cell behavior of mild hyperthermia in combination with chemical factors and/or nanomaterials. Exposure to 38°C for 4 days induced cell proliferation in the presence of growth factors and stimulated differentiation in absence of these factors (Hossain et al., 2017). Thermal stimulation at 39°C supported the fusion and elongation of myoblasts (Hayashi et al., 2019) and daily heat treatment could rescue oxidative stress, loss of mitochondria and muscle atrophy (Tamura et al., 2015). In PC12 cells, maintained at 39.5°C for 12 and 18 hours, projection length and Acetylcholinesterase (AChE) activity increased compared to control, whereas cells maintained at 42°C died after one day of treatment (Kudo et al., 2015). The last result indicates the importance of establishing a fine-tuning mechanism of thermal stimulation. In fact, heating is commonly used in cancer therapy, as it induces cell death, inhibits DNA repair and sensitizes cells to chemotherapeutic agents (Roti Roti, 2008). Hyperthermia could lead to protein unfolding, but this process is reversible in the range of 40-47°C; however, in the range 48-60°C, the protein unfolding is irreversible, and for this reason, these temperatures are applied for thermal ablation. Similarly, at extreme temperatures of 50-60°C, DNA damage was observed, but not in the range of 40-46°C (Lewis et al., 1977; Dewey et al., 1971). At temperature ≥42.5°C, cell death occurs mainly in S-phase cells (Mackey et al., 1988), and the nuclear matrix is also affected.

One example of fine-tuning mechanisms of thermal stimulation is shown in the study by Itoh and colleagues, in which heat pulses (2 or 150 seconds) from an infrared laser could induce Ca^{2+} bursts in fibroblasts, proposing a new method to control Ca^{2+} dynamics, which regulate several cellular functions (Itoh et al., 2014). Pulsed infrared light can also pace

embryonic intact hearts, inducing electrical activity in cardiomyocytes (Jenkins et al., 2010), and can penetrate the skin to directly interact with circulating lymphocytes which modulate immune functions (Roberts, 2000).

The heat produced by an infrared laser (IR) can alter the electrical capacitance of the cellular membrane, allowing a depolarization and consequently an action potential, by eliciting an inward current in *Xenopus* oocytes and in mammalian cells (Shapiro et al., 2012). The mechanisms by which these changes occur are so far unknown, but several studies on Transient Receptor Potential Vanilloid (TRPV) channels demonstrated that they might be involved in the response to heat.

1.2. TRP channels

TRP channels were identified in 1960 in a Drosophila mutant and successively cloned. The mammalian family contains 28 members (Gees et al., 2012) and thermo-TRPs are represented by several members of different subfamilies (TRPV, TRPC, TRPM and TRPA). They cover a range of responses to temperatures between 10°C and 52°C and are polymodal sensors, because they respond to both chemical and physical stimuli. They have a structure similar to other ion channels: the N-terminal contains ankyrin-repeated elements and the C-terminal probably plays a role in activation and desensitization, and it is likely to contain the thermal sensor (Castillo et al., 2018). These channels can be divided in two groups: cold and warm sensors.

TRPV1 is permeable to Ca^{2+} and Na^+ and is activated around 40-42°C. Its temperature sensing is linked to a voltage-dependent gating, as an increase in temperature results in a graded-shift of the voltage-dependent activation curves toward the physiological membrane potential. TRPV2 is activated over 52°C and is often associated with TRPV1, as seen in HEK293 and F-11 cells (Huang et al., 2006).

TRPV3 is activated at warm temperatures (34-39°C) and colocalizes with TRPV1 in DRG neurons to modulate the response to capsaicin, while TRPV4, as a polymodal ionotropic

receptor, could respond to thermal (>25°C), chemical (arachidonic acid and EETs, acidic pH) and physical (pulsatile stretch in endothelial cells and membrane swelling) stimuli (White et al., 2016), although it does not seem to massively contribute to peripheral thermosensation. TRPM8 responds to stimuli below 25°C, whereas TRPM2 is required to detect non-noxious warm from 23°C and above 32°C (Tan et al., 2016).

TRPA1 is activated below 17°C and colocalizes with TRPV1 in sensory cells, modulating the burning sensation of cold, and with TRPC5 (another cold-sensitive channel) in healthy teeth, providing cold sensing (Bernal et al., 2021).

TRPV1 seems to be the most involved in the response to heat, as in DRG neurons an inward current is activated at temperature above 43°C (Huang et al., 2006). It was also demonstrated that TRPV1 may contribute to the constitutive Na^+ conductance in hyperexcitable neurons and could desensitize, as no responses have been seen after repetitive stimuli (Kitamura et al., 2018).

TRP channels are also expressed in the central nervous system, with a lower temperature threshold and with a tonic activity of TRPV1 especially in the midbrain, in the hypothalamus and in the hippocampus (Kauer et al., 2009). TRPV1 responds also to the exogenous vanilloid capsaicin (CAPS), the main pungent ingredient of chilli peppers, which elicits burning pain through TRPV1 activation. Studies in HEK293 cell line showed that capsaicin- and high temperature- (46°C) evoked currents are strictly correlated and that also correlate with acidic pH (<5.9), at which channels open at room temperature instead of at high temperatures (Tominaga et al., 1998). Moreover, TRPV1 responds to endogenous lipid signalling molecules, such as eicosanoids and anandamide, and changes in their concentration could modify the thermal sensitivity of the channel: for example, TRPV1 phosphorylation by PKC results in an activation of this channel at room temperature (Benham et al., 2003). The channel is inhibited by Capsazepine (CAPZ), the first competitive antagonist of capsaicin described in literature, which is moderately potent and active both in *in vitro* and in *in vivo* systems (Walpole et al., 1994).

Thus, TRP channels modify membrane capacitance and elicit currents which sustain the depolarization induced by heat or cold, but the specific mechanism is not yet known. It was seen that they could collaborate with other types of channels involved in the warm/cold response, such as the TWIK-Related potassium channels (TREK), which seem to control the activation and inactivation of different TRP channels (Fig. 14). Moreover, these channels could respond to heat induced by the infrared light (Liang et al., 2009), and for these reasons, the potentialities of optical stimulation, especially in the near-infrared region (NIR), were investigated in the last years to set off a targeted technique to handle in different therapies, from cancer therapy to functional nerve recovery.
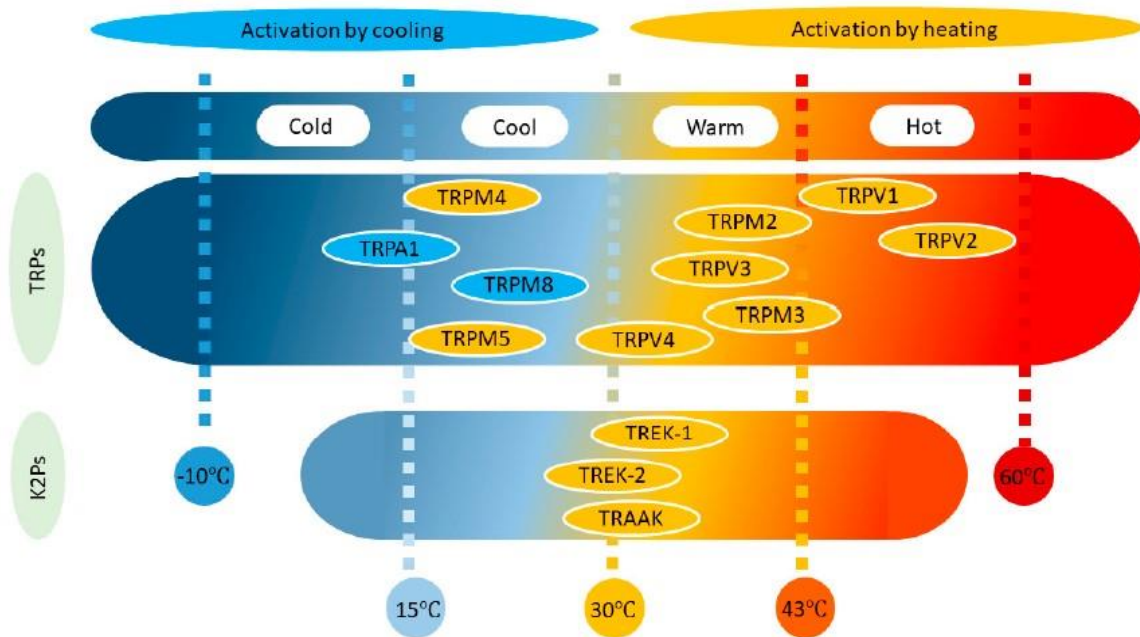

Figure 14. Thermal sensitivity of TRP and TREK channels. The position of the channel corresponds to the temperature at which the channel is activated (Lamas et al., 2019).

2. OPTICAL AND THERMAL STIMULATION

Light stimulation could influence neuronal behavior and its ability to trigger neuronal response without being invasive made it an interesting method to investigate. There are several approaches in which light stimulation is used, such as optogenetics, infrared neural stimulation (INS), a combined method of optical and electrical stimulation, and a combination of light and nanoparticles to convert light into targeted heat.

2.1. Optogenetics

Optogenetics includes the use of light to genetically control neurons modified with light-sensitive ion channels, such as channelrhodopsin-2, in a controlled spatial and temporal manner. This technique involves tools that can increase excitability, can regulate biochemical pathways in neurons of different animal models, and has the ability to target specific layers using viral expression systems or optical fibers (Fenno et al., 2011). However, despite the usefulness of this method into the neuroscience field, its potential for human purposes is limited because it requires gene transfection into neuronal cells, the expression efficiency is spatially heterogeneous, the high expression rate could lead to toxic accumulation of proteins within the tissue, and potential immunogenicity of viral particles could develop (Dugué et al., 2012). Another technique involves the use of photoactive molecules, consisting in neurotransmitters captured in a photosensitive cage, that can be released after the exposure to light, or molecules called photoswitches, which are able to change their conformation after light exposure. These compounds are promising for modulating specific targets, but their use in *in vivo* studies is limited due to the potential toxicity of the cage and the need to restock the cage with neurotransmitters (Kramer et al., 2009).

2.2. Infrared neural stimulation

The effect of an infrared neural stimulation (INS) is represented by a direct induction of an evoked potential in response to a transient targeted deposition of optical energy. It could be applied for the stimulation of peripheral nerves, cranial nerves, for the central auditory system *in vivo* and on different cell types *in vitro* (Richter et al., 2011). This technique has the advantage to stimulate nerves without genetic or chemical manipulations, as the light is directly absorbed by water; moreover, it has a high spatial resolution, does not require direct contact with the tissue and does not produce stimulation artefacts (Thompson et al., 2014). The mechanism behind INS involves a photothermal interaction due to water absorption of the light (Wells et al., 2007); therefore, the possible damage caused by heating is one of the disadvantages of this technique. High pulses rates from 5 to 8 Hz were more likely to cause damage than 2 Hz pulses, although in peripheral nerves the damage threshold seems to be higher than in central nervous system. Another disadvantage includes the limitation of depth penetration due to the absorption and refraction of light within the targeted tissue (Shapiro et al., 2012). However, INS has been often used in *in vivo* studies, and for this reason it would be useful to elucidate its mechanisms also on *in vitro* neuronal models (Richter et al., 2011).

Infrared neural stimulation can be coupled with electrical stimulation. This combination allows to stimulate neural activity through a contact-free, artefact-free and spatially precise modality. Delivering of an electrical stimulus combined with INS lowers the optical energy required to reach the tissue and increases the damage threshold of INS exposure, but an optimal combination of optical and electrical stimulation, which minimizes the tissue damage below the damage levels of INS alone, remains to be determined and further studies are needed to better understand this coupling mechanism (Duke et al., 2009).

2.3. Photothermal therapy

Phototherapy with near-infrared laser (NIR, Fig. 15) is currently used for different applications, such as traumatic brain injuries, strokes or psychiatric disorders. The parameters of irradiation needed to be considered in this therapy are wavelength (nm), energy (J), irradiance (W/cm²) and radiant exposure (J/cm²) (Jenkins et al., 2011).

Penetration of 40 mm depth within the brain, by using a 5-15 W laser at a wavelength between 810 and 980 nm, showed excellent responses in patients, with significant improvement of anxiety, cognitive ability, insomnia and depression. Moreover, the use of a LED-device with a wavelength of 600-1200 nm for 6-10 minutes for several months resulted in a neurophysiological improvement, which was maintained for 7-9 months after the treatment (Morries et al., 2015).
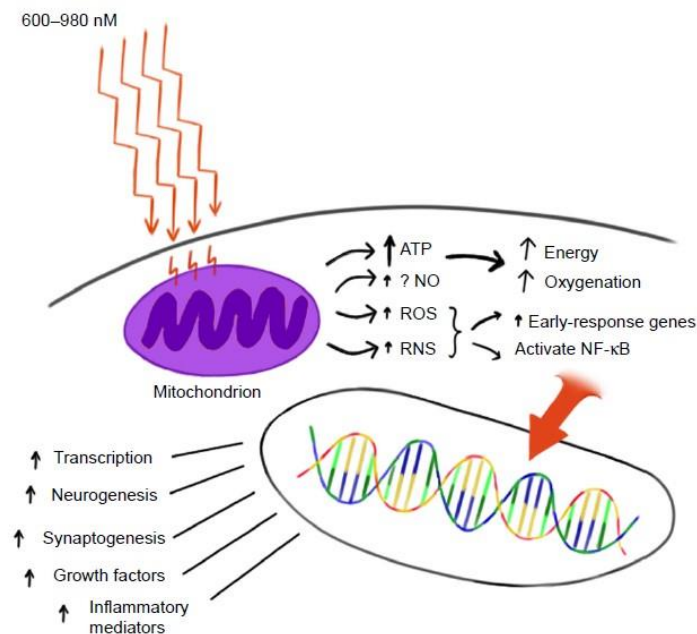
Figure 15. A hypothesized mechanism of action of NIR light therapy (Morries et al., 2015).

However, a lower laser power (0.5 W) at 670 or 830 nm showed no benefits, suggesting that the delivered energy was insufficient to reach the cortical tissue within the human brain (Giacci et al., 2014). In fact, NIR penetration into the human brain is attenuated by skin, skull, blood and cerebrospinal fluid which cause absorption, reflection and scattering of the light at lower wattage, although some studies showed that higher wattage could

avoid these issues without damaging tissues (Henderson et al., 2015). Moreover, electrophysiological studies in spiral ganglion neurons (SGNs) showed that increase in power, energy or duration of irradiation could decrease the membrane impedance of 30% and damage cells, although thermodynamics in *in vitro* and in *in vivo* models are different and cells in a non-physiological state may be more susceptible to thermal damage (Brown et al., 2020). Therefore, wavelength, delivery, intensity and duration of NIR phototherapy should be optimized, because the cells in the brain could have different sensitivity and require different treatment strategies (Giacci et al., 2014).

2.4. Use of nanoparticles

One optimization developed in the last years is the use of NIR laser in combination with nanomaterials or nanoparticles. Functional studies on cultured spiral ganglion neurons and on rat sciatic nerve demonstrated that NIR light at a wavelength of 780 nm in combination with gold nanoparticles induced a localized stimulation of neurons and enhanced the effects of infrared laser stimulation without cell damages (Paviolo et al., 2013a; Paviolo et al., 2013b). Light stimulated nanoparticles are notably useful for several treatments, such as anticancer therapy, immunomodulation, stem cell regulation, drug delivery and neuromodulation (Thang et al., 2019). In the next paragraphs, properties of two types of nanoparticles largely used in nanomedicine, Gold nanoparticles and Prussian Blue nanoparticles, will be explored. The use of a novel combination of NIR laser and nanoparticles to induce neuronal differentiation via thermal stimulation will be discussed in Chapter 4.

3. NANOPARTICLES AS LIGHT-TO-HEAT TRANSDUCERS

3.1. Gold Nanoparticles

Gold nanoparticles (AuNPs) have specific optical properties that attracted the interest of the biomedical field in the past decade. They can be developed in various shapes, such as stars (Fig. 16), cubes, spheres, prisms and rods. When reached by a NIR light, a resonant coherent oscillation, called plasmon excitation or localized surface plasmon resonance, occurs (Myroshnychenko et al., 2008). In particular, nanorods possess two plasmon excitation bands, for the long and for the short axis of the rods, respectively. Modifications of this ratio make these nanoparticles highly tunable and useful in biomedical applications (Zhan et al., 2009). Nanostars represent a versatile tool because they can be used as contrast agent for X-ray imaging *in vitro* and in *in vivo*, and as a dual-sensitive photosensitizer (PS) for Photothermal therapy (PTT), by inducing hyperthermia, and for Photodynamic therapy (PDT), by providing the release of ROS in cancer treatment (Wang et al., 2015).
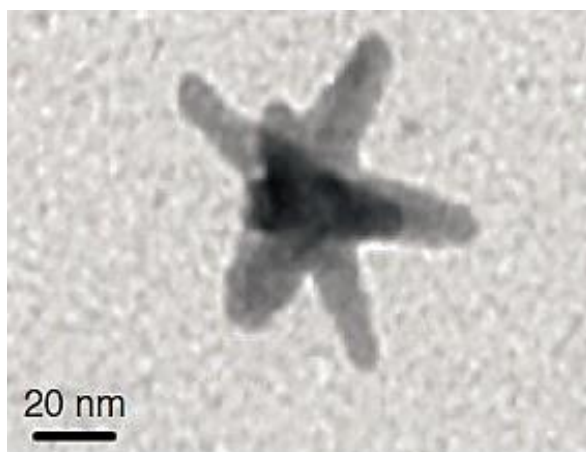

Figure 16. Transmission electron microscopy (TEM) image of a gold nanostar (GNST) (Wang et al., 2015).

Other applications in which AuNPs are largely used are electronics, drug delivery and as sensors. However, gold nanoparticles have a limit, which consists in the short-range effect of heating: therefore, they should be very close to the cell to produce an appreciable effect. To avoid this problem, AuNPs can be conjugated with functional groups which bind membrane proteins. In this form, AuNPs were able to stimulate neurons. AuNPs conjugated with neurotoxin Ts1 (which binds voltage-gated Na^+ channels), antibodies versus TRPV1 channels and antibodies versus $P2X_3$ channel receptors are able to trigger action potentials in DRG neurons at a low concentration and with a good resistance to washout (Carvalho-de-Souza et al., 2015). The capability to induce action potentials was confirmed in several studies which demonstrated that stimulated AuNPs could elicit neuronal outgrowth (even with a low-power device and a single irradiation of 1 minute), increasing neurite length, the number of neurites per neuron and the percentage of neurons with neurites, and could evoke Ca^{2+} transients (Paviolo et al., 2014).

Despite their flexibility and their usefulness in several applications, another strong limit of AuNPs is their cytotoxicity, therefore, the type of surface coating of these nanoparticles is extremely important. Citrate and biotin surfaces did not appear to be toxic, while Cetyltrimethylammonium Bromide (CTAB) showed a high cytotoxicity. Moreover, AuNPs can affect the immunological response of cells (Lewinski et al., 2008).

3.2. Prussian Blue Nanoparticles

Prussian Blue nanoparticles (PBNPs) are composed by inorganic salt of co-coordination complexes, with unique electro, photochemical, biochemical and magnetic properties (Johansson et al., 2005). Prussian Blue is a coordination polymer containing Fe^{3+} cations and a hexacyanoferrate complex, $[Fe(CN)_6]^{2+}$. Fe^{2+} cations are coordinated by the C atom of the CN^- ligand, which acts as a bridge with Fe^{3+} cations, that are octahedrally coordinated by 6 Nitrogen atoms (Fig. 17) (Da Carro et al., 2018). They represent excellent candidates for several applications such as photonic and optical devices, catalysis, drug delivery,

staining and chelating agents (Roy et al., 2011; Mukherjee et al., 2015), due to their biocompatibility, biodegradability, production facility and low production cost. Moreover, they have been approved by the U.S. *Food and Drug Administration* in 2003 as a safe oral antidote for the treatment of internal contamination of thallium or caesium in humans (Patra, 2016). PBNPs can be soluble or insoluble and can be prepared in a simple aqueous solution, without the need of adding organic compounds or polymers. Citrate coating is commonly used in their preparation and no detectable cytotoxicity in *in vitro* models has been referred, suggesting that this coating could have a good biocompatibility (Shokouhimehr et al., 2009).
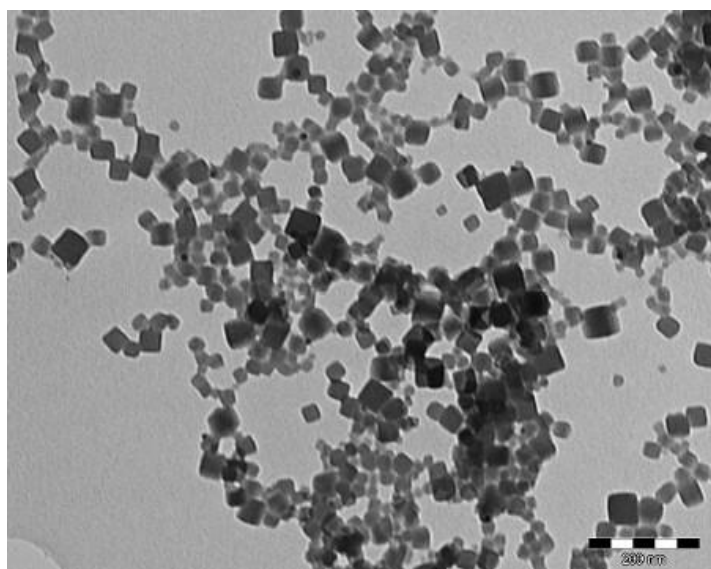
Figure 17. TEM image of stabilized PBNPs with citrate (DaCarro et al., 2018).

Nonetheless, polymeric matrices, reverse microemulsions and silica scaffolds, to form nanoparticles and to prevent their agglomeration, can be used as methods to prepare PBNPs, making them a versatile tool for different approaches (Vaucher et al., 2000; Moore et al., 2003, Fig.18). Inorganic or organic transparent PBNP films enzymatically modified could act as an electrocatalyst and could be used, for example, as urea or glucose biosensors (Koncki et al., 2001). PBNPs embedded in poly-vinyl alcohol films showed antibacterial effects after a high and localized increase of temperature, and this localized photothermal effect could also mitigate bacterial biofilm growth (Borzenkov et al., 2019).

PBNPs can be layered also on a functionalized glass surface, allowing temperature increase (Da Carro et al., 2017), albeit the glass is not a biocompatible material. In the nanoscale, PBNPs tend to aggregate and to be cleared easily from the physiological system, thus, in this case, they need a protection strategy, guaranteed by inorganic (carbon, iron oxide or manganese) or organic (proteins, antibodies, albumin) materials. These combinations do not show cytotoxic effects (Pearce, 1994) as, after PBNPs injection, T-cell levels in blood tend to decrease, but recover gradually within 7 days, and coatings could prolong circulation in blood and prevent the release of toxic metal ions (Kirchner et al., 2005). Notably, thanks to their biosafety in humans, they are excellent photothermal conversion agents in cancer treatment. As Phototherapy (PTT) alone has limited therapeutic efficacy, a combination of PTT with PBNPs could be a promising strategy to kill cancer cells (Gautam et al., 2018).
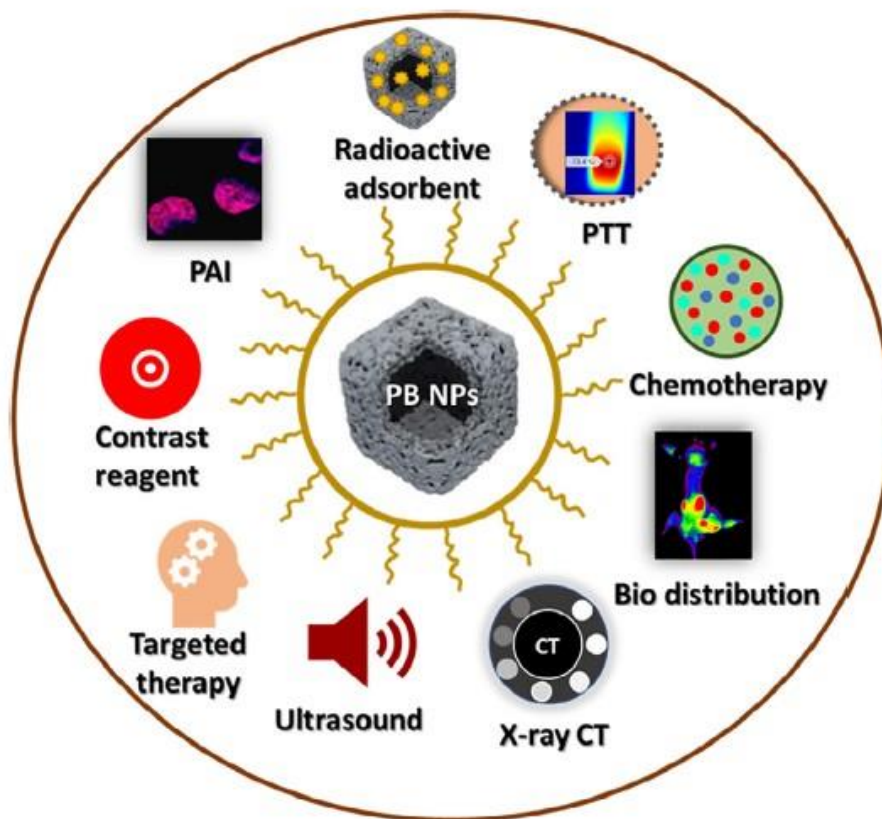

Figure 18. Applications of PBNPs (Gautam et al., 2018).

In fact, PBNPs in combination with PTT showed that when irradiated at 808 nm NIR laser, nanoparticles were able to selectively heat cancer cells in a murine model of neuroblastoma, leading to a significant tumor debulking, increasing tumor-free days and decreasing tumor growth rates (Hoffman et al., 2014). Moreover, the combination of PTT with PBNPs and chemotherapic agents enhanced the therapeutic efficacy compared to PTT or chemotherapy alone (Jing et al., 2016), suggesting that PBNPs in combination with PTT could be a promising approach in theranostics. Compared to AuNPs, PBNPs have a lower molar extinction coefficient and better photothermal stability, and were patented for electrochemistry, electrochromic material, sensing water and soil purification and as contrast agents for cellular imaging (Da Carro et al., 2018). However, only a few stabilizing agents and coatings, such as PVP- and citrate-capped, were investigated so far in the photothermal stimulation field (Da Carro et al., 2018). Chapter 4 will refer the use of poly-vinyl alcohol coating as a PBNP-stabilizing agent during neuronal stimulation.

4. Polymers for tissue engineering and nerve regeneration

The use of polymers for tissue engineering and biomaterial production has gained great interest in the last years thanks to their numerous potential applications and their tailorability. Some biomaterials could be fabricated in a 2D structure as monolayers, with the support of non-biological scaffolds; whereas in the last few years great attention has been given to the production of 3D-structure hydrogels, which could mimic the extracellular environment and could provide trophic and structural support. 3D-hydrogels designed with self-assembled peptides (SAP), a bioabsorbable biomaterial, had the ability to generate mature human neurons from human neural stem cells (hNSCs) and showed a functional neuroregenerative potential in rat spinal cord injuries (Marchini et al., 2019). Biodegradable polymeric materials can cross the blood brain barrier and are used as drug delivery systems (Amani et al., 2019), whereas conductive polymers such as poly-pyrrole

(Ppy), poly-aniline and poly(3,4-ethylene dioxythiophene) (P3HT) can be used to enhance neural adhesion and differentiation (Arzaghi et al., 2020), as well as poly-lysine (PLL).

4.1. Poly-pyrrole and poly-lysine

Films composed by PBNPs and N-substituted poly-pyrroles could be suitable for optical determination of pH in the range of 5-9 and result to be stable, thin, optically transparent, reproducible, and non-expensive (Koncki, 1998). Poly-l-lysine-coated iron nanoparticles showed biocompatibility, high saturation magnetization and, thanks to the PLL coating, were able to label mammalian cells, and further investigations on the capability of these coated NPs to facilitate the regeneration of peripheral nerves after injury are currently ongoing (Riggio et al., 2012). PLL-coated PBNPs can label human mesenchymal stem cells and can be used as biocompatible and efficient photoacoustic agents, through the propagation of ultrasounds, by dissipating heat from pulsing light, improving the stem cell therapy field for real-time imaging (Kim et al., 2017).

Other different polymers which could interact with nanoparticles to enhance neuronal recovery or outgrowth are Chitosan, Polydimethylsiloxane (PDMS) and poly-vinyl alcohol (PVA), that have been largely investigated and have well-known properties and, for these reasons, they are currently used in tissue bioengineering.

4.2. Chitosan

Chitosan is a linear co-polymer of β(1-4)-linked D-glucosamine and has a biocompatible and biodegradable structure (Fig. 19), exhibiting several biomedical properties. At acidic pH it becomes aqueous, whereas at alkaline pH it forms an easily manipulated gel that can be used as a matrix. Its nature gives cell affinity and pro-regenerative properties, and it allows to form mixed polymers with other molecules such as collagen (Taravel et al., 1995) or PLL and gelatin, which could promote neurite elongation in DRG neurons and

proliferation in astrocytes and olfactory ensheathing cells (Martín-López et al., 2010). Biosensors based on chitosan and PBNPs were developed to detect glucose, galactose and glutamate in human blood serum and fermented solutions and exhibit excellent performances, without any interference with ascorbic acid or uric acid thanks to the selective permeability of chitosan and electro-catalysis properties of nanoparticles (Wang et al., 2003). Another type of glucose sensor was developed through electrodeposition of PBNPs and chitosan directly on gold electrodes as mediators for hydrogen peroxide detection; in this system, PBNPs have a good stability in alkaline and neutral medium thanks to the hybridization with chitosan. This biosensor could act as redox mediator and could be used for the detection of blood sugar in real samples (Wang et al., 2009). Thus, chitosan films are suitable as a surface for mammalian cell growth, as their tensile properties, surface roughness and free energy give them reproducible physical and chemical properties, for example to optimize cell spreading and fibroblast growth (Ghanem et al., 2005). As efficient attachment and proliferation results in rapid and quick wound repair, these types of films became promising for their potential use as biomedical surfaces (Katalinich, 2001).

Blended hydrogel of chitosan and poly-vinyl alcohol (PVA) with high percentages of water content showed an excellent cell attachment and cell growth rate by increasing the chitosan component; this property is the result of the electrostatic interactions between the cells and the amino groups of chitosan (Koyano et al., 1997).

In summary, chitosan represents a biocompatible and tailorable material which can be used in several biomedical fields for different purposes.
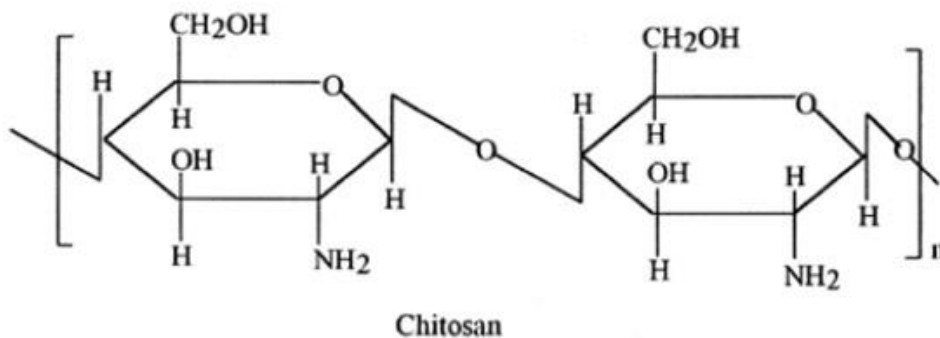
Figure 19. Chemical structure of Chitosan (Ranjha et al., 2016).

4.3. Polydimethylsiloxane

Polydimethylsiloxane (PDMS) or Dimethicone is an organosilicon polymer which belongs to the siloxane family (Fig. 20 and Fig. 21). In the non-crosslinking form, it can be liquid or semi-solid and has a high level of flexibility and viscoelasticity. These properties allow the use of PDMS for several applications: as film/membrane for microfluidic platforms, as surfactant, as cosmetic ingredient, as adhesive, in rubber molds and biomedical devices (Kuo, 1999). In particular, microfluidics, which studies the behavior of lesser amounts of liquid within microchannels or chambers, is a powerful tool in medical and biological research due to the possibility to modify biological samples in small chambers. In microfluidic systems, the microenvironment can be controlled by using chips that release fluids containing molecules in a time-controlled manner. Several microfluidic culture chambers are based on PDMS, that thanks to the low cost, fast way of fabrication, biocompatibility and optical transparency allows droplet generation, drug therapies, cell staining, screening and *in situ* observation (Torino et al., 2018). This material has high permeability to gases, hydrophobic and physiological inertness, resistance to UV radiation, and has a very good dielectric strength (Kuo, 1999). Moreover, it has an excellent thermal stability, as its thermal degradation in inert atmosphere and under vacuum leads to depolymerization over the range of 450-600°C (Camino et al., 2000). Thermal degradation occurs through two competitive mechanisms: a molecular mechanism, which takes place

with the formation of cyclic oligomers, and a radical mechanism, that occurs through homolytic Si-CH$_3$ bonds scissions, leading to methane. In this case, thermal stability can be reached through the formation of ceramic silicon-oxycarbide (Camino et al., 2001).
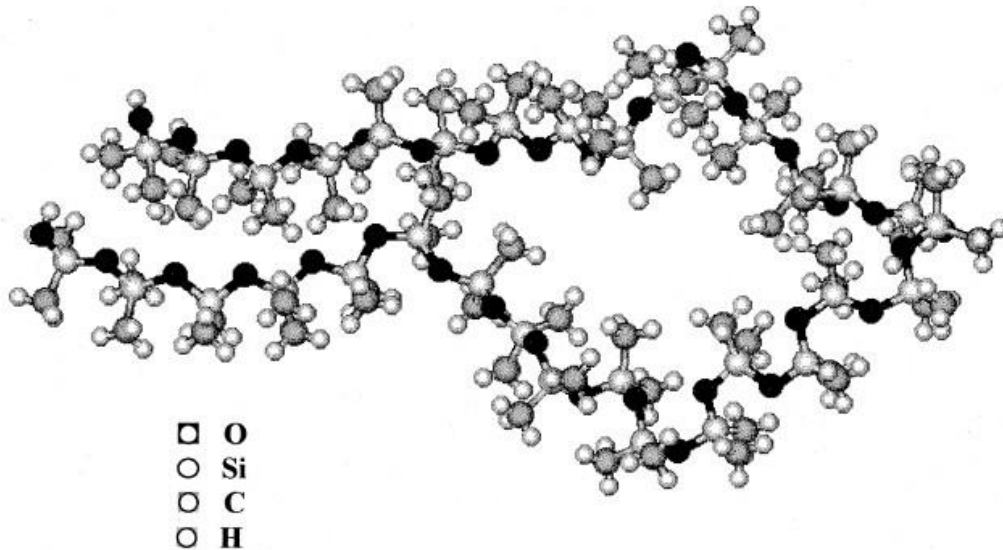
Figure 20. PDMS 3D structure (Camino et al., 2000).
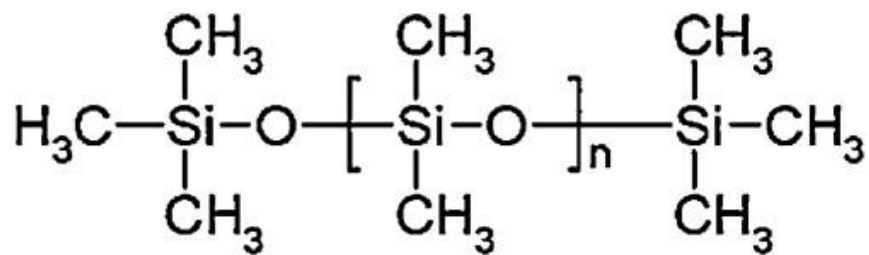
Figure 21. Chemical structure of PDMS (Seethapathy et al., 2012).

4.4. Poly-vinyl Alcohol

Poly-vinyl Alcohol (PVA) is a semi-cristalline synthetic polymer with a backbone composed of carbon atoms (Fig. 22), prepared by the hydrolysis of polyvinyl acetate, and classified into two groups: fully and partially hydrolized. By modifying the length of vinyl acetate and the hydrolysis conditions, PVA can have different molecular weights, adhesiveness and flexibility (DeMerlis et al., 2003). It has several specific properties such as high hydrophilicity, easiness to form films, process ability, biocompatibility, gel forming, chemical resistance (Ranjha et al., 2013) and it is currently used in the production of glues, clothes, pharmaceuticals and biomaterials (Hernández et al., 2004), for subcutaneous delivery of drugs and for growth factor delivery. It has a biocompatible structure that can absorb molecules and substances without any toxic effect and represents a versatile and flexible tool which can be blended with numerous other polymers or molecules, such as chitosan, alginate, starch, gelatin, polyethylene and so on.
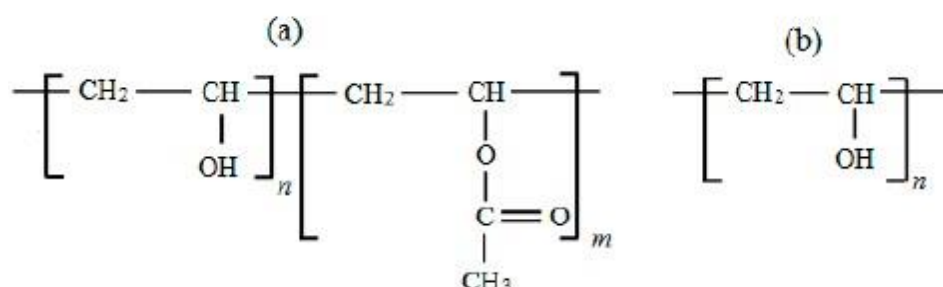
Figure 22. Chemical structure of partially hydrolized (a) and fully hydrolized (b) PVA (Gaaz et al., 2015).

For example, it can be blended with hallosyte nanotubes, which have good mechanical properties and thermal stability and can be utilized for cartilage replacement or transplantation, and for soft biomaterial implants in general (Gaaz et al., 2015). PVA

blended with chitosan results in hydrogels useful in several applications like contact lenses, wound dressing, biomedical prostheses, electrodes and coatings. These hydrogels can be classified based on the type of crosslinking they are subjected to, that can be chemical or physical. Chemically crosslinked hydrogels are permanent and involve interactions between different functional groups and crosslinkers, generating different types of bonds. Physically crosslinked hydrogels include ionic interactions, stereo complex formations and crystallization methods. Within these two macro categories, crosslinking can be obtained by casting/solvent evaporation method, UV irradiation, electrospinning technique and by using crosslinking agents, such as glutaraldehyde, through freeze/thaw cycles (Ranjha et al., 2013). The last one has the advantage to induce crosslinking without the introduction of chemical agents within the hydrogel, which could be toxic or evoke inflammatory response in the body, and the properties of the hydrogel can be controlled by regulating the number of freeze-thaw cycles, the temperature and the thawing rate. A complete cell adhesion and engineered endothelial layer can be obtained through the addition of adhesion promoting polymers, making PVA-blended hydrogels promising candidates for tissue engineering fields (Liu et al., 2009). Moreover, it has been seen that aqueous solutions of PVA can gradually form gels at room temperature with a visible increment in elasticity, due to the formation of network of PVA crystals. Thus, a good method to induce PVA physical crosslinking is the "freezing-and-melting" cycle, in which the solution is firstly frozen, then is gradually melted increasing the temperature above 0°C and the cycle is repeated. Therefore, the hydrogel passes through water phases with a low concentration of PVA, amorphous phases in which PVA is linked with water, and crystal phases which restrain the mobility of chains (Yokoyama et al., 1986). Overall, PVA results a very versatile and promising polymer for tissue engineering, cell outgrowth and adhesion and is currently used in several biomedical fields.

REFERENCES

Abe N., Cavalli V. (2008). Nerve injury signaling. Curr Opin Neurobiol, Jun;18(3):276-83. Doi: 10.1016/j.conb.2008.06.005

Abemayor E., Sidell N. (1989). Human neuroblastoma cell lines as models for the in vitro study of neoplastic and neuronal cell differentiation. *Environ Health Perspect.*, 80:3-15. Doi:10.1289/ehp.89803

Al-Majed A.A., Brushart T.M., Gordon T. (2000). Electrical stimulation accelerates and increases expression of BDNF and trkB mRNA in regenerating rat femoral motoneurons. Eur J Neurosci., Dec;12(12):4381-90. PMID: 11122348

Amani H., Kazerooni H., Hassanpoor H., Akbarzadeh A., Pazoki-Toroudi H. (2019). Tailoring synthetic polymeric biomaterials towards nerve tissue engineering: a review, Artificial Cells, Nanomedicine, and Biotechnology, 47:1, 3524-3539, Doi:10.1080/21691401.2019.1639723

Arslantunali D., Dursun T., Yucel D., Hasirci N., Hasirci V. (2014). Peripheral nerve conduits: technology update. Med Devices (Auckl)., Dec 1;7:405-24. Doi: 10.2147/MDER.S59124

Arzaghi H., Adel B., Jafari H., Askarian-Amiri S., Shiralizadeh Dezfuli A., Akbarzadeh A., Pazoki-Toroudi H. (2020). Nanomaterial integration into the scaffolding materials for nerve tissue engineering: a review. Rev Neurosci., Aug 10:/j/revneuro.ahead-of-print/revneuro-2020-0008/revneuro-2020-0008.xml. Doi: 10.1515/revneuro-2020-0008

Balint R., Cassidy N.J., Cartmell S.H. (2014). Conductive polymers: towards a smart biomaterial for tissue engineering. Acta Biomater., Jun;10(6):2341-53. Doi: 10.1016/j.actbio.2014.02.015

Bernal L, Sotelo-Hitschfeld P, König C, Sinica V, Wyatt A, Winter Z, Hein A, Touska F, Reinhardt S, Tragl A, Kusuda R, Wartenberg P, Sclaroff A, Pfeifer JD, Ectors F, Dahl A, Freichel M, Vlachova V, Brauchi S, Roza C, Boehm U, Clapham DE, Lennerz JK, Zimmermann K. Odontoblast TRPC5 channels signal cold pain in teeth. Sci Adv. 2021 Mar 26;7(13):eabf5567. doi: 10.1126/sciadv.abf5567

Bettinger C.J., Bruggeman J.P., Misra A., Borenstein J.T., Langer R. (2009). Biocompatibility of biodegradable semiconducting melanin films for nerve tissue engineering, Biomaterials, Volume 30, Issue 17, Pages 3050-3057, Doi: https://doi.org/10.1016/j.biomaterials.2009.02.018

Borzenkov M., D'Alfonso L., Polissi A., Sperandeo P., Collini M., Dacarro G., Taglietti A., Chirico G., Pallavicini P. (2019). Novel photo-thermally active polyvinyl alcohol-Prussian blue nanoparticles hydrogel films capable of eradicating bacteria and mitigating biofilms. Nanotechnology, Jul 19;30(29):295702. Doi: 10.1088/1361-6528/ab15f9

Brown W.G.A., Needham K., Begeng J.M., Thompson A.C., Nayagam B.A., Kameneva T., Stoddart P.R. (2020). Thermal damage threshold of neurons during infrared stimulation. Biomed Opt Express. Mar 27;11(4):2224-2234. Doi: 10.1364/BOE.383165

Brushart T.M., Tarlov E.C., Mesulam M.M. (1983). Specificity of muscle reinnervation after epineurial and individual fascicular suture of the rat sciatic nerve. The Journal of Hand Surgery, Volume 8, Issue 3, Pages 248-253. Doi: https://doi.org/10.1016/S0363-5023(83)80152-X

Bryan D.J., Tang J.B., Doherty S.A., Hile D.D., Trantolo D.J., Wise D.L., Summerhayes I.C. (2004). Enhanced peripheral nerve regeneration through a poled bioresorbable poly(lactic-co-glycolic acid) guidance channel. J Neural Eng., Jun;1(2):91-8. Doi: 10.1088/1741-2560/1/2/004

Burnett M.G., Zager E.L. (2004). Pathophysiology of peripheral nerve injury: a brief review. Neurosurg Focus., May 15;16(5):E1. Doi: 10.3171/foc.2004.16.5.2

Camino G., Lomakin S.M., Lazzari M. (2001). Polydimethylsiloxane thermal degradation Part 1. Kinetic aspects, Polymer, Volume 42, Issue 6, Pages 2395-2402, Doi: https://doi.org/10.1016/S0032-3861(00)00652-2

Camino G., S.M Lomakin S.M., M Lageard M. (2002). Thermal polydimethylsiloxane degradation. Part 2. The degradation mechanisms, Polymer, Volume 43, Issue 7, Pages 2011-2015. Doi: https://doi.org/10.1016/S0032-3861(01)00785-6

Campbell W.W. (2008). Evaluation and management of peripheral nerve injury, Clinical Neurophysiology, Volume 119, Issue 9, Pages 1951-1965. Doi: https://doi.org/10.1016/j.clinph.2008.03.018

Carvalho-de-Souza J.L., Treger J.S., Dang B., Kent S.B., Pepperberg D.R., Bezanilla F. (2015). Photosensitivity of neurons enabled by cell-targeted gold nanoparticles. Neuron, Apr 8;86(1):207-17. Doi: 10.1016/j.neuron.2015.02.033

Castillo K., Diaz-Franulic I., Canan J., Gonzalez-Nilo F., Latorre R. (2018). Thermally activated TRP channels: molecular sensors for temperature detection. IOP Publishing, Physical Biology, Gen(18), Issue 2, Vol 15, 1478-3975. doi:10.1088/1478-3975/aa9a6f

Clapham DE, Runnels LW, Strübing C. The TRP ion channel family. Nat Rev Neurosci. 2001 Jun;2(6):387-96. doi: 10.1038/35077544. PMID: 11389472.

Climent J.M., Mondejar-Gomez F., Rodriguez-Ruiz C., DiazLlopis I., Gomez-Gallego D., Martin-Medina P. (2013). Treatment of Morton neuroma with botulinum toxin A: a pilot study. Clin Drug Investig., 33:497-503. Doi: 10.1007/s40261-013-0090-0

Dacarro G., Grisoli P., Borzenkov M., Milanese C., Fratini E., Ferraro G., Taglietti A., Pallavicini P. (2017). Self-assembled monolayers of Prussian blue nanoparticles with photothermal effect. Supramolecular Chemistry, 823-833, Vol 29, Issue 11, Taylor & Francis. Doi: 10.1080/10610278.2017.1372582

Dacarro G., Taglietti A., Pallavicini P. (2018). Prussian Blue Nanoparticles as a Versatile Photothermal Tool. Molecules, Jun 11;23(6):1414. Doi: 10.3390/molecules23061414

Dahl E., Cohen S.P. (2008). Perineural injection of etanercept as a treatment for postamputation pain. Clin J Pain., 24:172-175. Doi: 10.1097/AJP.0b013e31815b32c8

De Ruiter G.C., Malessy M.J., Yaszemski M.J., Windebank A.J., Spinner R.J. (2009). Designing ideal conduits for peripheral nerve repair. Neurosurg Focus., Feb;26(2):E5. Doi: 10.3171/FOC.2009.26.2.E5

DeMerlis C.C., Schoneker D.R. (2003). Review of the oral toxicity of polyvinyl alcohol (PVA). Food Chem Toxicol., Mar;41(3):319-26. Doi: 10.1016/s0278-6915(02)00258-2

Devor M (1999). Unexplained peculiarities of the dorsal root ganglion. Pain, Aug;Suppl 6:S27-S35. Doi: 10.1016/S0304-3959(99)00135-9

Dewey W.C., Westra A., Miller H.H., Nagasawa H. (1971). Heat induced lethality and chromosomal damage in synchronized Chinese hamster cells treated with 5-bromodeoxyuridine. Int J Radiat Biol, 20:505–520. Doi: https://doi.org/10.1080/09553007114551421

Dubuisson A., Kline D.G. (1992). Indications for Peripheral Nerve and Brachial Plexus Surgery, Neurologic Clinics, Volume 10, Issue 4, Pages 935-951. Doi: https://doi.org/10.1016/S0733-8619(18)30189-0

Dugué G.P., Akemann W., Knöpfel T. (2012). A comprehensive concept of optogenetics. Prog Brain Res., 196:1-28. Doi: 10.1016/B978-0-444-59426-6.00001-X

Duke A.R., Cayce J.M., Malphrus J.D., Konrad P., Mahadevan-Jansen A., Jansen E.D. (2009). Combined optical and electrical stimulation of neural tissue in vivo. J Biomed Opt., Nov-Dec;14(6):060501. Doi: 10.1117/1.3257230

Edshage S. (1964). Peripheral nerve suture, A technique for improved intraneural topography, Evaluation of some suture materials. Acta Chir Scand Suppl., 15:Suppl 331:1+. OMID: 14131762

Edsjö A., Holmquist L., Påhlman S. (2007). Neuroblastoma as an experimental model for neuronal differentiation and hypoxia-induced tumor cell dedifferentiation. Semin Cancer Biol., Jun;17(3):248-56. Doi: 10.1016/j.semcancer.2006.04.005

Evans G.R. (2001). Peripheral nerve injury: a review and approach to tissue engineered constructs. Anat Rec., Aug 1;263(4):396-404. Doi: 10.1002/ar.1120

Fenno L., Yizhar O., Deisseroth K. (2011). The development and application of optogenetics. Annu Rev Neurosci., 34:389-412. Doi: 10.1146/annurev-neuro-061010-113817

Francel P.C., Harris K., Smith M., Fishman M.C., Dawson G., Miller R.J. (1987). Neurochemical characteristics of a novel dorsal root ganglion X neuroblastoma hybrid cell line, F-11. J. Neurochem., 48 (5) pp. 1624-1631. Doi: 10.1111/j.1471-4159.1987.tb05711.x

Fricker M,, Tolkovsky A.M., Borutaite V., Coleman M., Brown G.C. (2018). Neuronal Cell Death. Physiol Rev., Apr 1;98(2):813-880. Doi: 10.1152/physrev.00011.2017

Gaaz T.S., Sulong A.B., Akhtar M.N., Kadhum A.A., Mohamad A.B., Al-Amiery A.A. (2015). Properties and Applications of Polyvinyl Alcohol, Halloysite Nanotubes and Their Nanocomposites. Molecules, Dec 19;20(12):22833-47. Doi: 10.3390/molecules201219884

Gaudin R., Knipfer C., Henningsen A., Smeets R., Heiland M., Hadlock T. (2016). Approaches to Peripheral Nerve Repair: Generations of Biomaterial Conduits Yielding to Replacing Autologous Nerve Grafts in Craniomaxillofacial Surgery. Biomed Res Int., 2016:3856262. Doi: 10.1155/2016/3856262

Gautam M., Poudel K., Yong C.S., Kim J.O. (2018). Prussian blue nanoparticles: Synthesis, surface modification, and application in cancer treatment, International Journal of Pharmaceutics, Volume 549, Issues 1–2, Pages 31-49, Doi: https://doi.org/10.1016/j.ijpharm.2018.07.055

Gees, M., Owsianik, G., Nilius, B. and Voets, T. (2012). TRP Channels. In Comprehensive Physiology, R. Terjung (Ed.). https://doi.org/10.1002/cphy.c110026

Geremia N.M., Gordon T., Brushart T.M., Al-Majed A.A., Verge V.M. (2007). Electrical stimulation promotes sensory neuron regeneration and growth-associated gene expression. Exp Neurol., Jun;205(2):347-59. doi: 10.1016/j.expneurol.2007.01.040

Ghanem, A., Katalinich, M. (2005). Characterization of Chitosan Films for Tissue Engineering Applications., Applied Bionics and Biomechanics, 468645, Vol 2. Doi:10.1533/abbi.2004.0004

Ghasemi-Mobarakeh L., Prabhakaran M.P., Morshed M., Nasr-Esfahani M.H., Baharvand H., Kiani S., Al-Deyab S.S., Ramakrishna S. (2011). Application of conductive polymers, scaffolds and electrical stimulation for nerve tissue engineering. J Tissue Eng Regen Med., Apr;5(4):e17-35. doi: 10.1002/term.383

Giacci M.K., Wheeler L., Lovett S., Dishington E., Majda B. et al. (2014). Differential Effects of 670 and 830 nm Red near Infrared Irradiation Therapy: A Comparative Study of Optic Nerve Injury, Retinal Degeneration, Traumatic Brain and Spinal Cord Injury. PLOS ONE 9(8): e104565. Doi: https://doi.org/10.1371/journal.pone.0104565

Guimarda N.K., Gomezb N., Schmidt C.E. (2007). Conducting polymers in biomedical engineering. Progr Polym Sci 32: 876–921. Doi: https://doi.org/10.1016/j.progpolymsci.2007.05.012

Haberberger R.V., Barry C., Matusica D. (2020). Immortalized Dorsal Root Ganglion Neuron Cell Lines. Frontiers in Cellular Neuroscience, Vol 14, 184. Doi: 10.3389/fncel.2020.00184

Hall S.M. (1999). The biology of chronically denervated Schwann cells. Ann N Y Acad Sci., Sep 14;883:215-33. PMID: 10586247

Hayashi S., Yonekura S. (2019). Thermal stimulation at 39°C facilitates the fusion and elongation of C2C12 myoblasts. Anim Sci J., Aug;90(8):1008-1017. Doi: 10.1111/asj.13227

Heidland A., Fazeli G., Klassen A., Sebekova K., Hennemann H., Bahner U., Di Iorio B. (2013). Neuromuscular electrostimulation techniques: historical aspects and current possibilities in treatment of pain and muscle waisting. Clin Nephrol., Jan;79 Suppl 1:S12-23. PMID: 23249528

Henderson T.A., Morries L.D. (2015). Near-infrared photonic energy penetration: can infrared phototherapy effectively reach the human brain?. *Neuropsychiatr Dis Treat.*, 11:2191-2208. Published 2015 Aug 21. Doi:10.2147/NDT.S78182

Hernández R., Sarafian A., López D., Mijangos C. (2004). Viscoelastic properties of poly(vinyl alcohol) hydrogels and ferrogels obtained through freezing–thawing cycles, Polymer, Volume 45, Issue 16, Pages 5543-5549. Doi: https://doi.org/10.1016/j.polymer.2004.05.061

Hess J.R., Brenner M.J., Fox I.K., Nichols C.M., Myckatyn T.M., Hunter D.A., Rickman S.R., Mackinnon S.E. (2007). Use of cold-preserved allografts seeded with autologous Schwann cells in the treatment of a long-gap peripheral nerve injury. Plast Reconstr Surg., Jan;119(1):246-259. Doi: 10.1097/01.prs.0000245341.71666.97

Hoffman H.A., Chakrabarti L., Dumont M.F., Sandler A.D., Fernandes R. (2014). Prussian blue nanoparticles for laser-induced photothermal therapy of tumors. 29729-29734, RSC Advances, Vol 4, Issue 56,. The Royal Society of Chemistry. Doi: 10.1039/C4RA05209A

Hossain M.E., Matsuzaki K., Katakura M., et al. (2017). Direct exposure to mild heat promotes proliferation and neuronal differentiation of neural stem/progenitor cells in vitro. *PLoS One*, 12(12):e0190356. Published 2017 Dec 29. Doi:10.1371/journal.pone.0190356

Houdek M.T., Shin A.Y. (2015) Management and complications of traumatic peripheral nerve injuries. Hand Clin., May;31(2):151-63. Doi: 10.1016/j.hcl.2015.01.007

Huang J., Zhang X., McNaughton P.A. (2006). Modulation of temperature-sensitive TRP channels. Semin Cell Dev Biol., Dec;17(6):638-45. Doi: 10.1016/j.semcdb.2006.11.002

Huang L., Hu J., Lang L., et al. (2007); Synthesis and characterization of electroactive and biodegradable ABA block copolymer of polylactide and aniline pentamer. Biomaterials 28: 1741–1751. Doi: https://doi.org/10.1016/j.biomaterials.2006.12.007

Hussain G., Wang J., Rasul A., Anwar H., Qasim M., Zafar S., Aziz N., Razzaq A., Hussain R., de Aguilar J.L.G., Sun T. (2020). Current Status of Therapeutic Approaches against Peripheral Nerve Injuries: A Detailed Story from Injury to Recovery. Int J Biol Sci, 16(1):116-134. Doi:10.7150/ijbs.35653

Ichihara S., Inada Y., Nakamura T. (2008). Artificial nerve tubes and their application for repair of peripheral nerve injury: an update of current concepts. Injury, Oct;39 Suppl 4:29-39. Doi: 10.1016/j.injury.2008.08.029

Itoh H., Oyama K., Suzuki M., Ishiwata S. (2014). Microscopic heat pulse-induced calcium dynamics in single WI-38 fibroblasts, BIOPHYSICS, Volume 10, Pages 109-119, Released December 17, 2014. Doi: https://doi.org/10.2142/biophysics.10.109

Jenkins M.W., Duke A.R., Gu S., Chiel H.J., Fujioka H., Watanabe M., Jansen E.D., Rollins A.M. (2010). Optical pacing of the embryonic heart. Nat Photonics., Aug 15;4:623-626. Doi: 10.1038/nphoton.2010.166

Jenkins P.A., Carroll J.D. (2011). How to report low-level laser therapy (LLLT)/photomedicine dose and beam parameters in clinical and laboratory studies. Photomed Laser Surg., 29(12):785–787. Doi: 10.1089/pho.2011.9895

Jing L., Shao S., Wang Y., Yang Y., Yue X., Dai Z. (2016). Hyaluronic Acid Modified Hollow Prussian Blue Nanoparticles Loading 10-hydroxycamptothecin for Targeting Thermochemotherapy of Cancer. Theranostics, 6(1):40-53. Doi:10.7150/thno.13250

Johansson A., Widenkvist E., Lu J., Boman M., Jansson U. (2005). Fabrication of High-Aspect-Ratio Prussian Blue Nanotubes Using a Porous Alumina Template. Nano Letters, 1603-1606, vol 5, issue 8, American Chemical Society, 1530-6984. Doi: 10.1021/nl050964u

Johnson M.I., Bjordal J.M. (2011). Transcutaneous electrical nerve stimulation for the management of painful conditions: focus on neuropathic pain. Expert Rev Neurother., May;11(5):735-53. Doi: 10.1586/ern.11.48

Kamalesh S., Tan P., Wang J., et al. (2000). Biocompatibility of electroactive polymers in tissues. J Biomed Mater Res 52: 467–478. Doi: https://doi.org/10.1002/1097-4636(20001205)52:3<467::AID-JBM4>3.0.CO;2-6

Kandel E., Schwartz J and Jessel T.M. (1991). Principles of neural science. Appleton & Lange, pp. 329-366; 385-398

Kandel E., Schwartz J and Jessel T.M. (2013). Principles of neural science. Appleton & Lange, pp. 23; 441

Katalinich M. (2001). "Characterization of Chitosan Films for Cell Culture Applications". *Electronic Theses and Dissertations.* 245. https://digitalcommons.library.umaine.edu/etd/245

Kauer J.A., Gibson H.E. (2009). Hot flash: TRPV channels in the brain, Trends in Neurosciences, Volume 32, Issue 4, Pages 215-224. Doi: https://doi.org/10.1016/j.tins.2008.12.006

Kaur G., Dufour J.M. (2012). Cell lines: Valuable tools or useless artifacts. Spermatogenesis, Jan 1;2(1):1-5. Doi: 10.4161/spmg.19885

Kew J.N.C. and Davies C.H (2010). Ion channels: from structure to function. Oxford University Press, pp. 10-12; 22-155

Kim J., Hwang T., Aguilar L. *et al.* (2016). A Controlled Design of Aligned and Random Nanofibers for 3D Bi-functionalized Nerve Conduits Fabricated via a Novel Electrospinning Set-up. *Sci Rep* 6, 23761. Doi: https://doi.org/10.1038/srep23761

Kim S., Ghil S.H., Kim S.S., Myeong H.H., Lee Y.D., Suh-Kim H. (2002). Overexpression of neurogenin1 induces neurite outgrowth in F11 neuroblastoma cells. Exp Mol Med., Dec 31;34(6):469-75. Doi: 10.1038/emm.2002.65

Kim T., Lemaster J.E., Chen F., Li J., Jokerst J.V. (2017). Photoacoustic Imaging of Human Mesenchymal Stem Cells Labeled with Prussian Blue–Poly(l-lysine) Nanocomplexes ACS Nano, 9022-9032, Vol 11, Issue 9, American Chemical Society. Doi: 10.1021/acsnano.7b03519

Kirchner C., Liedl T., Kudera S., Pellegrino T., Muñoz J.A., Gaub H.E., Stölzle S., Fertig N.P., Wolfgang J. (2005). Cytotoxicity of Colloidal CdSe and CdSe/ZnS Nanoparticles. Nano Letters, 331-338, Vol 5, Issue 2. American Chemical Society. Doi: 10.1021/nl047996m

Kitamura N., Nagami E., Matsushita Y., Kayano T., Shibuya I. (2018). Constitutive activity of transient receptor potential vanilloid type 1 triggers spontaneous firing in nerve growth factor-treated dorsal root ganglion neurons of rats, IBRO Reports, Volume 5, Pages 33-42, Doi: https://doi.org/10.1016/j.ibror.2018.08.002

Kline D.G. (2008). 3 - Clinical and electrical evaluation, Editor(s): Daniel H. Kim, Rajiv Midha, Judith A. Murovic, Robert J. Spinner, Kline and Hudson's Nerve Injuries (Second Edition), W.B. Saunders, Pages 43-63. Doi: https://doi.org/10.1016/B978-0-7216-9537-2.50011-6

Koncki R., Lenarczuk T., Radomska A., Głąb S. (2001). Optical biosensors based on Prussian Blue films. 1080-1085, Analyst, vol 126, issue 7, The Royal Society of Chemistry. Doi: 10.1039/B103044M

Koncki R., Wolfbeis O.S. (1998). Composite Films of Prussian Blue and N-Substituted Polypyrroles: Fabrication and Application to Optical Determination of pH Analytical Chemistry, 2544-2550, Vol 70, Issue 13. American Chemical Society. Doi: 10.1021/ac9712714

Koo J., MacEwan M.R., Kang SK. et al. (2018). Wireless bioresorbable electronic system enables sustained nonpharmacological neuroregenerative therapy. Nat Med 24, 1830–1836. Doi: https://doi.org/10.1038/s41591-018-0196-2

Koyano T., Minoura N., Nagura M., Kobayashi K.I. (1998). Attachment and growth of cultured fibroblast cells on PVA/chitosan-blended hydrogels. J. Biomed. Mater. Res., 39: 486-490. Doi: https://doi.org/10.1002/(SICI)1097-4636(19980305)39:3<486::AID-JBM20>3.0.CO;2-7

Kramer R.H., Fortin D.L., Trauner D. (2009) New photochemical tools for controlling neuronal activity. Curr Opin Neurobiol., Oct;19(5):544-52. Doi: 10.1016/j.conb.2009.09.004

Kryger G.S., Kryger Z., Zhang F., Shelton D.L., Lineaweaver W.C., Buncke H.J. (2001). Nerve growth factor inhibition prevents traumatic neuroma formation in the rat. J Hand Surg Am., 26:635-644. Doi: https://doi.org/10.1053/jhsu.2001.26035

Kudo T-a., Kanetaka H., Mochizuki K., Tominami K., Nunome S., Abe G., et al. (2015). Induction of Neurite Outgrowth in PC12 Cells Treated with Temperature-Controlled Repeated Thermal Stimulation. PLoS ONE 10(4): e0124024. Doi: https://doi.org/10.1371/journal.pone.0124024

Kuo A. C. M. (1999). Poly(dimethylsiloxane). In Polymer Data Handbook; Mark, J. E., Ed.; Oxford University Press: Oxford, p 421

Lee S.K., Wolfe S.W. (2000). Peripheral nerve injury and repair. J Am Acad Orthop Surg., Jul-Aug;8(4):243-52. Doi: 10.5435/00124635-200007000-00005.

Lewinski N., Colvin V., Drezek R. (2008). Cytotoxicity of Nanoparticles. Small, 4: 26-49. Doi: https://doi.org/10.1002/smll.200700595

Lewis P.N. A thermal denaturation study of chromatin and nuclease-produced chromatin fragments. Can J Biochem 1977;55:736–746. Doi: 10.1139/o77-106

Liang, S., Yang, F., Zhou, C. et al. Temperature-dependent Activation of Neurons by Continuous Near-infrared Laser. Cell Biochem Biophys 53, 33 (2009). https://doi.org/10.1007/s12013-008-9035-2

Lisman J. (2015). The Challenge of Understanding the Brain: Where We Stand in 2015, Neuron, Volume 86, Issue 4, 864-882. Doi: 10.1016/j.neuron.2015.03.032

Liu Y., Vrana N.E., Cahill P.A., McGuinness G.B. (2009). Physically crosslinked composite hydrogels of PVA with natural macromolecules: structure, mechanical properties, and endothelial cell compatibility. J Biomed Mater Res B Appl Biomater., Aug;90(2):492-502. Doi: 10.1002/jbm.b.31310

Lundborg G. (1987). Nerve regeneration and repair. A review. Acta Orthop Scand., Apr;58(2):145-69. Doi: 10.3109/17453678709146461

Mackey M.A., Dewey W.C. (1988). Time-temperature analyses of cell killing of synchronous G1 and S phase Chinese hamster cells in vitro. Radiat Res., Feb;113(2):318-33. PMID: 3340736

Mackinnon S.E. (2018). Discussion: State-of-the-Art Techniques in Treating Peripheral Nerve Injury. Plast Reconstr Surg., Mar;141(3):711-712. Doi: 10.1097/PRS.0000000000004264

Mandolesi G., Madeddu F., Bozzi Y., Maffei L., Ratto G.M. (2004). Acute physiological response of mammalian central neurons to axotomy: ionic regulation and electrical activity. FASEB J., Dec;18(15):1934-6. Doi: 10.1096/fj.04-1805fje

Marchini A., Raspa A., Pugliese R., Abd El Malek M., Pastori V., Lecchi M., Vescovi A.L., Gelain F. (2019). Multifunctionalized hydrogels foster hNSC maturation in 3D cultures and neural regeneration in spinal cord injuries. Proceedings of the National Academy of Sciences Apr, 116 (15) 74837492; Doi: 10.1073/pnas.1818392116

Marquardt L.M., Sakiyama-Elbert S.E. (2013). Engineering peripheral nerve repair. Curr Opin Biotechnol., Oct;24(5):887-92. Doi: 10.1016/j.copbio.2013.05.006

Martín-López E., Alonso F.R., Nieto-Díaz M., Nieto-Sampedro M. (2012). Chitosan, gelatin and poly(L-lysine) polyelectrolyte-based scaffolds and films for neural tissue engineering. J Biomater Sci Polym Ed., 23(1-4):207-32. Doi: 10.1163/092050610X546426

Martins R.S., Bastos D., Siqueira M.G., Heise C.O., Teixeira M.J. (2013). Traumatic injuries of peripheral nerves: a review with emphasis on surgical indication. Arq Neuropsiquiatr., Oct;71(10):811-4. Doi: 10.1590/0004-282X20130127

Millesi H., Schmidhammer R. (2007). How to improve the results of peripheral nerve surgery. Springer-Verlag/Wien, pagg. 37-38

Mobbs R.J., Nair S., Blum P. (2007). Peripheral nerve stimulation for the treatment of chronic pain, Journal of Clinical Neuroscience, Volume 14, Issue 3, Pages 216-221, Doi: https://doi.org/10.1016/j.jocn.2005.11.007

Mogoşanu G.D., Grumezescu A.M. (2014). Natural and synthetic polymers for wounds and burns dressing, International Journal of Pharmaceutics, Volume 463, Issue 2, Pages 127-136, Doi: https://doi.org/10.1016/j.ijpharm.2013.12.015

Moore J.G., Lochner E.J., Ramsey C.D., Naresh S., Stiegman, A.E. (2003). Transparent, Superparamagnetic K^I_x Co^{II}_y [Fe^{III}(CN)6]–Silica Nanocomposites with Tunable

Photomagnetism. Angewandte Chemie International Edition, vol 42, issue 24, 1433-7851. Doi: https://doi.org/10.1002/anie.200250409

Morries L.D., Cassano P., Henderson T.A. (2015). Treatments for traumatic brain injury with emphasis on transcranial near-infrared laser phototherapy. Neuropsychiatr Dis Treat., Aug 20;11:2159-75. Doi: 10.2147/NDT.S65809

Muheremu A., Qiang A. (2015). Past, Present, and Future of Nerve Conduits in the Treatment of Peripheral Nerve Injury, 237507, 2314-6133. Doi: https://doi.org/10.1155/2015/237507

Mukherjee S., Rao B.R., Sreedhar B., Paik P., Patra C.R. (2015). Copper Prussian blue analogue: investigation into multifunctional activities for biomedical applications. 7325-7328. Chemical Communications, Vol51, Issue 34. The Royal Society of Chemistry. Doi: 10.1039/C5CC00362H

Murillo J.R., Goto-Silva L., Sánchez A., Nogueira F.C.S., omont G.B., Junqueira M. (2017). Quantitative proteomic analysis identifies proteins and pathways related to neuronal development in differentiated SH-SY5Y neuroblastoma cells. EuPA Open Proteomics, Volume 16, Pages 1-11, ISSN 2212-9685. https://doi.org/10.1016/j.euprot.2017.06.001

Myroshnychenko V., Rodríguez-Fernández J., Pastoriza-Santos I., Funston A.M., Novo C., Mulvaney P., Liz-Marzán L.M., García de Abajo F.J. (2008). Modelling the optical response of gold nanoparticles. 1792-1805. Chemical Society Reviews, vol 37, issue 9, The Royal Society of Chemistry. Doi: 10.1039/B711486A

Navarro X., Geuna S., Grothe C., Haastert-Talini, K. (2018). Introduction: Thematic Papers Issue on Peripheral Nerve Regeneration and Repair. Anat. Rec., 301: 1614-1617. Doi: https://doi.org/10.1002/ar.23941

Navarro X., Vivó M., Valero-Cabré A. (2007). Neural plasticity after peripheral nerve injury and regeneration. Prog Neurobiol., Jul;82(4):163-201. Doi: 10.1016/j.pneurobio.2007.06.005

Panahi-Joo Y., Karkhaneh A., Nourinia A., Abd-Emami B., Negahdari B., Renaud P., Bonakdar S. (2016). Design and fabrication of a nanofibrous polycaprolactone tubular nerve guide for peripheral nerve tissue engineering using a two-pole electrospinning system. Biomed Mater., Apr 12;11(2):025017. Doi: 10.1088/1748-6041/11/2/025017

Pastori V., D'Aloia A., Blasa S., Lecchi M. (2019). Serum-deprived differentiated neuroblastoma F-11 cells express functional dorsal root ganglion neuron properties. PeerJ, Oct 30;7:e7951. Doi: 10.7717/peerj.7951

Patra C.R. (2016). Prussian blue nanoparticles and their analogues for application to cancer theranostics. Nanomedicine, 11:6, 569-572. Doi: 10.2217/nnm.16.16

Paviolo C., Haycock J.W., Cadusch P.J., McArthur S.L., Stoddart P.R. (2014). Laser exposure of gold nanorods can induce intracellular calcium transients. J Biophotonics, Oct;7(10):761-5. Doi: 10.1002/jbio.201300043

Paviolo C., Haycock J.W., Yong J., Yu A., Stoddart P.R., McArthur S.L. (2013). Laser exposure of gold nanorods can increase neuronal cell outgrowth. Biotechnol Bioeng., Aug;110(8):2277-91. Doi: 10.1002/bit.24889

Paviolo C., Thompson A.C., Yong J., Brown W.G., Stoddart P.R. (2014). Nanoparticle-enhanced infrared neural stimulation. J Neural Eng., Dec;11(6):065002. Doi: 10.1088/1741-2560/11/6/065002

Pearce, J. (1994). Studies of any toxicological effects of Prussian blue compounds in mammals—a review. Food Chem. Toxicol. 32, 577–582. Doi: 10.1016/0278-6915(94)90116-3

Platika D., Boulos M.H., Baizer L., Fishman M.C. (1985). Neuronal traits of clonal cell lines derived by fusion of dorsal root ganglia neurons with neuroblastoma cells. Proc Natl Acad Sci U S A., May;82(10):3499-503. Doi: 10.1073/pnas.82.10.3499

Prince M.R., King A.H., Shin A.Y., Bishop A.T., Stuart M.J., Levy B.A. (2015). Peroneal Nerve Injuries: Repair, Grafting, and Nerve Transfers, Operative Techniques in Sports Medicine, Volume 23, Issue 4, Pages 357-361, Doi: https://doi.org/10.1053/j.otsm.2015.06.006

Ranjha N.M., Samiullah K. (2013). "Chitosan/Poly (vinyl alcohol) Based Hydrogels for Biomedical Applications: A Review." *Journal of Pharmacy and Alternative Medicine* 2, 30-41. ISSN 2222-4807

Ransom S.C., Shahrestani S., Lien B.V., et al. (2020). Translational Approaches to Electrical Stimulation for Peripheral Nerve Regeneration. *Neurorehabilitation and Neural Repair.*, 34(11):979-985. Doi:10.1177/1545968320962508

Reyes O., Sosa I., Kuffler D.P. (2005). Promoting neurological recovery following a traumatic peripheral nerve injury. PR Health Sci J., Sep;24(3):215-23. PMID: 16329686

Richter C.P., Matic A.I., Wells J.D., Jansen E.D., Walsh J.T. Jr. (2011). Neural stimulation with optical radiation. Laser Photon Rev., Jan 1;5(1):68-80. Doi: 10.1002/lpor.200900044

Riggio C., Calatayud M.P., Hoskins C., Pinkernelle J., Sanz B., Torres T.E., Ibarra M.R., Wang L., Keilhoff G., Goya G.F., Raffa V., Cuschieri A. (2012). Poly-l-lysine-coated magnetic nanoparticles as intracellular actuators for neural guidance. Int J Nanomedicine., 7:3155-66. Doi: 10.2147/IJN.S28460. Epub 2012 Jun 25

Rizzo M.A. (1997). Successful treatment of painful traumatic mononeuropathy with carbamazepine: insights into a possible molecular pain mechanism. J Neurol Sci., Nov 6;152(1):103-6. Doi: 10.1016/s0022-510x(97)00143-3

Roberts J.E. (2000). Light and Immunomodulation. Annals of the New York Academy of Sciences, 917: 435-445. Doi: https://doi.org/10.1111/j.1749-6632.2000.tb05408.x

Roti Roti J.L. (2008). Cellular responses to hyperthermia (40-46 degrees C): cell killing and molecular events. Int J Hyperthermia. Feb;24(1):3-15. Doi: 10.1080/02656730701769841

Roy X., Hui J.K.H., Rabnawaz M., Liu G., MacLachlan M.J. (2011). Prussian Blue Nanocontainers: Selectively Permeable Hollow Metal–Organic Capsules from Block Ionomer Emulsion-Induced Assembly. Journal of the American Chemical Society 2011 133 (22), 8420-8423. Doi: 10.1021/ja2016075

Ruijtenberg S. & van den Heuvel S. (2016). Coordinating cell proliferation and differentiation: Antagonism between cell cycle regulators and cell type-specific gene expression. Cell Cycle, 15:2, 196-212. Doi: 0.1080/15384101.2015.1120925

Sameem M., Wood T.J., Bain J.R. (2011). A systematic review on the use of fibrin glue for peripheral nerve repair. Plast Reconstr Surg., Jun;127(6):2381-2390. Doi: 10.1097/PRS.0b013e3182131cf5

Sanchvi A.B., Miller K.P.H., Belcher A.M. et al. (2005). Biomaterials functionalization using a novel peptide that selectively binds to a conducting polymer. Nat Mater 4: 496–502. Doi: 10.1038/nmat1397

Sassen W.A., Lehne F., Russo G., Wargenau S., Dübel S., Köster R.W. (2017). Embryonic zebrafish primary cell culture for transfection and live cellular and subcellular imaging. Dev Biol., Oct 1;430(1):18-31. Doi: 10.1016/j.ydbio.2017.07.014

Shapiro M., Homma K., Villarreal S. *et al.* (2012). Infrared light excites cells by changing their electrical capacitance. *Nat Commun* 3, 736. Doi: https://doi.org/10.1038/ncomms1742

Shokouhimehr M., Soehnlen E.S., Khitrin A., Basu S., Huang S.D. (2010) Biocompatible Prussian blue nanoparticles: Preparation, stability, cytotoxicity, and potential use as an MRI contrast agent, Inorganic Chemistry Communications, Volume 13, Issue 1, Pages 58-61, Doi: https://doi.org/10.1016/j.inoche.2009.10.015

Singh R.K., Sinha V.P., Pal U.S., Yadav S.C., Singh M.K. (2012). Pregabalin in post traumatic neuropathic pain: case studies. Natl J Maxillofac Surg., 3:91-95. Doi: 10.4103/0975-5950.102175

Smith J.W. (1964). Microsurgery of peripheral nerves. Plast Reconstr Surg, Apr;33:317-29. Doi: doi: 10.1097/00006534-196404000-00002

Spitzer N.C., Lautermilch N.J., Smith R.D., Gomez T.M. (2000). Coding of neuronal differentiation by calcium transients. Bioessays, Sep;22(9):811-7. Doi: 10.1002/1521-1878(200009)22:9<811::AID-BIES6>3.0.CO;2-G

Subia B., Kundu J., Kundu S.C. (2010). Biomaterial Scaffold Fabrication Techniques for Potential Tissue Engineering Applications, Tissue Engineering, Daniel Eberli, IntechOpen, Doi: 10.5772/8581

Subramanian A., Krishnan U.M., Sethuraman S. (2009). Development of biomaterial scaffold for nerve tissue engineering: Biomaterial mediated neural regeneration. *J Biomed Sci.*, 16(1):108. Published 2009 Nov 25. Doi:10.1186/1423-0127-16-108

Tamura Y., Kitaoka Y., Matsunaga Y., Hoshino D., Hatta H. (2015). Daily heat stress treatment rescues denervation-activated mitochondrial clearance and atrophy in skeletal muscle. *J Physiol.*, 593(12):2707-2720. Doi:10.1113/JP270093

Tan, CH., McNaughton, P. The TRPM2 ion channel is required for sensitivity to warmth. Nature 536, 460–463 (2016). https://doi.org/10.1038/nature19074

Taravel M.N., Domard A. (1996). Collagen and its interactions with chitosan, III some biological and mechanical properties. Biomaterials., Feb;17(4):451-5. Doi: 10.1016/0142-9612(96)89663-3

Tecoma E.S., Monyer H., Goldberg M.P., Choi D.W. (1989). Traumatic neuronal injury in vitro is attenuated by NMDA antagonists. Neuron., Jun;2(6):1541-5. doi: 10.1016/0896-6273(89)90042-1

Thang D.C., Wang Z., Lu X., Xing B. (2019). Precise cell behaviors manipulation through light-responsive nano-regulators: recent advance and perspective. Theranostics, 9(11):3308-3340. Doi:10.7150/thno.33888

Thomas P.K., Holdorff B. (1993). Neuropathy due to physical agents. In: Dyck PJ, Thomas PK, editors. *Griffin JW editors. Peripheral neuropathy,* 3rd ed. W.B. Saunders; Piladelphia, p 990

Thompson A.C., Stoddart P.R., Jansen E.D. (2014). Optical Stimulation of Neurons. *Curr Mol Imaging,* 3(2):162-177. doi:10.2174/2211555203666141117220611.

Tominaga M., Caterina M.J., Malmberg A.B., Rosen T.A., Gilbert H., Skinner K., Raumann B.E., Basbaum A.I., Julius D. (1998). The cloned capsaicin receptor integrates multiple pain-producing stimuli. Neuron., Sep;21(3):531-43. Doi: 10.1016/s0896-6273(00)80564-4

Torino S.; Corrado B.; Iodice M.; Coppola G. (2018). PDMS-Based Microfluidic Devices for Cell Culture. *Inventions, 3,* 65. Doi: https://doi.org/10.3390/inventions3030065
Vaucher S., Li M., Mann, S. (2000). Synthesis of Prussian Blue Nanoparticles and Nanocrystal Superlattices in Reverse Microemulsions. Angew. Chem. Int. Ed., 39: 1793-1796. Doi: https://doi.org/10.1002/(SICI)1521-3773(20000515)39:10<1793::AID-ANIE1793>3.0.CO;2-Y

Vijayavenkataraman S. (2020). Nerve guide conduits for peripheral nerve injury repair: A review on design, materials and fabrication methods, Acta Biomaterialia, Volume 106, Pages 54-69, Doi: https://doi.org/10.1016/j.actbio.2020.02.003

Walpole C.S.J., Bevan S., Bovermann G., Boelsterli J.J., Breckenridge R., Davies J.W., Hughes G.A., James I., Oberer L., Winter J., Wrigglesworth R. (1994). The Discovery of Capsazepine, the First Competitive Antagonist of the Sensory Neuron Excitants Capsaicin and Resiniferatoxin. Journal of Medicinal Chemistry , 37 (13), 1942-1954. Doi: 10.1021/jm00039a006

Wang L., Meng D., Hao Y., Zhao Y., Li D., Zhang B., Zhang Y., Zhang Z. (2015). Gold nanostars mediated combined photothermal and photodynamic therapy and X-ray imaging for cancer theranostic applications. J Biomater Appl., Nov;30(5):547-57. Doi: 10.1177/0885328215594481

Wang X., Gu H., Yin F., Tu Y. (2009). A glucose biosensor based on Prussian blue/chitosan hybrid film. Biosens Bioelectron., Jan 1;24(5):1527-30. Doi: 10.1016/j.bios.2008.09.025

Wang Y., Zhu J., Zhu R., Zhu Z., Lai Z., Chen Z. (2003). Chitosan/Prussian blue-based biosensors. IOP Publishing, 831-836, Vol 14, Issue 6. Doi: 10.1088/0957-0233/14/6/317

Wells J., Kao C., Konrad P. et al. (2007). Biophysical mechanisms of transient optical stimulation of peripheral nerve. *Biophys J.,* 93(7):2567-2580. doi:10.1529/biophysj.107.104786

Weng W., Zhao B., Lin D., Gao W., Li Z., Yan H. (2016). Significance of alpha smooth muscle actin expression in traumatic painful neuromas: a pilot study in rats. Sci Rep., 6:23828. Doi: https://doi.org/10.1038/srep23828

White JP, Cibelli M, Urban L, Nilius B, McGeown JG, Nagy I. TRPV4: Molecular Conductor of a Diverse Orchestra. Physiol Rev. 2016 Jul;96(3):911-73. doi: 10.1152/physrev.00016.2015. PMID: 27252279.

Wong J.Y., Langer R., Ingber D.E. (1994). Electrically conducting polymers can noninvasively control the shape and growth of mammalian cells. *Proc Natl Acad Sci U S A.*, 91(8):3201-3204. Doi:10.1073/pnas.91.8.3201

Yao C., Zhou X., Zhao B., Sun C., Poonit K., Yan H (2017). Treatments of traumatic neuropathic pain: a systematic review. Oncotarget., Apr 7;8(34):57670-57679. doi: 10.18632/oncotarget.16917

Yokoyama F., Masada I., Shimamura K. *et al.* (1986). Morphology and structure of highly elastic poly(vinyl alcohol) hydrogel prepared by repeated freezing-and-melting. *Colloid & Polymer Sci* 264, 595–601. Doi: https://doi.org/10.1007/BF01412597

Yu W., Zhao W., Zhu C., Zhang X., Ye D., Zhang W., Zhou Y., Jiang X., Zhang Z. (2011). Sciatic nerve regeneration in rats by a promising electrospun collagen/poly(ε-caprolactone) nerve conduit with tailored degradation rate. BMC Neurosci., Jul 15;12:68. Doi: 10.1186/1471-2202-12-68

Yusaf S.P., Goodman J., Pinnock R.D., Dixon A.K., Lee K. (2001). Expression of voltage-gated calcium channel subunits in rat dorsal root ganglion neurons. Neurosci Lett., Sep 28;311(2):137-41. Doi: 10.1016/s0304-3940(01)02038-9

Zhan Q., Qian J., Li X., He S. (2010). A study of mesoporous silica-encapsulated gold nanorods as enhanced light scattering probes for cancer cell imaging. Nanotechnology, Feb 5;21(5):055704. Doi: 10.1088/0957-4484/21/5/055704

Zhang B.G., Quigley A.F., Myers D.E., Wallace G.G., Kapsa R.M., Choong P.F. (2014). Recent advances in nerve tissue engineering. Int J Artif Organs., Apr;37(4):277-91. Doi: 10.5301/ijao.5000317

Zhang Q., Esrafilzadeh D., Crook J. *et al.* (2017). Electrical Stimulation Using Conductive Polymer Polypyrrole Counters Reduced Neurite Outgrowth of Primary Prefrontal Cortical Neurons from NRG1-KO and DISC1-LI Mice. *Sci Rep* 7, 42525. Doi: https://doi.org/10.1038/srep42525

CHAPTER 2: Experimental Design

1.1. Background

The preliminary studies, conducted on different time and temperature combinations to establish the stimulation procedure, showed that the best protocol for morphological differentiation was 41,5°C for 30 minutes, as described in detail in the chapter 4. In order to verify which approach could be the best to increase the medium temperature of F-11 cell cultures as desired, several materials were tested, such as coated glasses, biopolymers and different types of nanoparticles. Firstly, a glass coverslips covered with a monolayer of nanoparticles was used. Further, several biopolymers such as chitosan, poly-lysine, polydimethylsiloxane (PDMS) and poly-vinyl alcohol (PVA) were tested to select the most suitable for the embedding of nanoparticles for the *in vitro* experiments. Initially, they were subjected to a thermal increase to verify their response to heat. Therefore, they were exposed for 30 minutes at 41,5°C, which is the protocol identified with the bulk heating stimulation.

This project was developed in collaboration with the chemistry's group of Prof. Piersandro Pallavicini, who provided us the nanoparticles and the coverslips, and the biophysics group of Prof. Maddalena Collini and Prof. Giuseppe Chirico, who provided the instruments for the irradiation experiments and for the morphological analysis. The protocol of the irradiation experiments will be described in the chapter 4.

1.2. Gold Nanostar and Prussian Blue Nanoparticle slides

In the first preliminary experiments, F-11 cells were seeded on a glass monolayer of gold nanostars (GNSTs) and were stimulated using a near infrared (NIR) laser with a wavelength of 800 nm for 5 minutes; initially the temperature was set at 39°C, according to literature. Pictures were taken for three days after stimulation. After 24 hours, irradiated cells showed longer neurites compared to the control and seemed to be able to differentiate in the standard medium without the presence of chemical agents.

GNST slides were coated with Triton, (3-aminopropyl)triethoxysilane (APTES) or polyethyleneimine (PEI). Some toxic effects on cells were evident during the experiment, however, considering the promising results on differentiation, other types of nanoparticles were tested.

Prussian Blue nanoparticles (PBNPs) were chosen because of their non-cytotoxicity and biocompatibility and glass monolayers of PBNPs coated with citrate were tested. As the coverslips were not sterile, they were exposed to UV light for 2 hours and then washed with 2 ml EtOH 70% and 3 ml PBS. The glass coverslips were placed into the petri dishes and covered with 2 ml of 1% FBS medium, containing antibiotics (penicillin-streptomycin) 1:100, and cells were seeded 1:30 on the monolayer.

The coverslips coated with PBNPs were irradiated with a NIR laser with a power of 230 mW for 2 consecutive days for 10 minutes, and images were taken each day, to find the best protocol for irradiation.

Despite the sterilization protocol and the use of antibiotics, contamination often emerged into the petri dishes. However, cells tended to have longer neurites compared to the control, and for this reason and the biocompatibility of PBNPs, the later experiments were conducted by this type of nanoparticles, using biopolymers within sight of a future use of this method in clinical applications.

1.3. Prussian Blue Nanoparticles and biopolymers

The polymers chosen for the experiments were chitosan, PDMS and PVA, thanks to their specific and unique chemical and physical properties and their flexibility.

First of all, a blended polymer with chitosan, PVA and poly-lysine was tested.

A solution of acetic acid 1% with 0.2g (2%) of chitosan was prepared and stirred, and an aqueous solution of 10 ml H_2O with 0.9g (9%) PVA was prepared and put in an oven. Then, chitosan and PVA solutions were mixed and 90 µl of Poly-lysine were added to the mixture, stirring continuously. After 3 hours in oven, a physical crosslinking was performed to avoid adding of chemical or toxic agents; the films were maintained at -20°C overnight, then exposed for 3 hours at room temperature, for 5 consecutive times.

Three concentrations of chitosan and PVA were prepared:

-75% PVA and 25% chitosan (plus 90 µl of Poly-lysine);

-50% PVA and 50% chitosan (plus 90 µl of Poly-lysine);

-25% PVA and 75% chitosan (plus 90 µl of Poly-lysine).

After 10 days, a stability test through swelling measurements was performed by placing the material in contact with the culture medium and, since chitosan tends to be acid, pH was measured for each film. The swelling rate tended to change during the experiment, increasing within 48 hours. The pH values, measured after 24 hours of incubation within the medium, also increased (Table 1).

	Initial pH	pH after 24 h
25% PVA – 75% Chitosan	4,8	5,4
50% PVA – 50% Chitosan	5,1	5,8
75% PVA – 25% Chitosan	5,3	6,5

Table 1. pH measurement for different film composition.

Another test was performed by preparing a film of poly-lysine in which PBNPs were dissolved. Poly-lysine was treated following the standard protocol. In both cases, the absorbance of PBNPs decreased after 12 hours, and for this reason this method was not considered further.

Since PBNPs could react with the culture medium, containing phenol red, which could alter the absorbance, a coating of PDMS was made to shield nanoparticles from the medium. The PVA solution was prepared with 0.29g of PVA and 400g of PBNPs, and a volume of 2.6 ml of H_2O was added to the mixture. The PDMS was prepared following the standard protocol, with 1g of elastomer and 10% of crosslinking agent.

A coating of 2 ml of poly-lysine was added to allow cell adhesion and cells were seeded following the same previous protocol. Results at 24 hours showed no effects on cell viability, neither swelling nor absorbance decrease, and a differentiation phenotype was seen in the cultures; however, after 48 hours, PDMS tended to aggregate, and the optical quality started to decline.

1.4. Prussian Blue Nanoparticles and PVA

Considering the promising results obtained concerning morphological differentiation, a test with a drop of PVA and PBNPs in the middle of the petri dish was performed to avoid material aggregation and to direct the temperature increase to a localized area of the dish. A temperature calibration was carried out to allow the laser power to locally increase the temperature up to 41,5°C, starting from a temperature of 36,7°C; during the calibration, the volume of 1% FBS medium placed in the petri dish was 2 ml, as during the experiments with the cells. Each test was performed for 6 minutes. The results of the temperature calibration at different laser powers are shown in Table 2.

Laser Power (mW)	Final Temperature (C°)
771	49
598	48
407	46,8
199	42
187	41,8
169	41,6

Table 2. Temperature calibration of medium at different laser power.

With a biocompatible material such as PVA, which protects nanoparticles from the medium, and with an accurate temperature calibration of the material, cells tended to differentiate and to have longer neurites compared to the control.

Although the approach used caused neither cytotoxicity nor nanoparticle contamination of the medium, a test with a PVA-PBNP drop on the outer surface of the petri dish was performed, to verify if the same results could be obtained without a direct contact between the material, the nanoparticles and the cells.

A solution of 3 ml (total volume) containing 7% Poly Vinyl Alcohol and 800 µl of PBNPs was prepared and 70 µl of this solution were placed on the outer surface of the petri dish, forming a blue disc with a diameter corresponding to the laser beam (~ 1 cm^2). A temperature calibration was also made and, in this condition, the best laser power to reach the temperature of 41,5°C on the PVA-PBNP disc with 700 nm wavelength was 260 mW.

Thus, cells were seeded following the previous protocol and preliminary results showed a significant increase in neurite length. Moreover, cells tended to form several networks and connections compared to the control.

Considering these results, the approach represented by a PVA-PBNP disc placed on the outer surface of the petri dish was chosen for the subsequent experiments. PVA was

selected as the most suitable material because it allowed a homogeneous nanoparticle distribution within the disc.

1.5. The cellular model

The cellular model used for these experiments is the F-11 cell line. It is a hybrid derived from mouse neuroblastoma and embryonic rat dorsal root ganglion (DRG) neurons (Platika et al., 1985). These cells have been largely used to study DRG neuron properties, but their gene expression profile is not consistent with any specific DRG subclass and their functional properties as sensory neurons have not been described so far. In standard conditions, these cells are maintained in a 10% FBS (foetal bovine serum) medium, which allows cells proliferation. In our study, they were incubated in serum-deprived (1% FBS) medium for 10-14 days, which induced differentiation, and a functional characterization was performed to verify the eventual presence of similarities with DRG neurons.

Results of this investigation are reported in the following chapter.

CHAPTER 3: Serum-deprived differentiated neuroblastoma F-11 cells express functional dorsal root ganglion neuron properties

Valentina Pastori[1], Alessia D'Aloia[2], Stefania Blasa[2] and Marzia Lecchi[1*]

[1] Department of Biotechnology and Biosciences and Milan Center for Neuroscience, University of Milano-Bicocca, Milan, Italy

[2] Department of Biotechnology and Biosciences, University of Milano-Bicocca, Milan, Italy

*Corresponding author

1. Abstract

The isolation and culture of dorsal root ganglion (DRG) neurons cause adaptive changes in the expression and regulation of ion channels, with consequences on neuronal excitability. Considering that not all neurons survive the isolation and that DRG neurons are heterogeneous, it is difficult to find the cellular subtype of interest. For this reason, researchers opt for DRG-derived immortal cell lines to investigate endogenous properties. The F-11 cell line is a hybridoma of embryonic rat DRG neurons fused with the mouse neuroblastoma line N18TG2. In the proliferative condition, F-11 cells do not display a gene expression profile correspondent with specific subclasses of sensory neurons, but the most significant differences when compared with DRGs are the reduction of voltage-gated sodium, potassium and calcium channels, and the small amounts of TRPV1 transcripts. To investigate if functional properties of mature F-11 cells showed more similarities with those of isolated DRG neurons, we differentiated them by serum deprivation. Potassium and sodium currents significantly increased with differentiation, and biophysical properties of tetrodotoxin (TTX)-sensitive currents were similar to those characterized in small DRG neurons. The analysis of the voltage-dependence of calcium currents demonstrated the lack of low threshold activated components. The exclusive expression of high threshold activated Ca^{2+} currents and of TTX-sensitive Na^+ currents correlated with the generation of a regular tonic electrical activity, which was recorded in the majority of

the cells (80%) and was closely related to the activity of afferent TTX-sensitive A fibers of the proximal urethra and the bladder. Responses to capsaicin and substance P were also recorded in ~20% and ~80% of cells, respectively. The percentage of cells responsive to acetylcholine was consistent with the percentage referred for rat DRG primary neurons and cell electrical activity was modified by activation of non-NMDA receptors as for embryonic DRG neurons. These properties and the algesic profile (responses to pH5 and sensitivity to both ATP and capsaicin), proposed in literature to define a sub-classification of acutely dissociated rat DRG neurons, suggest that differentiated F-11 cells express receptors and ion channels that are also present in sensory neurons.

2. Introduction

The F-11 cell line is a hybrid obtained by fusion of embryonic rat dorsal root ganglion (DRG) and mouse neuroblastoma by Platika et al. (1985). These cells have been widely used in the past years in proliferating conditions to study properties of DRG neurons, but their transcriptomic analysis appeared only 2 years ago by means of Illumina next-generation sequencing, revealing that their gene expression profile did not resemble any specific defined DRG subclass (Yin, Baillie & Vetter, 2016).

F-11 cells could also be differentiated into functional neurons by retinoic acid incubation (Chiesa et al., 1997; Ambrosino et al., 2013), and by their maintenance on biocompatible substrates (neoglucosylated collagen matrices, Russo et al., 2014). Although the acquisition by differentiated F-11 cells of characteristic neuronal electrophysiological properties, such as sodium, potassium and calcium currents, and action potential (AP) firing, have been described, their properties as sensory neurons have not been documented so far.

Here, we show for the first time an exhaustive characterization of the electrophysiological properties of F-11 cells differentiated by serum deprivation. Our aim was to investigate if differentiated F-11 cells manifest similarities with DRG neurons in order to verify whether

they are an adequate model for studying mechanisms involved in the detection and transmission of noxious stimuli.

3. Materials and methods

3.1. Cell cultures

F-11 cells (mouse neuroblastoma N18TG-2 x rat DRG, ECACC Cat#08062601 RRID:CVCL_H605; Platika et al., 1985) were seeded at 60,000 cells/35 mm dish and were maintained without splitting in low serum medium for almost 2 weeks to induce differentiation. The complete composition of the medium was: Dulbecco's modified Eagle's medium (Cat#D6546; Sigma-Aldrich, St. Louis, MO, USA), 2 mM glutamine (Sigma-Aldrich, St. Louis, MO, USA), 1% fetal bovine serum (FBS, Cat# F2442; Sigma-Aldrich, St. Louis, MO, USA). The cells were incubated at 37 °C in a humidified atmosphere with 5% CO_2, receiving fresh medium twice per week. F-11 cells maintained in 10% FBS medium were used as control. Morphological and functional analysis were performed at 10–14 days of differentiation, whereas cells growing in the non-differentiation medium underwent the same analysis at 7 days to avoid dramatic cell death due to confluence.

3.2. Immunofluorescence

F-11 cells were plated at a density of 60,000 cells on coverslips pre-treated with gelatin from porcine skin (Sigma-Aldrich, St. Louis, MO, USA). Cells were then maintained in DMEM medium supplemented with 1% or 10% serum. After 10 and 7 days, respectively, differentiated and undifferentiated cells were fixed for 10 min in 3.7% paraformaldehyde in phosphate-buffer saline (PBS), permeabilized for 4 min with 0.1% Triton X-100 in PBS, and stained with monoclonal anti-NeuN/Fox3 produced in mouse primary antibody (1:150, Cat#MAB-94161; Immunological Sciences, Rome, Italy). Incubation with secondary antibody Cyanine3 goat anti-mouse IgG (H+L) (1:200, Cat#A10521, RRID: AB_2534030; Thermo Fisher, Waltham, MA, USA) was maintained for 45 min. After washout in 1× PBS,

DAPI (Sigma-Aldrich, St. Louis, MO, USA) was added at the final concentration of 1 µg/ml in 1× PBS and incubation was maintained for 10 min at room temperature. After washing, the slides were mounted and photographed using an A1RNikon (Nikon, Tokyo, Japan) laser scanning fluorescence confocal microscope at 40× magnification. A total of 16–20 z-stack images from 10 different fields for each condition were taken. For this analysis three coverslips of cells maintained in 10% serum and three coverslips of cells in 1% serum were prepared. Transmission images were captured with a Leica TCSSP2 confocal microscope equipped with a 100×/PH3 oil immersion objective. The images were acquired from three cultures of cells maintained in 10% serum and from three cultures of cells in 1% serum.

3.3. Functional analysis by the patch-clamp technique

Functional characterization of the electrophysiological properties of F-11 cells was performed by the patch-clamp technique in the whole-cell configuration. For the experiments, culture media were replaced by a standard extracellular solution which contained (mM): NaCl 135, KCl 2, CaCl2 2, $MgCl_2$ 2, hepes 10, glucose 5, pH 7.4. The standard pipette solution contained the following (mM): potassium aspartate 130, NaCl 10, $MgCl_2$ 2, $CaCl_2$ 1.3, EGTA 10, hepes 10, pH 7.3. Recordings were acquired by the pClamp8.2 software (pClamp, RRID:SCR_011323) and the MultiClamp 700A amplifier (Axon Instruments; Molecular Devices, LLC., San Jose, CA, USA). Resting membrane potential (Vrest) and APs were monitored in the current-clamp mode. Cells that did not exhibited spontaneous firing were depolarized with 1 s-long current pulses under conditioning hyperpolarization at −75/−80 mV to verify their capability to generate repetitive spiking. In the voltage-clamp mode, series resistance errors were compensated for a level of up to 85–90%. Sodium (I_{Na}) and potassium (I_K) currents were recorded by applying a standard protocol: starting from a holding potential of −60 mV, cells were conditioned at −90 mV for 500 ms and successively tested by depolarizing potentials in 10 mV-increments, from −80 to +40 mV. Na^+ and K^+ currents were isolated by applying 0.3–1

µM tetrodotoxin (TTX) or 10 mM tetraethylammonium (TEA) in the bath. To determine current densities (I_{Na} and I_K), the maximal inward and outward current intensities were respectively chosen for Na^+ and K^+ currents. Na^+ channel biophysical properties of activation and inactivation were studied by using a pipette solution containing (mM): CsF 105, CsCl 27, NaCl 5, $MgCl_2$ 2, EGTA 10, hepes 10, pH 7.3. The voltage-dependence of activation was determined by the above mentioned protocol, whereas for the inactivation properties the protocol consisted in a conditioning step with amplitude from −105 to 0 mV and duration of 600 ms, followed by a test at −10 mV.

Ether-à-go-go-related gene (ERG) potassium currents (Ierg) were recorded by using an extracellular solution containing a higher K^+ concentration (40 mM), and by imposing a standard protocol which, starting from an holding potential of −60 mV, conditioned the cell membrane for 15 s from −80 to +20 mV (20 mV increments) and successively hyperpolarized at −120 mV to evoke the tail current. Normalized tail currents were interpolated with a Boltzmann function to obtain the activation curve. To study the voltage-dependence of ERG channel inactivation, a stimulation protocol was applied which, starting from a holding potential of 0 mV, applied voltage steps with duration of ~200 ms and amplitude from +20 mV to −140 mV. ERG potassium current was analyzed by using WAY-123,398 (1 µM) as selective blocker and CsCl (5 mM) as further inhibitor.

Ba^{2+} currents through voltage-dependent Ca^{2+} channels were recorded under conditions which suppressed Na^+ and K^+ currents: the culture medium was replaced by an external solution composed by TEA-chloride 130 mM, $BaCl_2$ 10 mM, $MgCl_2$ 1 mM, hepes 10 mM, TTX 1 µM, glucose 10 mM, pH 7.3; the internal pipette solution contained CsCl 140 mM, MgCl2 4 mM, hepes 10 mM, EGTA 10 mM, Na-ATP 2 mM, pH 7.2. To examine the current-voltage relationship (IV) of I_{Ba}, the cells were depolarized with increasing 10 mV steps from −60 to +50 mV. Moreover, to analyze the contribution of high threshold (I_{Ba}(high)) and low threshold (I_{Ba}(low)) currents, cells were stimulated by two different protocols: IBa(high) were elicited by depolarizing pulses to 0 mV for 150 ms from a holding potential of −80

mV, whereas for I_{Ba}(low) the holding potential was imposed at −90 mV and the test potential was clamped at −50 mV. Addition of 200 μM CdCl$_2$ (Sigma-Aldrich, St. Louis, MO, USA) in the extracellular solution confirmed that I_{Ba} flowed through voltage-dependent calcium channels, and nifedipine (5 μM, Sigma-Aldrich, St. Louis, MO, USA) was used to isolate the component of I_{Ba} through L-type voltage-dependent calcium channels.

Acetylcholine (ACh) currents were evoked by applying ACh (1 mM, Sigma-Aldrich, St. Louis, MO, USA) and were inhibited by the nicotinic ACh receptor antagonist d-tubocurarine (DTC, 1 μM, Sigma-Aldrich, St. Louis, MO, USA). Glutamate (1 mM, Sigma-Aldrich, St. Louis, MO, USA), CNQX (6-cyano-7-nitroquinoxaline-2,3-dione, 10 μM, Tocris, Bristol, UK) and AP5 ((2R)-amino-5-phosphonovaleric acid, 40 μM, Tocris, Bristol, UK) were bath applied to evaluate the functional expression of α-amino-3-hydroxy-5-methyl-4-isoxazolepropionic acid (AMPA) and N-methyl-D-aspartic acid (NMDA) receptors, respectively. To allow NMDA receptor activation, Mg^{2+}-free extracellular solution was used. To study acidic condition responses mediated by transient receptor potential vanilloid 1 (TRPV1) non-selective cation channel and acid-sensing ion channels (ASIC), cells were superfused with a solution containing (mM): NaCl 135, KCl 2, CaCl$_2$ 2, MgCl$_2$ 2, MES 10, glucose 5, pH 5, or pH 6. To investigate the expression of proteins involved in nociception, capsaicin (CAPS, 3 μM, Sigma-Aldrich, St. Louis, MO, USA) and substance P (SP, 2 μM, Sigma-Aldrich, St. Louis, MO, USA) were applied.

3.4. Data analysis

Patch-clamp experiments were performed on a minimum of two and on a maximum of twenty independent cultures for each condition. For the analysis, Origin 8 (RRID:SCR_014212; Microcal Inc., Northampton, MA, USA) and Excel (Microsoft, Redmond, WA, USA) were routinely used. Data are presented as mean ± s.e.m. Mean comparisons were obtained using the unpaired t-test or the non parametric Mann–Whitney

test. The number of responsive cells in the two conditions was compared using the X^2 test. The significance level was set for $p < 0.05$.

4. Results

4.1. Neuronal differentiation of neuroblastoma F-11 cells

After 12–14 days in 1% FBS medium, F-11 cells stained positively for the neuronal nuclear protein NeuN (Fig. 1) and about 50% of the culture was characterized by neuronal networks of cells exhibiting typical neuronal morphology. When 1% FBS cultures were analyzed by the patch-clamp technique, only cells with neuronal morphology showed electrophysiological properties characteristic of mature neurons (Fig. 2). These cells, defined as "differentiated cells" throughout the article, compared to cells maintained in 10% FBS medium ("undifferentiated cells"), had more hyperpolarized resting membrane potentials (V_{rest}: −50.5 ± 1.9 mV vs. −17.1 ± 3.8 mV), and exhibited increased sodium and potassium current densities (for I_{Na}: 114 ± 10.2 pA/pF vs. 42.5 ± 15 pA/pF; for I_K: 181.4 ± 17.9 pA/pF vs. 40.9 ± 5.5 pA/pF). Moreover, a significantly higher percentage of cells was able to fire induced or spontaneous APs. Cells endowed with APs were 85% in differentiating conditions vs. 13% in control conditions (X^2 test); moreover cells with spontaneous spiking reached 61% vs. 18% (X^2 test) (Figs. 2E and 2F). Therefore, we investigated in the differentiated cells the presence of ion channels expressed in DRG neurons.

4.2. Expression of voltage-dependent sodium and potassium channels in differentiated cells

Sodium currents were fast and completely blocked by 1 µM TTX, indicating that differentiated F-11 cells did not express TTX-resistant sodium currents which are conversely present in some classes of DRG neurons. Activation and inactivation properties were consistent with those of TTX-sensitive currents characterized in small DRG neurons

by Cummins & Waxman (1997) (for activation: V1/2 = −22 ± 0.5 mV, k = 6.2 ± 0.4 mV, n = 5; for inactivation: V1/2 = −68 ± 2 mV, k = 5 ± 1 mV, n = 7) (Figs. 3A and 3B). Potassium current kinetic and voltage-dependence (Fig. 3A) were consistent with delayed rectifier potassium currents. Potassium current amplitude was reduced of 84% ± 1% by 10 mM TEA administration (n = 17). F-11 cells also expressed ERG potassium current Ierg (Figs. 3E–3G), as already referred for undifferentiated F-11 cells in Faravelli et al. (1996) and for cells differentiated in retinoic acid by Chiesa et al. (1997). In our conditions, Ierg current density significantly increased in differentiated compared to undifferentiated cells (42 ± 9 pA/pF, n = 8, vs. 14 ± 2 pA/pF, n = 14). Thus voltage-dependence of activation and inactivation were also compared. V1/2 and k values for activation and inactivation in undifferentiated cells were: −29.7 ± 2.4 and 9 mV (n = 6); −64.8 ± 4.4 and 18 mV (n = 7), respectively. Activation properties did not change in differentiated cells and were V1/2 = −32 ± 3 mV and k = 5 mV, n = 12. Concerning the voltage-dependence of inactivation, V1/2 was −56 ± 3 mV and k was 12 mV, n = 4. Ierg currents from both undifferentiated and differentiated cells were almost completely inhibited by WAY-123,398 (block fractions were respectively, 77% ± 4%, n = 6, and 71% ± 6%, n = 9). Moreover, they were also blocked by 5 mM Cs^{2+} (mean inhibition was 70% for both undifferentiated and differentiated cells). Cs^{2+} had no effects on the outward potassium components, which conversely were almost completely inhibited by 10 mM TEA (Fig. 3H).

4.3. Barium currents through voltage-dependent calcium channels

In DRG neurons all the different types of voltage-dependent calcium channels have been described, but low voltage-activated calcium currents (I_{Ca}(low)) have been identified only in small and medium diameter cells (Scroggs & Fox, 1992). To verify the functional expression of calcium channels in F-11 cells, whole-cell Ba^{2+} currents were recorded under conditions which suppressed Na^+ and K^+ currents, by adding TTX and TEA in the extracellular solution, and CsCl in the patch-pipette (see Materials and Methods for details). The I–V

curve was determined by measuring the peak current evoked at potentials from −60 and +50 mV. It showed a peak between −20 and −10 mV in undifferentiated cells (n = 9) and around −10 mV in differentiated cells (n = 8) (Figs. 4A and 4B). To discriminate between high threshold (I_{Ba}(high)) and low threshold-activated currents (I_{Ba}(low)), two different protocols were applied as described in Materials and Methods. Test at 0 mV from a holding potential of −80 mV could evoke Ba_{2+} currents in 15 out of 21 undifferentiated cells (74%); the mean current amplitude was 107 ± 26 pA (current density 3 ± 0.4 pA/pF) (Fig. 4C). In differentiated cells currents had mean amplitude of 203 ± 44 pA (current density 5 ± 1 pA/pF, recorded in 16 out of 24 cells, Fig. 4C). Test at −50 mV from a holding potential of −90 mV evoked responses in neither undifferentiated nor differentiated cells (13 and 10 cells tested, respectively), indicating that low voltage-activated Ca^{2+} channels were not expressed. Cadmium application (200 µM) completely blocked I_{Ba} in all the differentiated cells (n = 10) and in all the undifferentiated cells (n = 11). The L-type voltage-gated calcium channel antagonist nifedipine (5 µM) blocked high threshold currents equivalently in differentiated (63% ± 7% of block, 7 out of 7 cells) and undifferentiated cells (51% ± 11% of block, 5 out of 5 cells) (Figs. 4D–4F).

4.4. Capsaicin

Capsaicin, the pungent ingredient of the hot chili pepper, is the agonist of the transient receptor potential vanilloid 1 (TRPV1) non-selective cation channel, highly expressed in DRG sensory neurons (Goswami et al., 2006; Masuoka et al., 2017). In undifferentiated cells, 3 µM CAPS did not evoke any response (n = 12). In differentiated cells, it induced appreciable inward currents (≥20 pA) in 13 out of 62 cells (21%). Mean current amplitude was 41 ± 9 pA (current density: 1.2 ± 0.3 pA/pF, n = 13). The effects of CAPS are shown in Figs. 5A–5E. In our study, no correlation between responses and cell capacitance was evident (mean capacitance of responsive cells: 38.2 ± 2.7 pF; mean capacitance of non-responsive cells: 38.2 ± 4.4 pF).

4.5. Substance P

Substance P modulates the excitability of sensory neurons in pain pathways. In DRG neurons it can increase or decrease excitability, by modulating ligand-gated channels including P2X3 ATP receptors, TRPV1 CAPS receptors and ASIC3 channels, as well as several types of voltage-gated channels (sodium, calcium and potassium channels, and the hyperpolarization-activated I_h current). In our experiments, undifferentiated cells did not respond to SP (n = 12). On the contrary, in differentiated cells, SP depolarized the cells of about 12 mV (from −48 ± 4 to −36 ± 4 mV, n = 9). No cell tested underwent hyperpolarization in presence of the substance. When tested in the voltage-clamp mode, SP promoted small inward currents in 11 cells. Mean current amplitude calculated for currents ≥20 pA was 24.5 ± 3.3 pA (n = 4) (Figs. 5F–5J). Responses to SP were recorded in 79% of cells (15 out of 19) overall. No correlation between responses to SP and cell capacitance was evident.

4.6. Acidic solutions

Acid-sensing channels are expressed by neurons throughout the nervous system and are involved in acidotoxicity related to several pathological conditions and the perception of pain. F-11 cells maintained at holding potential of −70 mV responded to the application of acidic (pH 5 and pH 6) solutions with fast inward currents (Figs. 5K–5T) which were recorded in <40% of undifferentiated cells (pH 6: 31%, 5 out of 16 cells, mean current: 8.6 ± 1.8 pA; pH 5: 37%, 6 out of 16 cells, mean current: 11.6 ± 2.8 pA). On the contrary, they were evoked in all the differentiated cells with a mean current amplitude of 1,021 ± 181 pA (n = 22) at pH 6 and of 931 ± 131 pA (n = 32) at pH 5.

4.7. Acetylcholine and nicotinic acetylcholine receptors

Functional nicotinic acetylcholine receptors (nAChRs) have been described in heterogeneous populations of dissociated rat and mouse DRG neurons (Smith et al., 2013) and they are known to be involved in pain modulation. The pathway in which nAChRs operate to modulate pain is actually of great interest since it has been suggested that the anti-allodynic effect of their agonists may have a peripheral component (Rueter et al., 2003). In undifferentiated cells, ACh evoked currents in 14 out of 14 cells, with mean amplitude 43.6 ± 12 pA at −70 mV. In differentiated F-11 cells, currents were recorded in 89% of cells and displayed a significantly higher mean amplitude (136 ± 35 pA, n = 34 out of 38). In differentiated cells the effects of ACh administration was also evident on the resting membrane potential (mean depolarization: +44% ± 8%, n = 20). Since ACh-evoked currents were completely inhibited by 1 µM DTC, they were consistent with nAChRs (Figs. 6A–6D). Approximately the same percentage (70–80%) of rat DRG primary neurons was referred to express functional nAChRs in Genzen, Van Cleve & McGehee (2001).

4.8. Glutamate receptors

The localization of AMPA, Kainate, and NMDA receptor subunits has been demonstrated in rat DRGs by immunohistochemistry and in situ hybridization histochemistry, suggesting that the glutamatergic system plays an important role in the primary sensory afferent systems (Sato et al., 1993). In our experiments 1 mM glutamate was effective on only 1 out of 13 undifferentiated cells, but on 28 out of 33 differentiated cells (85%). In the current-clamp mode, it depolarized differentiated cells of 27% ± 5% (n = 14), and in voltage-clamp recordings it evoked currents with amplitude ranging from 20 to 227 pA (mean amplitude: 77 ± 25 pA, n = 10) (Figs. 6E–6H). Currents were inhibited by 71% ± 9% during CNQX and AP5 co-application. However, glutamate administration in the Mg^{2+}-free extracellular solution and at the holding potential of −40 mV evoked no AP5-sensitive

currents, demonstrating that differentiated F-11 cells expressed non-NMDA receptors prevalently.

5. Discussion

The DRG neuron-derived immortal cell line F-11 is routinely used as in vitro model of peripheral sensory neurons. However, expression analysis of RNA transcripts using next-generation sequencing (Yin, Baillie & Vetter, 2016) has stressed the need for the exploration on the functional receptors they present to validate this cell line as a model of DRG neurons. In this paper, for the first time, we show an extensive characterization by the patch-clamp technique of the functional properties of this cell line, comparing undifferentiated cells (7 days in 10% FBS medium) with the ones differentiated by a very simple and economic procedure, represented by cell incubation in serum deprived medium for 10–14 days in culture.

Undifferentiated cells showed immature neuronal morphology and behavior, with low expression of voltage-dependent channels and reduced capability of generating APs, and did not react to CAPS and SP administration. In contrast, differentiated cells revealed typical features of neurons (long processes and NeuN expression) and, when analyzed by the patch-clamp technique, they were functional, firing APs spontaneously or after current injection, and expressing voltage-gated sodium, potassium, and calcium channels. Sodium currents evoked in differentiated F-11 cells were consistent with those exhibited by primary DRG neurons, although TTX-resistant currents typical of nociceptors were not detected. Literature refers that in dissociated rat DRG neurons, calcium currents and calcium transients are sustained by different voltage-dependent calcium channels (N-, P/Q-, R-type, and T-type channels), whose variable expression was related to different cell body diameters; currents through N-type channels instead remained constant between the diameter ranges (Scroggs & Fox, 1992; Fuchs et al., 2007). In differentiated F-11 cells, the largest barium current activated at 0 mV, and was consistent with high threshold activated

Ca^{2+} channel subtypes, whereas no current was attributed to low threshold activated channels. The absence of low threshold activated (T-type channels) Ca^{2+} currents and the expression of TTX-sensitive Na+ channels in the differentiated F-11 cells of our study correlated with the generation of a regular tonic firing of APs, as it has been described for afferent TTX-sensitive A fibers innervating the proximal urethra and the bladder (Yoshimura et al., 2003).

It is known that voltage-gated currents recorded from neurons are distorted due to the lack of space clamp and in fact the results published on DRG neurons are often obtained from cells without processes. In the simulations of all the neuronal morphologies, even of neurons with relatively short dendrites, the membrane potential imposed at the soma decayed by ~10–20 mV over the first 100 μm along the dendrite away from the somatic voltage-clamp (Bar-Yehuda & Korngreen, 2008). However, since indications from both morphology and function are needed to define the level of neuronal maturation, in this manuscript we confirmed that cells displaying elongated processes expressed the typical electrical activity of mature neurons. Even if we are aware of the limits of our analysis and of the distortion of the biophysical properties we described for Na^{+}, K^{+}, and Ca^{2+} channels, nevertheless we show that this properties sustain a neuronal behavior which is consistent with the one described for primary sensory neurons (see Table S1 for the electrophysiological properties we described in undifferentiated and differentiated F-11 cells, and for the same properties referred in literature for primary DRG neurons and for other sensory neuron models for comparison).

Concerning ligand-gated channels, we verified differentiated F-11 cell sensitivity to ACh since nAChRs are expressed on rat DRG neurons (Genzen, Van Cleve & McGehee, 2001) with a role in pain modulation (Rueter et al., 2003). In differentiated F-11 cells, ACh evoked responses in 89% of recorded cells, consistent with the percentage referred by Genzen, Van Cleve & McGehee (2001) in rat DRG primary neurons. The complete inhibition by DTC confirmed that ACh-evoked currents were sustained by nAChRs. We also investigated the

effects of glutamate, since it has been suggested that glutamatergic system plays an important role in the primary sensory afferent pathway (Sato et al., 1993). In fact, the localization of AMPA, Kainate and NMDA receptor subunits has been demonstrated in rat DRGs, in the peripheral axons of small diameter fibers in the rat and human skin, and in the peripheral terminals of primary afferent nerves innervating somatic tissues (Sato et al., 1993; Coggeshall & Carlton, 1997; Carlton & Coggeshall, 1999; Kinkelin et al., 2000). Moreover, activation of non-NMDA receptors has been shown to modify the electrical activity of embryonic DRG neurons (Lee et al., 2004). In our experiments 1 mM glutamate was predominantly effective on non-NMDA receptors.

Capsaicin sensitivity is a hallmark of nociceptive sensory neurons and we investigated its effect, together with the action of SP, on differentiated F-11 cells. CAPS can have both irritating and analgesic effects (Fitzgerald, 1983). It is the agonist of the transient receptor potential vanilloid 1 (TRPV1) non-selective cation channel, a polymodal sensor sensitive to heat, acid pH, and irritant vanilloids, highly expressed in a subset of DRG sensory neurons (Goswami et al., 2006; Masuoka et al., 2017). The painful sensation induced by CAPS is consequent to its binding to TRPV1, and to Ca^{2+} and cation influx through them, which activates several mechanisms (Takayama et al., 2015; Frias & Merighi, 2016; Goswami et al., 2006). Although very small amounts of TRPV1 transcript were identified in proliferating F-11 cells by Yin, Baillie & Vetter (2016), patch-clamp recordings revealed that CAPS was able to evoke calcium currents in roughly 30% of the cells examined (Kusano & Gainer, 1993). In our conditions, differentiation induced responses to CAPS in 21% of cells, a percentage consistent with the one referred by Kusano & Gainer, but inferior to the one found by Ambrosino et al. (2013) in F-11 cells differentiated in retinoic acid.

Substance P is released by DRG neurons at regions in the CNS associated with pain transmission, and at the periphery, where it contributes to neurogenic inflammation in many tissues. Moreover, it can increase or decrease excitability of sensory neurons, by modulating various ligand- and voltage-gated channels, depending on cell diameter and

on the time course of AP after-hyperpolarization (Moraes, Kushmerick & Naves, 2014). In our experiments, responses to SP were recorded in 79% of cells. When investigations were performed in the voltage-clamp mode, SP evoked small inward currents. In the current-clamp mode, administration of SP depolarized the cells. Contrary to rat primary DRG neurons (Moraes, Kushmerick & Naves, 2014), responses to CAPS and SP coexisted in the same differentiated F-11 cell.

Dorsal root ganglion neurons are also sensitive to variation in extracellular pH because of the proton-activated cation channels they express. In particular, two principal proton-gated inward currents were recorded from them and described in literature: fast and rapidly inactivating currents, with maximum activation at pH 6, and sustained, slowly inactivating currents, activated only at pH below 6.2, observed exclusively in DRG neurons responsive to CAPS (Bevan & Yeats, 1991). In our work, proton activated currents were recorded in 100% of the differentiated cells we tested.

Although F-11 cells have been classically used as a model of authentic type C peptidergic nociceptive neurons, for their ability to synthesize and secrete SP, to express sensory neuron antigens, functional voltage-dependent calcium channels and CAPS receptor TRPV1 (Francel et al., 1987; Boland & Dingledine, 1990; Jahnel et al., 2001), our experiments confirm the heterogeneity of these cells already hypothesized by Kusano & Gainer (1993). Since in the past years different culture conditions have been used to attain F-11 cell differentiation, it is possible that these conditions are responsible for the heterogeneous characteristics described in literature.

Referring to the sub-classification of acutely dissociated cells of rat DRGs, which was proposed by Petruska et al. (2000) by using a "current signature" method based on the algesic profile (responses to pH5 and sensitivity to both ATP and CAPS), in our study it seems that ~80% of differentiated F-11 cells showed similarities with "type 3," CAPS and ATP insensitive cells, whereas ~20% of cells seemed to show a partial correspondence with "type 7," CAPS and ATP weakly sensitive cells. As shown in Fig. 7, the cells stimulated by

pH5 responded with desensitizing currents, which were in the 50% of the cells inhibited by 100 μM amiloride (maximum block was 89%; mean block for six cells was 57%, n = 6). None of the cells responded at 10 μM ATP administration with appreciable currents, whereas 19% of cells responded to 3 μM CAPS.

6. Conclusions

Dissociated human DRGs represent the ideal model for investigating sensory neurons and the molecular mechanisms of pain (Valeyev et al., 1996; Dib-Hajj et al., 1999: Davidson et al., 2014; Zhang et al., 2017). However, their limited availability and the incomplete characterization of ion channel expression and biophysical properties force researchers to make do with rodent DRG neurons, even if the obtained results are controversial. Cell lines are also a debated alternative. In this paper, we show that serum deprived differentiated F-11 cells express some ion channels described in sensory neurons. Moreover, compared to neurons differentiated from immortalized human DRG by Raymon et al. (1999) they represent a more accessible model, simple and less expensive. In conclusion, differentiated F-11 cells represent a useful model for research on DRG neurons and, since they express some ion channels and receptors that are also expressed in sensory neurons, might be employed for studying mechanisms involved in the detection and transmission of noxious stimuli.

7. Acknowledgments

8. Funding Statement

9. Competing Interests

The authors declare that they have no competing interests.

10. References

Ambrosino et al. (2013) Ambrosino P, Soldovieri MV, Russo C, Taglialatela M. Activation and desensitization of TRPV1 channels in sensory neurons by the PPARα agonist palmitoylethanolamide. British Journal of Pharmacology. 2013;168(6):1430–1444. doi: 10.1111/bph.12029.

Bar-Yehuda & Korngreen (2008) Bar-Yehuda D, Korngreen A. Space-clamp problems when voltage clamping neurons expressing voltage-gated conductance. Journal of Neurophysiology. 2008;99(3):1127–1136. doi: 10.1152/jn.01232.2007.

Bevan & Yeats (1991) Bevan S, Yeats J. Protons activate a cation conductance in a sub-population of rat dorsal root ganglion neurones. Journal of Physiology. 1991;433(1):145–161. doi: 10.1113/jphysiol.1991.sp018419.

Boland & Dingledine (1990) Boland LM, Dingledine R. Multiple components of both transient and sustained barium currents in a rat dorsal root ganglion cell line. Journal of Physiology. 1990;420(1):223–245. doi: 10.1113/jphysiol.1990.sp017909.

Carbone & Lux (1987) Carbone E, Lux HD. Kinetics and selectivity of a low-voltage-activated calcium current in chick and rat sensory neurones. Journal of Physiology. 1987;386(1):547–570. doi: 10.1113/jphysiol.1987.sp016551.

Carlton & Coggeshall (1999) Carlton SM, Coggeshall RE. Inflammation-induced changes in peripheral glutamate receptor populations. Brain Research. 1999;820(1–2):63–70. doi: 10.1016/S0006-8993(98)01328-6.

Chen et al. (2007) Chen W, Mi R, Haughey N, Oz M, Höke A. Immortalization and characterization of a nociceptive dorsal root ganglion sensory neuronal line. Journal of the Peripheral Nervous System. 2007;12(2):121–130. doi: 10.1111/j.1529-8027.2007.00131.x.

Chiesa et al. (1997) Chiesa N, Rosati B, Arcangeli A, Olivotto M, Wanke E. A novel role for HERG K+ channels: spike-frequency adaptation. Journal of Physiology. 1997;501(2):313–318. doi: 10.1111/j.1469-7793.1997.313bn.x.

Coggeshall & Carlton (1997) Coggeshall RE, Carlton SM. Receptor localization in the mammalian dorsal horn and primary afferent neurons. Brain Research Reviews. 1997;24(1):28–66. doi: 10.1016/S0165-0173(97)00010-6.

Cummins & Waxman (1997) Cummins TR, Waxman SG. Downregulation of tetrodotoxin-resistant sodium currents and upregulation of a rapidly repriming tetrodotoxin-sensitive sodium current in small spinal sensory neurons after nerve injury. Journal of Neuroscience. 1997;17(10):3503–3514. doi: 10.1523/JNEUROSCI.17-10-03503.1997.

Davidson et al. (2014) Davidson S, Copits BA, Zhang J, Page G, Ghetti A, Gereau RW., IV Human sensory neurons: membrane properties and sensitization by inflammatory mediators. Pain. 2014;155(9):1861–1870. doi: 10.1016/j.pain.2014.06.017.

Dib-Hajj et al. (1999) Dib-Hajj SD, Tyrrell L, Cummins TR, Black JA, Wood PM, Waxman SG. Two tetrodotoxin-resistant sodium channels in human dorsal root ganglion neurons. FEBS Letters. 1999;462(1–2):117–120. doi: 10.1016/S0014-5793(99)01519-7.

Faravelli et al. (1996) Faravelli L, Arcangeli A, Olivotto M, Wanke E. A HERG-like K+ channel in rat F-11 DRG cell line: pharmacological identification and biophysical characterization. Journal of Physiology. 1996;496(1):13–23. doi: 10.1113/jphysiol.1996.sp021661.

Fitzgerald (1983) Fitzgerald M. Capsaicin and sensory neurones—a review. Pain. 1983;15(1):109–130. doi: 10.1016/0304-3959(83)90012-X.

Francel et al. (1987) Francel PC, Harris K, Smith M, Fishman MC, Dawson G, Miller RJ. Neurochemical characteristics of a novel dorsal root ganglion x neuroblastoma hybrid cell line, F-11. Journal of Neurochemistry. 1987;48(5):1624–1631. doi: 10.1111/j.1471-4159.1987.tb05711.x.

Frias & Merighi (2016) Frias B, Merighi A. Capsaicin, nociception and pain. Molecules. 2016;21(6):797. doi: 10.3390/molecules21060797.

Fuchs et al. (2007) Fuchs A, Rigaud M, Sarantopoulos CD, Filip P, Hogan QH. Contribution of calcium channel subtypes to the intracellular calcium signal in sensory neurons: the effect of injury. Anesthesiology. 2007;107(1):117–127. doi: 10.1097/01.anes.0000267511.21864.93.

Genzen, Van Cleve & McGehee (2001) Genzen JR, Van Cleve W, McGehee DS. Dorsal root ganglion neurons express multiple nicotinic acetylcholine receptor subtypes. Journal of Neurophysiology. 2001;86(4):1773–1782. doi: 10.1152/jn.2001.86.4.1773.

Goswami et al. (2006) Goswami C, Dreger M, Otto H, Schwappach B, Hucho F. Rapid disassembly of dynamic microtubules upon activation of the capsaicin receptor TRPV1.

Journal of Neurochemistry. 2006;96(1):254–266. doi: 10.1111/j.1471-4159.2005.03551.x.

Hall, Sima & Wiley (1995) Hall KE, Sima AA, Wiley JW. Voltage-dependent calcium currents are enhanced in dorsal root ganglion neurones from the Bio Bred/Worchester diabetic rat. Journal of Physiology. 1995;486(2):313–322. doi: 10.1113/jphysiol.1995.sp020814.

Jahnel et al. (2001) Jahnel R, Dreger M, Gillen C, Bender O, Kurreck J, Hucho F. Biochemical characterization of the vanilloid receptor 1 expressed in a dorsal root ganglia derived cell line. European Journal of Biochemistry. 2001;268(21):5489–5496. doi: 10.1046/j.1432-1033.2001.02500.x.

Kinkelin et al. (2000) Kinkelin I, Bröcker E-B, Koltzenburg M, Carlton SM. Localization of ionotropic glutamate receptors in peripheral axons of human skin. Neuroscience Letters. 2000;283(2):149–152. doi: 10.1016/S0304-3940(00)00944-7.

Kusano & Gainer (1993) Kusano K, Gainer H. Modulation of voltage-activated Ca currents by pain-inducing agents in a dorsal root ganglion neuronal line, F-11. Journal of Neuroscience Research. 1993;34(2):158–169. doi: 10.1002/jnr.490340203.

Lee et al. (2004) Lee CJ, Labrakakis C, Joseph DJ, MacDermott AB. Functional similarities and differences of AMPA and Kainate receptors expressed by cultured rat sensory neurons. Neuroscience. 2004;129(1):35–48. doi: 10.1016/j.neuroscience.2004.07.015.

Lei et al. (2014) Lei Z, Li X, Wang G, Fei J, Meng T, Zhang X, Yu J, Yu J, Li J. Inhibition of acid-sensing ion channel currents by propofol in rat dorsal root ganglion neurons. Clinical

and Experimental Pharmacology and Physiology. 2014;41(4):295–300. doi: 10.1111/1440-1681.12215.

Masuoka et al. (2017) Masuoka T, Kudo M, Yamashita Y, Yoshida J, Imaizumi N, Muramatsu I, Nishio M, Ishibashi T. TRPA1 channels modify TRPV1-mediated current responses in dorsal root ganglion neurons. Frontiers in Physiology. 2017;8:272. doi: 10.3389/fphys.2017.00272.

Moraes, Kushmerick & Naves (2014) Moraes ER, Kushmerick C, Naves LA. Characteristics of dorsal root ganglia neurons sensitive to Substance P. Molecular Pain. 2014;10(1):73. doi: 10.1186/1744-8069-10-73.

Petruska et al. (2000) Petruska JC, Napaporn J, Johnson RD, Gu JG, Cooper BY. Subclassified acutely dissociated cells of rat DRG: histochemistry and patterns of capsaicin-, proton-, and ATP-activated currents. Journal of Neurophysiology. 2000;84(5):2365–2379. doi: 10.1152/jn.2000.84.5.2365.

Platika et al. (1985) Platika D, Boulos MH, Baizer L, Fishman MC. Neuronal traits of clonal cell lines derived by fusion of dorsal root ganglia neurons with neuroblastoma cells. Proceedings of the National Academy of Sciences of the United States of America. 1985;82(10):3499–3503. doi: 10.1073/pnas.82.10.3499.

Raymon et al. (1999) Raymon HK, Thode S, Zhou J, Friedman GC, Pardinas JR, Barrere C, Johnson RM, Sah DWY. Immortalized human dorsal root ganglion cells differentiate into neurons with nociceptive properties. Journal of Neuroscience. 1999;19(13):5420–5428. doi: 10.1523/JNEUROSCI.19-13-05420.1999.

Rueter et al. (2003) Rueter LE, Kohlhaas KL, Curzon P, Surowy CS, Meyer MD. Peripheral and central sites of action for A-85380 in the spinal nerve ligation model of neuropathic pain. Pain. 2003;103(3):269–276. doi: 10.1016/s0304-3959(02)00455-4.

Russo et al. (2014) Russo L, Sgambato A, Lecchi M, Pastori V, Raspanti M, Natalello A, Doglia SM, Nicotra F, Cipolla L. Neoglucosylated collagen matrices drive neuronal cells to differentiate. ACS Chemical Neuroscience. 2014;5(4):261–265. doi: 10.1021/cn400222s.

Sato et al. (1993) Sato K, Kiyama H, Park HT, Tohyama M. AMPA, KA and NMDA receptors are expressed in the rat DRG neurones. NeuroReport. 1993;4(11):1263–1265. doi: 10.1097/00001756-199309000-00013.

Scroggs & Fox (1992) Scroggs RS, Fox AP. Calcium current variation between acutely isolated adult rat dorsal root ganglion neurons of different size. Journal of Physiology. 1992;445(1):639–658. doi: 10.1113/jphysiol.1992.sp018944.

Sculptoreanu & de Groat (2007) Sculptoreanu A, de Groat WC. Neurokinins enhance excitability in capsaicin-responsive DRG neurons. Experimental Neurology. 2007;205(1):92–100. doi: 10.1016/j.expneurol.2007.01.038.

Smith et al. (2013) Smith NJ, Hone AJ, Memon T, Bossi S, Smith TE, McIntosh JM, Olivera BM, Teichert RW. Comparative functional expression of nAChR subtypes in rodent DRG neurons. Frontiers in Cellular Neuroscience. 2013;7:225. doi: 10.3389/fncel.2013.00225.

Takayama et al. (2015) Takayama Y, Uta D, Furue H, Tominaga M. Pain-enhancing mechanism through interaction between TRPV1 and anoctamin 1 in sensory neurons.

Proceedings of the National Academy of Sciences of the United States of Amrica. 2015;112(16):5213–5218. doi: 10.1073/pnas.1421507112.

Valeyev et al. (1996) Valeyev AY, Hackman JC, Wood PM, Davidoff RA. Pharmacologically novel GABA receptor in human dorsal root ganglion neurons. Journal of Neurophysiology. 1996;76(5):3555–3558. doi: 10.1152/jn.1996.76.5.3555.

Yin, Baillie & Vetter (2016) Yin K, Baillie GJ, Vetter I. Neuronal cell lines as model dorsal root ganglion neurons: a transcriptomic comparison. Molecular Pain. 2016;12:1–17.

Yoshimura et al. (2003) Yoshimura N, Seki S, Erickson KA, Erickson VL, Chancellor MB, De Groat WC. Histological and electrical properties of rat dorsal root ganglion neurons innervating the lower urinary tract. Journal of Neuroscience. 2003;23(10):4355–4361. doi: 10.1523/JNEUROSCI.23-10-04355.2003.

Yu et al. (2014) Yu Y-Q, Chen X-F, Yang Y, Yang F, Chen J. Electrophysiological identification of tonic and phasic neurons in sensory dorsal root ganglion and their distinct implications in inflammatory pain. Physiological Research. 2014;63:793–799.

Zhang et al. (2017) Zhang X, Priest BT, Belfer I, Gold MS. Voltage-gated Na+ currents in human dorsal root ganglion neurons. Elife. 2017;6:e23235.
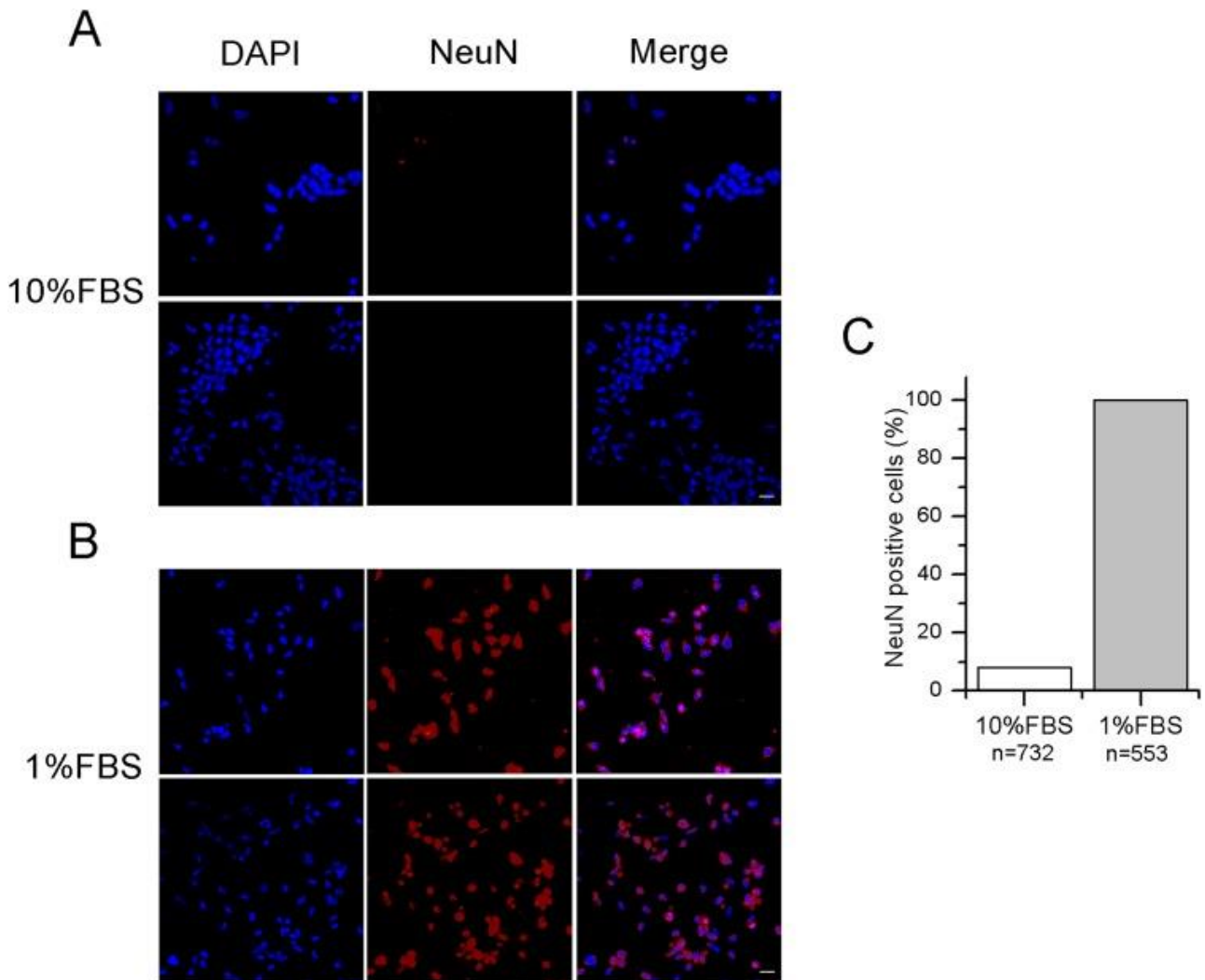
11. Figures and legends

Figure 1: Differentiated F-11 cells express the neuronal nuclear antigen NeuN. (A, B) The panels illustrate NeuN staining in red, DAPI in blue and the color overlay (merged) in F-11 cells maintained in 10% FBS and 1% FBS, respectively. A total of 16–20 z-stack images from for each condition were taken. (C) Quantification of NeuN positive cells (histograms) in 10 different fields confirmed no or minor expression of this nuclear marker in 10% FBS compared to 1% FBS cultures. Fluorescence images were captured with a laser scanning fluorescence confocal microscope at 40× magnification. Scale bar, 20 μm.
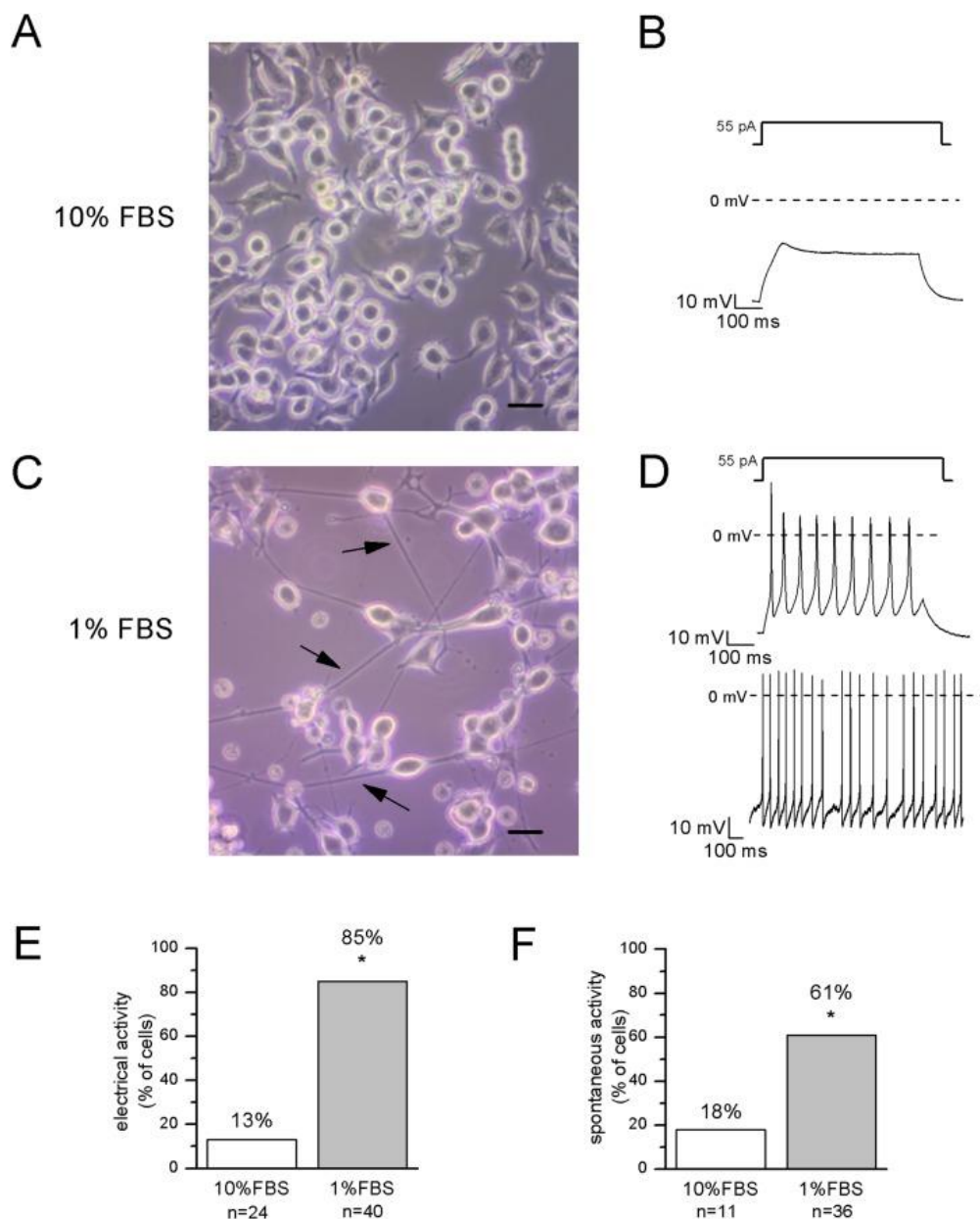
Figure 2: Differentiated cells with neuronal morphology were selected for electrophysiological recordings. (A, B) In undifferentiated F-11 cells, the round cell bodies and the absence of neuronal processes were consistent with the lack of electrical activity. Scale bar, 20 µm. (C, D) Differentiated F-11 cells showed oval cell bodies and long processes (indicated by arrows) which were consistent with the discharge of spontaneous or induced action potentials. Scale bar, 20 µm. (E) A significantly higher percentage of differentiated cells was able to fire action potentials compared to undifferentiated cells. (F) Moreover, cells able to generate spontaneous spiking were significantly more represented in the differentiated culture. Asterisks represent significance.
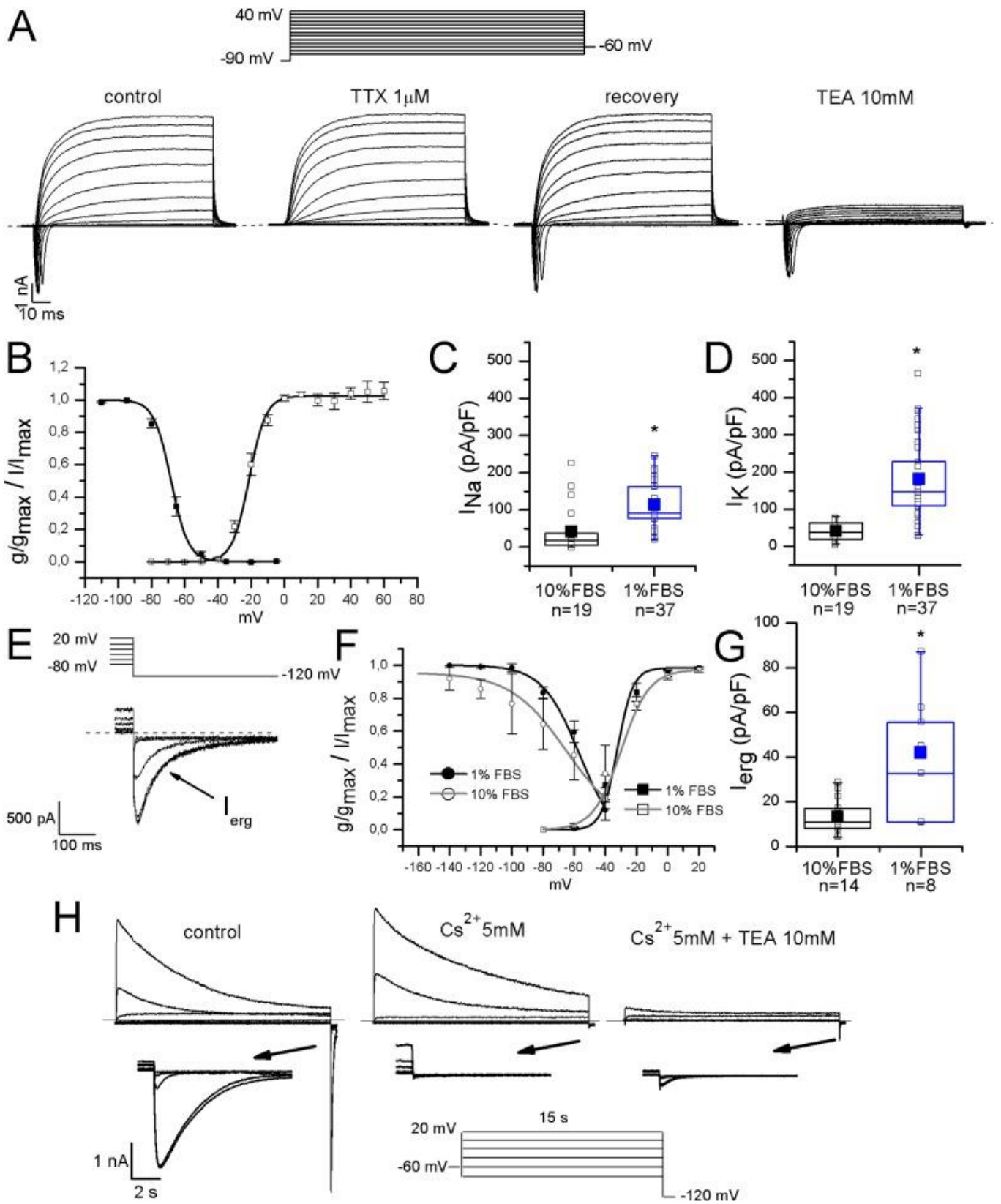
Figure 3: Differentiated F-11 cells expressed voltage-dependent sodium and potassium currents. (A) Sodium and potassium currents evoked by depolarizing steps from a preconditioning potential of −90 mV. Sodium currents were isolated by the application of the selective blocker TTX. All sodium currents were TTX-sensitive. Potassium outward currents exhibited properties consistent with delayed rectifier currents and they were inhibited by 10 mM TEA. (B) Activation (g/gmax, empty square symbols) and inactivation (I/Imax, filled square symbols) properties of voltage-dependent sodium channels. For activation, $V1/2 = -22 \pm 0.5$ mV, $k = 6.2 \pm 0.4$ mV (n = 5); for inactivation: $V1/2 = -68 \pm 2$ mV, $k = 5 \pm 1$ mV (n = 7). (C, D) Sodium (INa) and potassium (IK) current densities in undifferentiated and differentiated F-11 cells. Bar graphs were overlaid with scatter plots. Both INa and IK densities were significantly higher in differentiated cells. (E–G) ERG potassium current (Ierg) density increased in differentiated cells compared to undifferentiated cells (42 ± 9 pA/pF, n = 8, vs. 14 ± 2 pA/pF, n = 14) but the biophysical properties of activation (I/Imax, square symbols) were not different in differentiated cells compared to undifferentiated cells ($V1/2 = -32 \pm 3$ mV and $k = 5$ mV (n = 12) for differentiated cells vs. $V1/2 = -29.7 \pm 2.4$ mV and $k = 9$ mV (n = 6) for undifferentiated cells). Instead, the voltage-dependence of inactivation (g/gmax, round symbols), was ~8 mV more depolarized in differentiated cells ($V1/2 = -56 \pm 3$ mV and $k = 12$ mV (n = 4) for differentiated cells vs. $V1/2 = -64.8 \pm 4.4$ mV and $k = 18$ mV (n = 7) for undifferentiated cells). Extracellular potassium concentration in these experiments was 40 mM. (H) Potassium current sensitivity to Cs2+ and TEA block. As represented in the middle panel, inward currents showed sensitivity to Cs2+ (mean inhibition was $70\% \pm 5\%$, n = 15). When TEA was administered with Cs2+ (right panel), outward currents were also blocked. Mean inhibition by TEA was $76\% \pm 2\%$, n = 15. The arrows indicate the enlargement of the tail currents evoked at −120 mV in the different conditions (control, during Cs2+ and during Cs2+ and TEA coapplication). Extracellular potassium concentration was 40 mM. Asterisks represent significance.
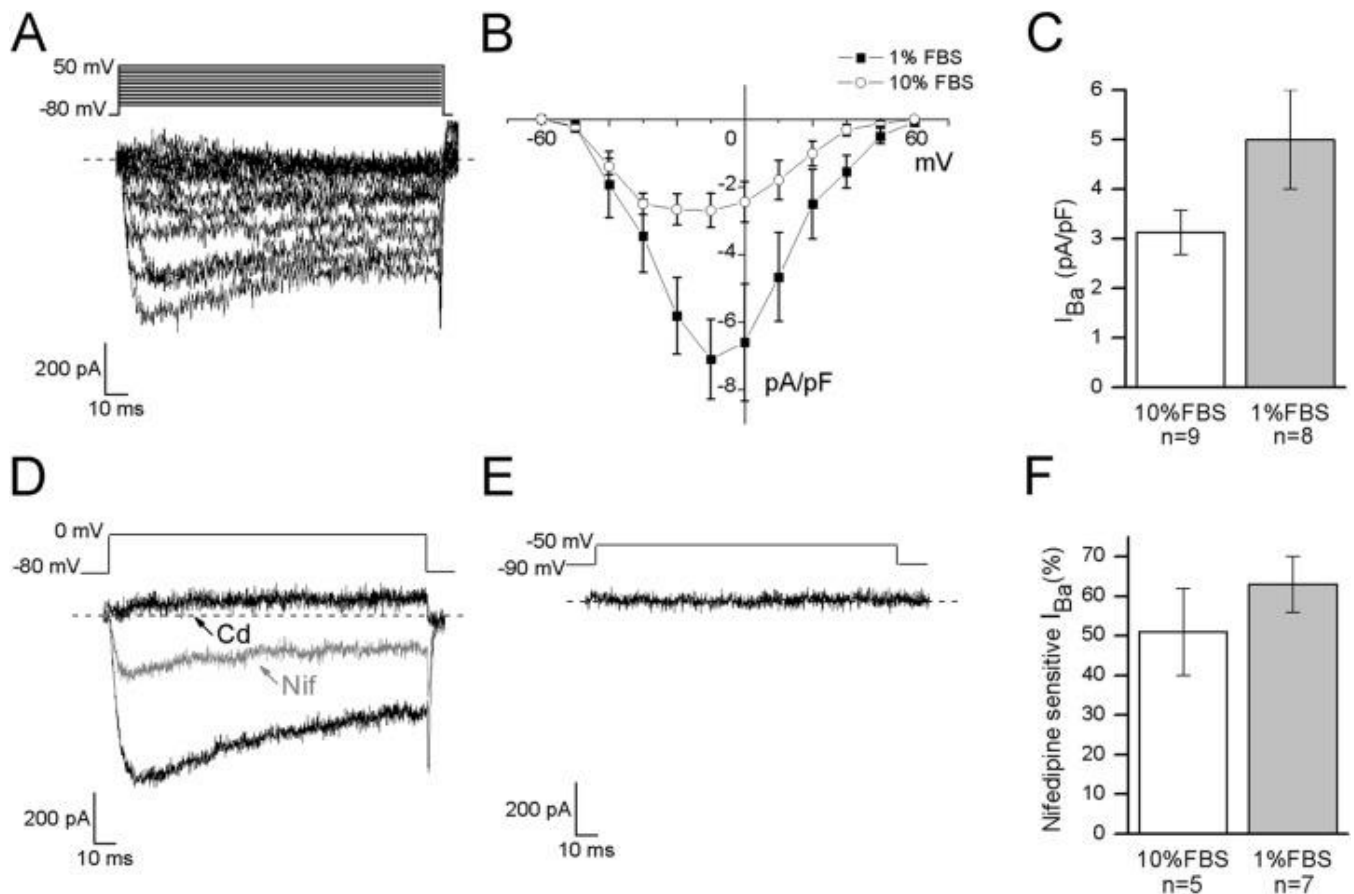
Figure 4: Differentiated cells expressed high voltage-activated barium currents. (A, B) Depolarized test potentials (from −60 to 50 mV) from a holding potential of −80 mV evoked barium currents with an I–V relationship which peaked around −10 mV in differentiated cells and between −20 and −10 mV in undifferentiated cells. (C) Current densities showed a tendency to increase in differentiated compared to undifferentiated cells (5 ± 1 pA/pF, n = 16 cells, vs. 3 ± 0.4 pA/pF, n = 15 cells, respectively). (D) To define the contribution of high threshold (IBa(high)) and low threshold (IBa(low)) activated channels the holding and the test potentials were varied opportunely. In both the culture conditions, test potential at 0 mV from a holding of −80 mV evoked currents, which were completely blocked by cadmium application (Cd, 200 μM) and partially inhibited by nifedipine (Nif, 5 μM). (E) On the contrary, no currents were elicited by testing at −50 mV from a holding potential of −90 mV, demonstrating that low threshold-activated Ca2+ channels were not present in cell membranes (n = 13 undifferentiated cells and n = 10 differentiated cells). (F) As shown in the histograms, nifedipine-sensitive currents were equivalently expressed in both the culture conditions.
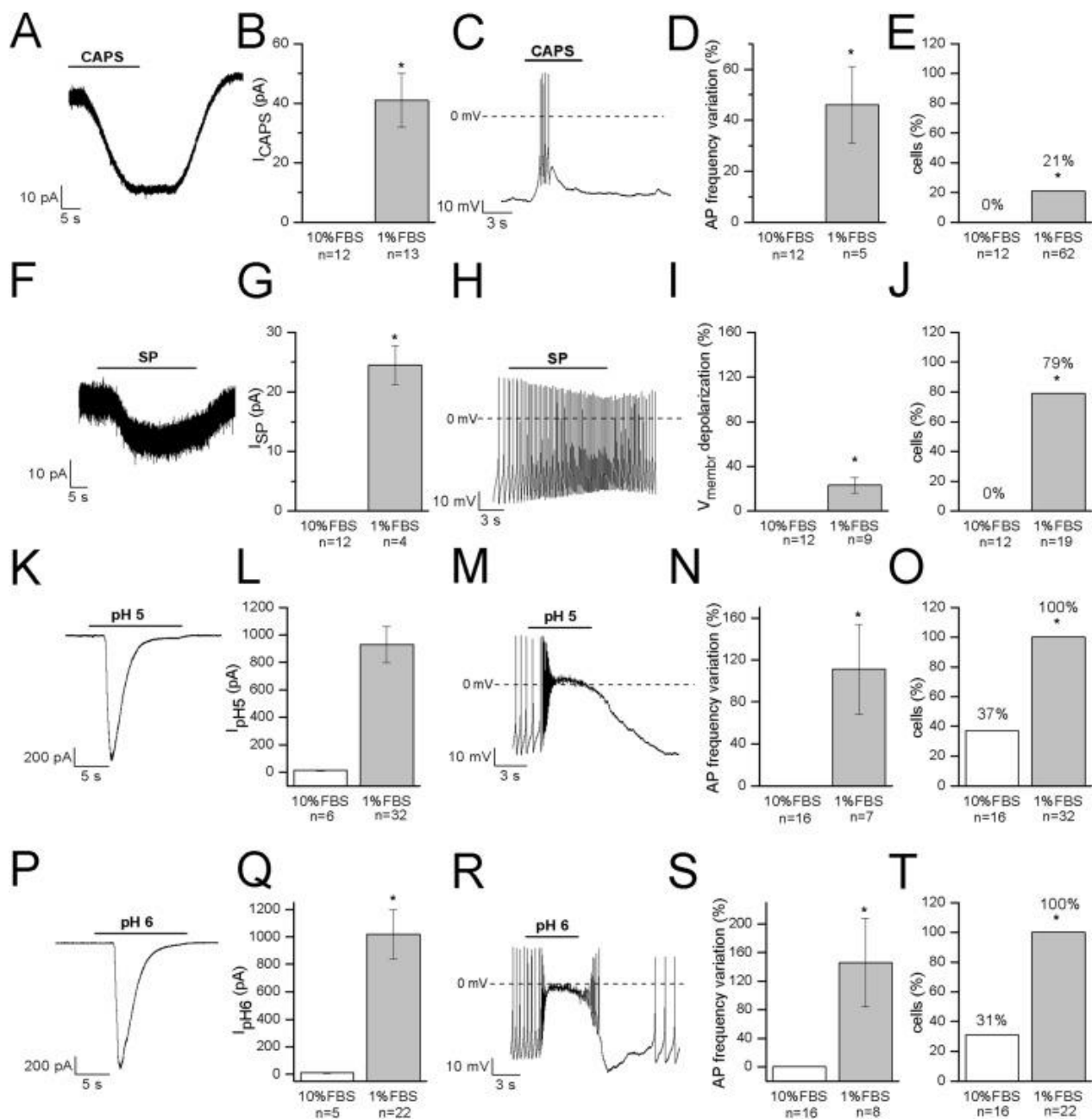
Figure 5: Differentiated F-11 cells express receptors and ion channels of nociceptors. The representative currents and the effects on the electrical activity evoked by capsaicin, substance P and acidic pH values are shown. (A–E) Capsaicin (CAPS) evoked responses in differentiated but not in undifferentiated cells. (F–J) Substance P (SP) induced currents and high frequency action potential discharges in differentiated cells but had no effect on undifferentiated cells. Responses to acidic extracellular solutions, (K–O) pH 5 and (P–T) pH 6, were recorded in all the differentiated cells and in 31% and 37% of undifferentiated cells, respectively. Cell membrane potential was clamped at −70 mV during all the experiments. Asterisks represent significance.
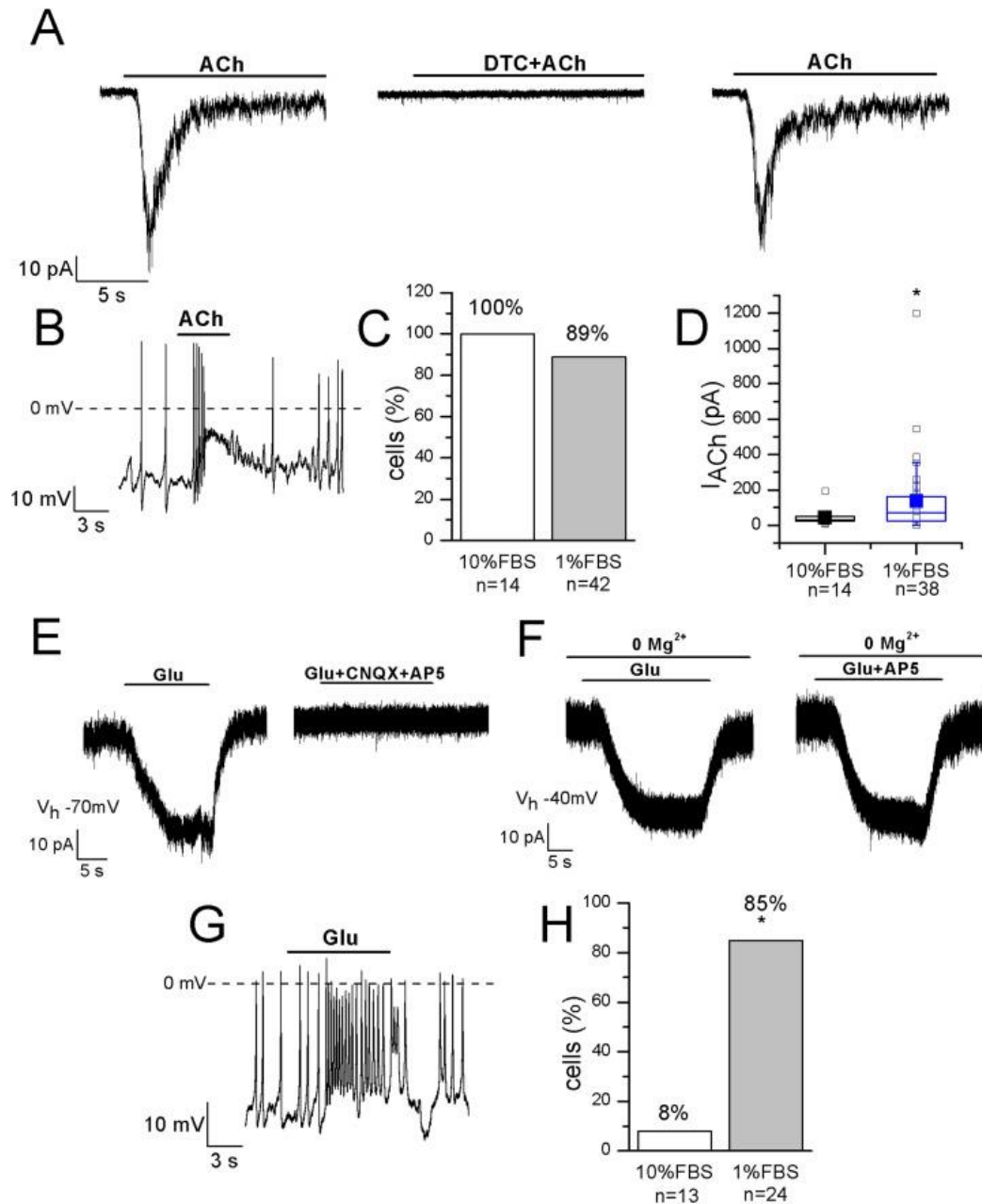
Figure 6: Differentiated F-11 cells display responses to acetylcholine and glutamate. The representative currents and the effects on the electrical activity evoked by acetylcholine (ACh) and glutamate (Glu) are shown. (A–D) ACh was effective on 100% of undifferentiated and on 89% of differentiated cells and its action was mediated by nAChRs, as demonstrated by d-tubocurarine (DTC) block. Cell membrane potential was clamped at −70 mV. (E–H) On the contrary, the percentage of Glu-responsive cells was significantly higher in differentiated than in undifferentiated cells. Glu-evoked effects were principally mediated by non-NMDA receptors, since AP5 administration in Mg2+-free extracellular solution and at −40 mV did not affected them. Asterisks represent significance.
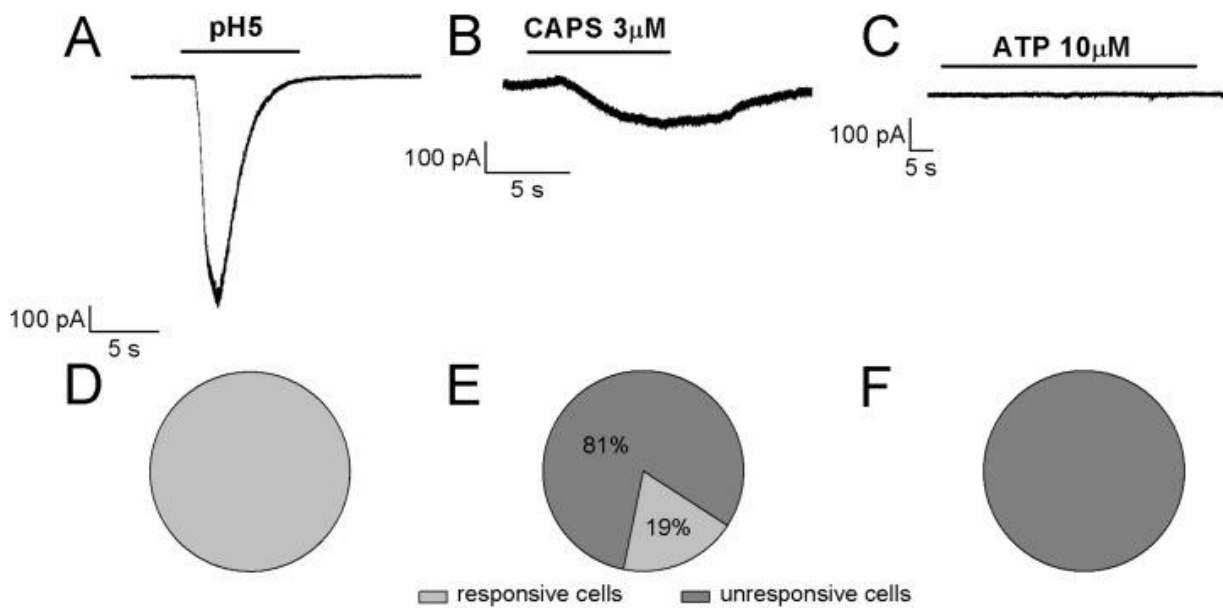
106

Figure 7: Algesic profile of differentiated F-11 cells. Responses to (A) pH5, (B) ATP, and (C) capsaicin (CAPS) were investigated in differentiated cells to define the "current signature" used by Petruska et al. (2000) to subclassify acutely dissociated cells of rat DRGs. (D–F) While all the cells responded to an extracellular acidic solution at pH 5, no cells showed appreciable sensitivity to ATP and only a small fraction of cells (19%) responded to CAPS.

CHAPTER 4: Neuronal differentiation induced by scalable thermal stimulation

Stefania Blasa[a], Mykola Borzenkov[b], Valentina Pastori[a], Lavinia Doveri[c], Piersandro Pallavicini[c], Giuseppe Chirico[d], Marzia Lecchi[a]* and Maddalena Collini[d]

[a]Department of Biotechnology and Biosciences, University of Milano-Bicocca, Piazza della Scienza 2, 20126 Milan, Italy

[b]Department of Medicine and Surgery, Nanomedicine Center, University of Milano-Bicocca, Via Alfred Nobel, 20854 Vedano al Lambro (MB), Italy

[c]Department of Chemistry, University of Pavia, Via Torquato Taramelli 12, 27100 Pavia, Italy

[d]Department of Physics «G. Occhialini», University of Milano-Bicocca, Piazza della Scienza 3, 20126 Milan, Italy

*Corresponding author

1. Abstract

Heating has been recently used as an alternative application to electrical stimulation to modulate excitability and to induce neuritogenesis and the expression of neuronal markers, but a long-term functional differentiation has not been described so far.

Here we present the results obtained by a new approach for scalable thermal stimulation on the behavior of a model of dorsal root ganglion neurons, the F-11 cell line. Initially, we performed experiments of bulk stimulation in incubator for different time intervals and temperatures, and significant differences in neurite elongation and in electrophysiological properties were observed in cultures exposed at 41,5°C for 30 minutes. Thus, we exposed the cultures to the same temperature increase by irradiating, with a near infrared laser, a disc of Prussian Blue nanoparticles and poly-vinyl alcohol, that we stuck on the outer surface of the petri dish. Neurite elongation in irradiated cells was significantly increased compared to the control and the electrophysiological properties (action potential firing frequency and spontaneous activity) were consistent with those of differentiated neurons. These results suggest that a targeted thermal stimulation could be a promising technique

to induce differentiation and support the future application of this method as a strategy to modify neuronal behavior in vivo.

2. Graphical Abstract
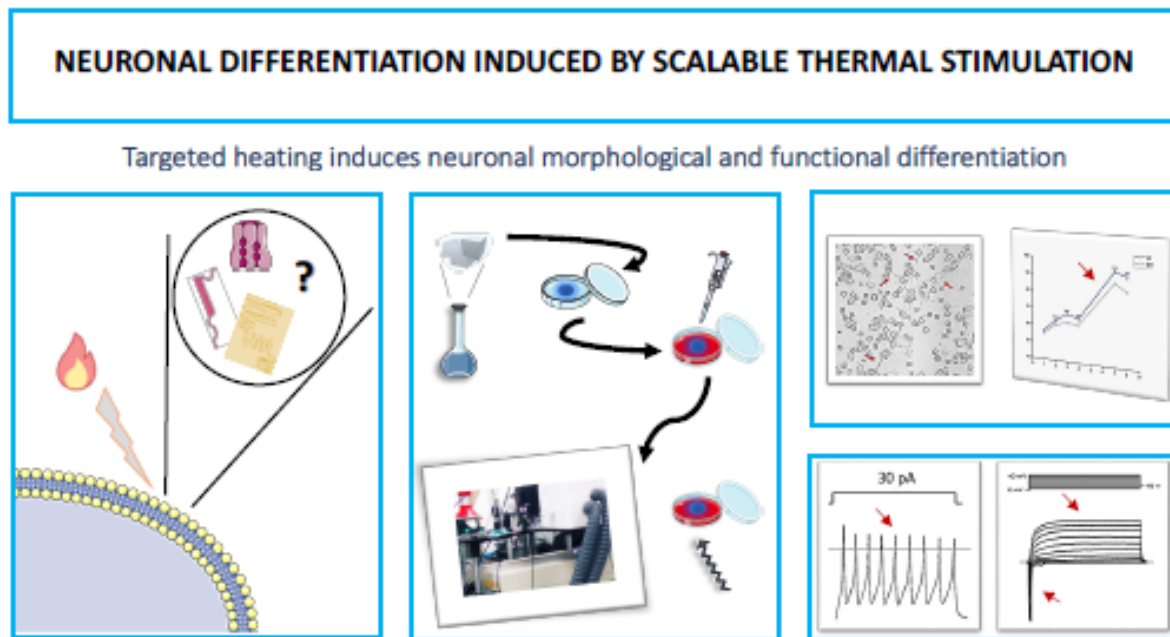
3. Introduction

Heating has been the subject of increasing attention in the last years for its ability to modify cell behavior and modulate the electrical activity of excitable tissues. Previous studies showed that different combinations of time and temperature, from milliseconds at high temperature to several hours/days at mild temperature, could elicit depolarizing currents or promote neuritogenesis and induce the expression of neuronal markers (Shapiro et al., 2012, Akhavan et al., 2015, Kudo et al., 2015, Hossain et al., 2017). These effects are probably due to changes in cell membrane capacitance and in ion channel properties (Shapiro et al., 2012, Thang et al., 2019), and to the activation of differentiation pathways (Kudo et al., 2015), but the underlying mechanism by which these changes occur remains so far unknown. In many studies, infrared neuronal stimulation (INS) has been applied mainly by exploiting the absorption properties of water in the infrared (IR) region

(Shapiro et al., 2012). Recently, the combination of near infrared (NIR) with photo-thermally active nanomaterials has been employed in order to scale the excitation wavelength to the interval 700-1000 nm, which lies in the transparent optical windows for tissues (Paviolo et al., 2013, Paviolo et al., 2014, Akhavan et al., 2015, Paviolo et al., 2015). IR photo- thermally active nanomaterials are explored as mediators to convert light, as primary stimulus, to a secondary stimulus, such as heat, which can be localized to stimulate neurons (Eom et al., 2014, Yong et al., 2014, Pallavicini et al., 2021). These photo-thermal nanoparticles, alone or together with probes and conjugates, can penetrate biological tissues and can be used for hyperthermic treatments arising from either localized surface plasmon resonances or charge transfer transitions (Weissleder 2001). Nanoparticles are also applied in photothermal (PTT) and photobiomodulation (PBT) therapy, which have become two of the most common therapies used in the last few years (Wang et al., 2015). However, for the opto-thermal stimulation, internalization of nanoparticles may cause spatial distribution variability, instability and cytotoxicity. Nanoparticles could undergo biodegradation in cell environment and damage cell components such as plasma membrane and intracellular organelles. They could compromise cell membrane integrity through lipid peroxidation, generate oxidative stress or inflammation, and they could have a genotoxic potential for cells. For this reason, it is important to study the cytotoxic effect of nanoparticles in order to choose the safest type to use for cell treatments (Lewinski et al., 2008).

Prussian Blue nanoparticles (PBNPs) have been approved in 2003 by the U.S Food and Drug Administration (FDA) as a safe and non-toxic compound available in commerce (Patra, 2016). They consist of a coordination polymer containing Fe^{3+} hexa-coordinated by the N atoms of $[Fe(CN)_6]^{2+}$ and they can be soluble or insoluble, depending on the exact formulation, namely $Fe_4[Fe(CN)_6]_3 \cdot xH2O$ (x=14-16, "insoluble" PB) and $KFe[Fe(CN)_6] \cdot xH2O$ (x=1-5, "soluble" PB). Soluble PBNPs show lower dimensioned crystals that reach the size typical of the mesophase, forming clear deep-blue colored colloidal solutions, whereas

insoluble PBNPs form larger crystals that easily aggregate and give a precipitate. However, all these formulas correspond to the same crystal and molecular structure by X-ray diffraction (Dacarro et al., 2017). PBNPs are used in several applications such as antimicrobial therapy (Borzenkov et al., 2019) or cancer treatment, often combined with a NIR laser (Gautam et al., 2018). They can convert light into heat thanks to a metal-to-metal charge transfer between Fe^{2+} and Fe^{3+} through a cyanide bridge, resulting in an intense, large absorption band with maximum at ~700 nm; the light irradiation in the 700-750 nm region results in a thermal relaxation.

In this study, we took advantage of using PBNPs, dispersed in a polymeric matrix and not in direct contact with cells, in order to obtain a scalable and controlled thermal stimulation to modulate neuronal behavior and properties of an in vitro model of dorsal root ganglion (DRG) neurons, the neuroblastoma F-11 cell line. A systematic study has been carried out to evaluate the effects of this stimulation on cell morphology and electrophysiological properties on a large statistical scale, in order to establish a reproducible protocol for optical stimulation.

4. Materials and methods

4.1. Cell cultures

F-11 cells (mouse neuroblastoma N18TG-2 x rat DRG, ECACC Cat#08062601 RRID: CVCL_H605; Platika et al., 1985) were seeded at 50,000 cells/35 mm dish (Corning®; Sigma- Aldrich, St. Louis, MO, USA) and maintained in a serum-deprived medium to reduce proliferation. The complete composition of the medium was as previously described (Pastori et al., 2019): Dulbecco's modified Eagle's medium (Cat#D6546; Sigma-Aldrich, St. Louis, MO, USA), 2 mM glutamine (Sigma-Aldrich, St. Louis, MO, USA), 1% fetal bovine serum (FBS, Cat# F2442; Sigma-Aldrich, St. Louis, MO, USA) and penicillin/streptomycin (10000 U/ml, lot#753901 ref#15140; Gibco™, Waltham, MA, USA). 24 hours after seeding, the cells were thermally stimulated. The stimulation was repeated the following day, with

the same parameters of duration and temperature. After each stimulation the cells were replaced in the incubator at 37°C, in a humidified atmosphere with 5% CO_2. Medium was replaced with fresh medium twice per week to prevent cell starvation. Cells maintained at 37°C in incubator were used as control.

Morphological and functional analysis were performed for 8 days after seeding for both stimulated and control samples.

4.2. Bulk heating protocol

In order to verify if heating could effectively induce cell differentiation, experiments were performed in bulk configuration to find out the best protocol to be applied in irradiation experiments. In particular, the temperature of the incubator (Jouan IGO150 CELLife CO_2 Incubator, Thermo Fisher Scientific, Rodano, MI, Italy) was increased from the standard 37°C to higher temperatures for 10 minutes/day for two consecutive days. The temperatures chosen were 39°C, 41,5°C or 43°C. Another series of experiments consisted in heating the cells for 10, 20, 30, 45 or 60 minutes/day for two consecutive days in order to find the best time duration of the heating protocol. Each experiment was performed on two or three independent cultures. After heating, cells were maintained in an incubator at 37°C.

4.3. Prussian Blue nanoparticle preparation

PBNPs were prepared according to literature (Dacarro et al., 2017) but increasing from 1 mM to 10 mM the concentration of the reagents; 100 ml of a 10 mM FeCl3 solution were mixed with 10 mM K4[Fe(CN)6] in 0.025 M citric acid and heated to 60°C under stirring. After 1 minute stirring at 60°C, the solution was cooled at room temperature. The solution was centrifuged for 25 minutes at 13,000 rpm in 10 ml test tubes for purification. Centrifuged PBNP pellet was resuspended in half the original volume. The absorbance peak of PBNP aqueous solution was evaluated with Jasco, V-570 spectrophotometer.

4.4. PBNP-PVA layer preparation

A solution containing 7% of poly vinyl alcohol (PVA, average molecular weight 72000 g mol-1, degree of hydrolysis 98%, Sigma-Aldrich, St. Louis, MO, USA) and 27-30% of 10 mM PBNPs was made. The PVA powder was dissolved in water and was maintained in oven at 70°C for at least one hour. Then the PBNP solution was added and the mixture was achieved by 1 hour under continuous stirring. 70 µl of the final solution was dropped on the outer surface of the petri dishes and dried in an oven at 70°C for at least 1 hour. The PVA-PBNP patch (blue colored) covered approximately a circular area of 1 cm². A circle of the same area was drawn on the control petri dishes to compare similar size regions.

4.5. Irradiation protocol by heating nanoparticles layers

A Ti:Sa laser (Mai-Tai DeepSea Ti:Sapphire®, Spectra Physics®, Santa Clara, CA, USA), tunable between 690 nm and 1100 nm, was used to increase the temperature of the medium into the petri dish in correspondence of the PVA-PBNP layer. By exploiting the 720 nm wavelength, the power was chosen to reach the desired temperatures, which were defined according to the results obtained by bulk heating experiments. Temperature calibrations were made either on dry petri dishes, to check the reproducibility of the layers, and on petri dishes with 2 ml of culture medium, in order to determine the power needed for temperature increase. Accurate temperature measurements were performed by a thermocamera (FLIR E40, FLIR Systems Inc., OR, USA) and by a needle thermocouple (Omega Engineering Ltd., Stamford, CT). The laser spot size has also been accurately calibrated in order to match the beam size with the photothermally active area. To this aim, a beam expander has been placed on the beam path and the spot size has been measured by recording the power after passing through a variable diameter iris. The final spot size was obtained by fitting the curve of power versus the iris diameter. The petri dish was placed on the sample holder and the laser beam irradiated it from below. During the

irradiation, the petri dishes were maintained at 37°C by a home-made chamber whose temperature was controlled by The Cube (Life Imaging Services, Basel, CH).

4.6. Morphological analysis

Morphology was determined by imaging the cells for 8 days from seeding. Cells were seeded on day 0, and on day 1 images were taken in transmitted light mode; after a recovery of at least 2 hours, they were heated for the first time. The same procedure was repeated on day 2. Electrophysiological recordings were performed on days 7 and 8. Transmitted images were acquired on a Leica SP5 microscope (Leica Microsystems, Wetzlar, D) with an air objective (20X HCX PL Fluoter, Leica Microsystems, Wetzlar, D). Six tiles mode images were acquired to fully cover the irradiated area, where the PBNP-PVA disc was present, or an equivalent one for control and bulk heating samples, in order to acquire images of the same region for the 8 days of the experiment, and a comparative statistical analysis was achieved among different experiments. The images were processed by FIJI ImageJ, version 2.0.0, Opensource code (Schindelin et al., 2012). Neurites were manually traced, then a homemade macro, which subtracts each traced image from the raw one, was run. The new image, on which only the traced neurites were visible, was binary converted and skeletonized. The characteristics of the traced neurites were eventually extracted in a .txt file and statistical analysis were performed.

4.7. Electrophysiological analysis

The functional characterization of the electrophysiological properties of F-11 cells was performed by the patch-clamp technique in the whole-cell configuration. Before recordings, culture medium was replaced by a standard extracellular solution which contained (mM): NaCl 135, KCl 2, $CaCl_2$ 2, $MgCl_2$ 2, hepes 10, glucose 5, pH 7.4. The standard pipette solution contained (mM): potassium aspartate 130, NaCl 10, $MgCl_2$ 2, $CaCl_2$ 1.3, EGTA 10, hepes 10, pH 7.3. Recordings were acquired by the pClamp8.2 software (pClamp,

RRID:SCR_011323) and the MultiClamp 700A amplifier (Axon Instruments; Molecular Devices, LLC., San Jose, CA, USA). Resting membrane potential and action potentials were monitored in the current-clamp mode. In the voltage-clamp mode, the resistance error was compensated up to 50-70%. Sodium (INa) and potassium (IK) currents were recorded by applying a standard voltage protocol, which started from a holding potential of −60 mV, conditioned cells at −90 mV for 500 ms, and successively clamped the membrane at depolarizing test potentials in 10 mV-increments, from −80 to +40 mV. Both round-shaped cells and cells with neurite-like processes were tested for this characterization.

4.8. Lactate-Dehydrogenase (LDH) assay

In order to verify if heating could induce cell stress, we tested cell viability by measuring the lactate-dehydrogenase (LDH) activity on both stimulated and control samples. LDH is an ubiquitous enzyme usually localized in the cytosol and is released into the medium by damaged cells. The samples used for the assay were maintained at -20°C. According to the protocol, they were defrosted in ice, centrifuged at 1000 rpm for 4 minutes and the supernatant was collected for the assay. The total solution volume of 1 ml was made, which contained (µl): K-phosphate Buffer, 850; NADH, 20, and stimulated or control sample, 70. The reaction started by adding 60 µl of Pyruvate. The rate of the absorbance decrease over time was measured and the ratio of LDH activity (U/ml) into the cell culture medium was calculated by using the standard formula.

4.9. Statistical analysis

For the data analysis, Origin 9 (OriginPro, Version 2019, OriginLab corporation, Northampton, MA, USA) and Excel (Microsoft, Redmond, WA, USA) were used. Data are presented as mean ± S.E. Mean comparisons were obtained using the parametric One-Way ANOVA test or the non- parametric Mann-Whitney test. Percentages of cells with spontaneous electrical activity were compared using the x^2 test. The significance level was set for $p \le 0.05$.

5. Results

5.1. Effects of bulk heating: morphological and functional characterization

Experiments in bulk heating were performed to evaluate the eventual effects on the morphology and the electrical activity of F-11 cells. This is a neuroblastoma cell line, which expresses functional properties of mature sensory neurons under appropriate culture conditions (Pastori et al., 2019) or when seeded on matrices mimicking the extracellular environment (Russo et al., 2014). Temperatures ranging from 39°C and 43°C and exposure timing from 10 to 60 minutes were tested. Concerning the morphological properties, the most efficient time/temperature combination was 30 minutes at 41,5°C (Fig. 1 and Supplementary Fig. 1), which induced significant elongation in neurites (about 27% of increase on day 8). On the contrary, the lowest temperature, 39°C, induced no effect on cell morphology, whereas the highest temperature, 43°C, seemed to determine cell suffering which became particularly evident after the fourth day. Since a visible decrease in neurite length and an increase in cell stress/mortality was seen in samples maintained at ≥43°C, chosen temperatures did not exceed 42°C. Moreover, cells at 41,5°C showed the tendency to sprout a higher number of processes than cells in control condition (Fig. 2A). According to the results obtained by morphological analysis, an electrophysiological investigation was performed by the patch-clamp technique, both on cells with neuronal morphology and cells with round shape, to verify if the established protocol could also

116

induce functional differentiation. The electrophysiological parameters investigated were the resting membrane potential, the electrical activity and sodium and potassium current densities. The resting membrane potential was more hyperpolarized in cells exposed at 41,5°C compared to control cells (-42 mV ± 1 mV versus -32 mV ± 2 mV, p<0,001, Mann-Whitney Test). Moreover, in heated cultures a significantly higher percentage of cells with spontaneous activity was present (67% versus 25%, p<0,01, Chi-Square Test) and a higher action potential firing frequency was measured compared to control (4,6 ± 0,7 Hz versus 2,6 ± 0,9 Hz, p<0,05, Mann-Whitney Test) (Fig. 2B, C). Consistently with the electrical activity, heated cells had a trend to express higher sodium and potassium current densities compared to cells maintained at 37°C (Fig. 3). Since these parameters are the hallmarks of neuronal maturation, these results indicate that bulk heating could also induce functional differentiation in the F-11 cell line.

To exclude that this approach could induce cell stress, a lactate-dehydrogenase (LDH) assay was performed. The results, shown in Table 1, suggested that heated cells released in the medium levels of LDH equivalent to control cells (p=0,94, One-Way ANOVA Test, n=8 samples for each condition), indicating that the treatment was not detrimental to F-11 cell survival.

5.2. Smart Petri dish characterization

Considering the efficacy of bulk heating on cell differentiation, the combination of 41,5°C for 30 minutes of exposure was chosen also for inducing a localized and selective stimulation by means of a NIR laser irradiation of PBNP-based polymer layer, applied on the bottom of the petri dishes (smart petri dishes). PBNPs were evenly dispersed in the hosting polymer matrix as it has been verified by imaging the smart layer on the petri dish by means of an optical confocal microscope in reflection mode (Fig. 4). A z-scan performed on the overall extension of the layer revealed a thickness of 90±10 μm in agreement with the estimate obtained with a gauge.

In order to measure accurately the temperature reached within the medium, the exact conditions used in the NIR laser irradiation experiments were reproduced, and a needle thermocouple was mounted and fixed inside the chamber and fed inside the 2 ml solution in the petri dish by a custom drilled lid. The temperature increase was recorded versus time at different powers in order to select the proper power value necessary to obtain the requested temperature increase. Two examples of the curves obtained are shown in fig. 5. As can be inferred from the figure, after 2 minutes an equilibrium temperature was reached and it was maintained for all the irradiation time. The plateau value depends on the irradiation intensity and the nanoparticle concentration.

5.3. Effects of thermal increase by PBNP irradiation

During the irradiation procedure, petri dishes were maintained in a box at 37°C. The temperature of 41,5°C was reached only on the PBNP-PVA disc by using the laser beam. Cultures maintained at 37°C in incubator were used as control. The morphological characterization showed that irradiated cells had longer neurites compared to control especially on day 7 and 8 (Fig. 6A, B) as already found in bulk heating experiments. Moreover, stimulated cells showed an increase in mean neurite number starting from day 2 and especially on day 2 and 3 compared to the control (Fig. 6C), suggesting that this method of thermal stimulation could induce neuronal differentiation.

A control experiment in which cells were irradiated without the support of PBNPs was performed to verify if the use of NIR laser could induce differentiation by itself. Cells irradiated without PBNPs had a trend comparable to the control on all days of the experiment; moreover, they had shorter neurites compared to cultures irradiated with PBNPs, suggesting that the single NIR laser did not induce differentiation of F-11 cells (Supplementary Fig. 2A).

Furthermore, in order to verify the highest temperature the cells could tolerate, we irradiated samples at 43°C. After being irradiated at this temperature, cells showed shorter

neurites compared to the control (Supplementary Fig. 2B) for all the examined time points. Interestingly, although the number of cells seeded on day 0 was the same in each petri dish (5×10^4 cells), in 43°C-treated samples, starting from day 4, cells attached in the middle of the irradiated PBNP- PVA disc were fewer, suggesting that this temperature caused excessive cellular stress.

Irradiated cells at 41,5°C had a typical neuronal morphology and were able to form several small neuronal networks. In order to verify the eventual development of the typical properties of electrically mature neurons, we performed an electrophysiological investigation on day 7.

Irradiated cells had a resting membrane potential more hyperpolarized compared to the control (-39 ± 1 mV versus -30 ± 2 mV, p<0,001, Mann-Whitney Test) and a higher action potential firing frequency (5,9 ± 0,5 Hz versus 2,5 ± 0,5 Hz, p<0,001, Mann-Whitney Test, Fig. 7A) compared to control cells. Moreover, in irradiated cultures a significantly higher percentage of cells with spontaneous activity was found (68% versus 19%, p<0,001, Chi-Square Test, Fig. 7A). Cells exposed to the thermal increase showed a higher sodium current density (110 ± 11 pA/pF versus 80 ± 11 pA/pF, p≤0,05, One-Way ANOVA Test) and a trend to a higher potassium current density compared to control cells (Fig. 7B). These results confirm that thermal increase by irradiated PBNPs could induce a functional differentiation in F-11 cell line.

As for the cultures exposed to bulk heating, the LDH assay was performed both on irradiated and control samples on day 7 and 8. The analysis showed that LDH levels in the medium of thermally stimulated cultures were not significantly different from the control, indicating that this treatment did not impair cell viability (p=0,11, One-Way ANOVA Test, n=8 samples for each condition).

6.   Discussion

In this paper, we showed the effect of a new approach for in vitro neuronal scalable thermal stimulation, constituted by irradiating PBNPs by a NIR laser. PBNPs were embedded in a PVA disc stuck on the outer surface of the petri dish, in which cells to be stimulated were maintained in culture. By this approach we demonstrated that a temperature increase at 41,5°C for 30 minutes, repeated for two days, was efficient to induce neuronal differentiation of F-11 cells, an in vitro model of DRG neurons. Neuronal differentiation was investigated and demonstrated by both morphological and functional analysis. Cell imaging for 8 days after seeding showed that neurites had a trend to increase in number and were significantly longer in thermally stimulated cultures compared to the control. Moreover, electrical properties (resting membrane potential, Na^+ and K^+ current densities, action potential firing frequency and spontaneous activity), recorded on days 7 and 8, also reached values characteristic of mature neurons, confirming that thermally stimulated cultures acquired a significant functional differentiation compared to control cultures. These results indicate that the new approach of thermal stimulation we propose could induce long-term modifications (maintained for at least 8 days) of neuronal properties without the support of genetics or chemical compounds.

The modifications observed in cell membrane properties and in electrical activity of F-11 cells after thermal stimulation could be due, beside other factors, to certain thermo-sensitive channels, whose activation induces a Ca^{2+} influx, which induces several biochemical pathways into the cell (Xiao et al., 2011). In particular, thermosensitive transient receptor potential vanilloid channels TRPV are known to be involved in the chain reaction generated by INS (Albert et al., 2012) and are activated by different temperatures, from noxious heat to noxious cold (Huang et al., 2006). It has been demonstrated that TRPV1 channels, which are activated at temperatures above 41°C, can be triggered by heating induced by nanoparticles in hippocampal neurons (Huang et al., 2010). These channels are permeable to Ca^{2+} and Na^+ and their higher expression or persistent

activation could induce depolarization and changes in the cell membrane capacitance (Kitamura et al., 2018). TRPV3 channels, which are activated at temperatures above 39°C, could also be involved in this process.

Since brain is one of the most temperature-sensitive organs, infrared laser has already been used to stimulate neurons, alone or in combination with nanoparticles (Yong et al., 2014; Carvalho- De-Souza et al., 2015). However, in several previous studies, the effects obtained on neurons consisted in transient variations of cell properties (membrane depolarization, action potential firing modulation). Some articles showed significant changes in the morphology, which are maintained for few days, but no electrophysiological analysis has been performed to demonstrate functional modifications. Moreover, in articles showing the capability of thermal stimulation to induce neuronal differentiation, cell culture media were enriched with differentiating components or factors, preventing the isolation of the real efficacy of temperature increase (Jung et al., 2021).

PBNPs are versatile tools endowed with photothermal effect and are excellent candidates for in vivo treatments due to their biocompatibility and biodegradability. PBNPs have been explored so far for imaging and chemotherapy, especially for their cancer cell-killing ability (Wang et al., 2013), and their biostability and capability to convert light into heat allow their employment in the field of the regenerative medicine.

In this work, our decision to develop a polymer matrix, which embed the photothermal nanoparticles thereby obtaining a "smart" petri dish supporting cell culturing, has the large advantage to avoid any contact with the cells, and also to allow the design of a precise and required geometry of the active heating area, thereby inducing differentiation on a selected region of the cell culture. Moreover, with this approach, the irradiation temperature can be finely tuned and selected by a calibration of the laser spot size and power on one hand, and the photothermal particle concentration in the smart region on the other.

The ability to induce neuronal differentiation by means of a scalable heating opens up new possibilities to treat peripheral nerve injuries and/or neurodegeneration. Among the techniques available, surgery, cell-based therapy and optogenetics are the most used so far. Surgery is the most common therapy, but in general the functional recovery does not exceed 50% of patients and the intervention could lead to neuronal atrophy (Hussain et al., 2020). Cell-based therapy is a promising approach, but is an invasive process, and safety cell preparations are time-consuming and expensive (Hussain et al., 2020). Optogenetics, in which neurons are genetically modified with light-sensitive ion channels, has gained great interest in the last years, but it requires gene transfection into neuronal cells which has several limits: the expression efficiency is spatially heterogeneous, the high expression rate could lead to toxic accumulation of protein within the tissue, and the light could be refracted or absorbed by the multiple tissue layers (Maimon et al., 2017). The approach described in this paper has several advantages: it has no direct contact with cells, the preparation is quite fast and economic and the ability of the nanoparticles to convert the light into heat allows to use the NIR laser at a low potency compared to the laser alone. In the perspective of the clinical translatability of this approach and its potential application in the biomedical field, other cellular models should be considered to verify the reproducibility of the effects described in this paper. Moreover, in vitro models of nerve injuries already available for studying peripheral nerve regeneration, such as DRG/Schwann co-coltures, embryonic spinal cord motor neurons, pluripotent stem cells or organotypic models (Geuna et al., 2015), would provide a reliable confirmation of the efficacy of the approach and would permit the investigation of the molecular mechanisms underlying the neuronal differentiation induced by this scalable thermal stimulation technique.

7. Conclusions

In this paper, we show for the first time a novel method to induce neuronal differentiation by using a combination of light sensitive nanoparticles and NIR laser that we applied with success on a neuroblastoma cell line, maintained in culture without chemical differentiating agents or genetic techniques and without any contamination with the photothermal material. The smart matrix delivering heat can be tuned to the temperature/shape needed for the region to be stimulated. Results showed that targeted heating could be a promising approach for in vivo therapy to induce neurite outgrowth and neuronal behavior modifications.

10. Competing Interests

Stefania Blasa, Mykola Borzenkov, Piersandro Pallavicini, Maddalena Collini, Giuseppe Chirico and Marzia Lecchi are inventors of the nanoparticles-near infrared laser technology that induces cell differentiation mentioned in this publication. The patent application was filed by Botti & Ferrari S.p.A. in accordance with the conflict of interest policy. The other authors, Valentina Pastori and Lavinia Doveri, do not have any competing interests.

11. References

Akhavan, O., Ghaderi, E., Shirazian, S.A., 2015. Near infrared laser stimulation of human neural stem cells into neurons on graphene nanomesh semiconductors. Colloids Surf B Biointerfaces. 2015 Feb 1;126:313-21. https://doi.org/10.1016/j.colsurfb.2014.12.027

Albert, E.S., Bec, J.M., Desmadryl, G., Chekroud, K., Travo, C., Gaboyard, S., Bardin, F., Marc, I., Dumas, M., Lenaers, G., Hamel, C., Muller, A., Chabbert, C., 2012. TRPV4 channels mediate the infrared laser-evoked response in sensory neurons. J Neurophysiol. 2012 Jun;107(12):3227- 34. doi: 10.1152/jn.00424.2011. Epub 2012 Mar 21. PMID: 22442563

Borzenkov, M., DAlfonso, L., Polissi, A., Sperandeo, P., Collini, M., Dacarro, G., Taglietti, A., Chirico, G., Pallavicini, P., 2019. Novel photothermally active polyvinyl alcohol-prussian blue nanoparticles hydrogel films capable of eradicating bacteria and mitigating biofilms. Nanotechnology 30 no. 29, 295702. doi: 10.1088/1361-6528/ab15f9

Carvalho-de-Souza, J.L., Treger, J.S., Dang, B., Kent, S.B.H., Pepperberg, D.R., Bezanilla, F., 2015. Photosensitivity of Neurons Enabled by Cell-Targeted Gold Nanoparticles, Neuron, Volume 86, Issue 1, Pages 207-217, ISSN 0896-6273. https://doi.org/10.1016/j.neuron.2015.02.033

Dacarro, G., Grisoli, P., Borzenkov, M., Milanese, C., Fratini, E., Ferraro, G., Taglietti, A., Pallavicini, P., 2017. Self-assembled monolayers of Prussian blue nanoparticles with

photothermal effect. Supramolecular Chemistr. 29:11, 823-833. doi: 10.1080/10610278.2017.1372582

Eom, K., Kim, J., Choi, J.M., Kang, T., Chang, J.W., Byun, K.M., Jun, S.B. and Kim, S.J.,2014. Enhanced Infrared Neural Stimulation using Localized Surface Plasmon Resonance of Gold Nanorods. Small, 10: 3853-3857. https://doi.org/10.1002/smll.201400599

Gautam, M., Poudel, K., Yong, C.S., Kim, O.J., 2018. Prussian blue nanoparticles: Synthesis, surface modification, and application in cancer treatment. International Journal of Pharmaceutics, Volume 549, Issues 1–2, 31-49, ISSN 0378-5173. https://doi.org/10.1016/j.ijpharm.2018.07.055

Geuna, S., Raimondo, S., Fregnan, F., Haastert-Talini, K., Grothe, C.,2016. In vitro models for peripheral nerve regeneration. Eur J Neurosci, 43: 287-296. https://doi.org/10.1111/ejn.13054

Hossain, M.E., Matsuzaki, K., Katakura, M., Sugimoto, N., Mamun, A.A., Islam, R., et al., 2017. Direct exposure to mild heat promotes proliferation and neuronal differentiation of neural stem/progenitor cells in vitro. PLoS ONE 12(12): e0190356. https://doi.org/10.1371/journal.pone.0190356

Huang, H., Delikanli, S., Zeng, H. et al., 2010. Remote control of ion channels and neurons through magnetic-field heating of nanoparticles. Nature Nanotech 5, 602–606. https://doi.org/10.1038/nnano.2010.125

Huang, J., Zhang, X., McNaughton, P.A.., 2006. Modulation of temperature-sensitive TRP channels. Semin Cell Dev Biol. 2006 Dec;17(6):638-45. doi: 10.1016/j.semcdb.2006.11.002. Epub 2006 Nov 11. PMID: 17185012

Hussain, G., Wang, J., Rasul, A., Anwar, H., Qasim, M., Zafar, S., Aziz, N., Razzaq, A., Hussain, R., de Aguilar, J.L.G., Sun, T., 2020. Current Status of Therapeutic Approaches against Peripheral Nerve Injuries: A Detailed Story from Injury to Recovery. Int J Biol Sci 2020; 16(1):116-134. doi:10.7150/ijbs.35653

Jung, S., Harris, N., Niyonshuti, I.I., Jenkins, S.V., Hayar, A.M., Watanabe, F., Jamshidi-Parsian, A., Chen, J., Borrelli, M.J., Griffin, R.J., 2021. Photothermal Response Induced by Nanocage- Coated Artificial Extracellular Matrix Promotes Neural Stem Cell Differentiation. Nanomaterials 2021, 11, 1216. https://doi.org/10.3390/nano11051216

Kitamura, N., Nagami, E., Matsushita, Y., Kayano, T.,i Shibuya, I., 2018. Constitutive activity of transient receptor potential vanilloid type 1 triggers spontaneous firing in nerve growth factor- treated dorsal root ganglion neurons of rats, IBRO Reports, Volume 5, 2018, Pages 33-42, ISSN 2451-8301, https://doi.org/10.1016/j.ibror.2018.08.002

Kudo, T-a., Kanetaka, H., Mochizuki, K., Tominami, K., Nunome, S., Abe, G., et al., 2015. Induction of Neurite Outgrowth in PC12 Cells Treated with Temperature-Controlled Repeated Thermal Stimulation. PLoS ONE 10(4): e0124024. https://doi.org/10.1371/journal.pone.0124024

Lewinski, N., Colvin, V., Drezek, R., 2008. Cytotoxicity of Nanoparticles. Small, 4: 26-49. https://doi.org/10.1002/smll.200700595

Maimon, B.E., Zorzos, A.N., Bendell, R., Harding, A., Fahmi, M., Srinivasan, S., Calvaresi, P., Herr, H.M., 2017. Transdermal optogenetic peripheral nerve stimulation. J. Neural Eng. 14 034002. https://doi.org/10.1088/1741-2552/aa5e20

Pallavicini, P., Chirico, G., Taglietti, A., 2021. Harvesting light to produce heat: photothermal nanoparticles for technological applications and biomedical devices. Chem. Eur. J. 27, 15361- 15374. Doi: 10.1002/chem.202102123

Pastori, V., D'Aloia, A., Blasa, S., Lecchi, M., 2019. Serum-deprived differentiated neuroblastoma F-11 cells express functional dorsal root ganglion neuron properties. PeerJ, 7:e7951. doi: 10.7717/peerj.7951

Patra, C.R., 2016. Prussian blue nanoparticles and their analogues for application to cancer theranostics. Nanomedicine 2016 11:6, 569-572. Doi: 10.2217/nnm.16.16

Paviolo, C., Thompson, A.C., Yong, J., Brown, W.G., Stoddart, P.R., 2014. Nanoparticle-enhanced infrared neural stimulation. J Neural Eng. 2014 Dec;11(6):065002

Paviolo, C., Stoddart, P.R., 2015. Metallic nanoparticles for peripheral nerve regeneration: is it a feasible approach? Neural Regen Res. 2015 Jul;10(7):1065-6

Paviolo, C., Haycock, J.W., Yong, J., Yu, A., Stoddart, P.R. and McArthur, S.L., 2013. Laser exposure of gold nanorods can increase neuronal cell outgrowth. Biotechnol. Bioeng., 110: 2277- 2291. https://doi.org/10.1002/bit.24889

Platika, D., Boulos, M.H., Baizer, L., Fishman, C.M., 1985. Neuronal traits of clonal cell lines derived by fusion of dorsal root ganglia neurons with neuroblastoma cells. Proceedings of the National Academy of Sciences of the United States of America. 82. 3499-503. 10.1073/pnas.82.10.3499. doi: 10.1073/pnas.82.10.3499

Russo, L., Sgambato, A., Lecchi, M., Pastori, V., Raspanti, M., Natalello, A., Doglia, S.M., Nicotra, F., Cipolla, L., 2014. Neoglucosylated collagen matrices drive neuronal cells to differentiate. ACS Chem Neurosci. 2014;5(4):261-265. doi:10.1021/cn400222s

Schindelin, J., Arganda-Carreras, I., Frise, E. et al., 2012. "Fiji: an open-source platform for biological-image analysis", Nature methods 9(7): 676-682, PMID 22743772. https://doi.org/10.1038/nmeth.2019
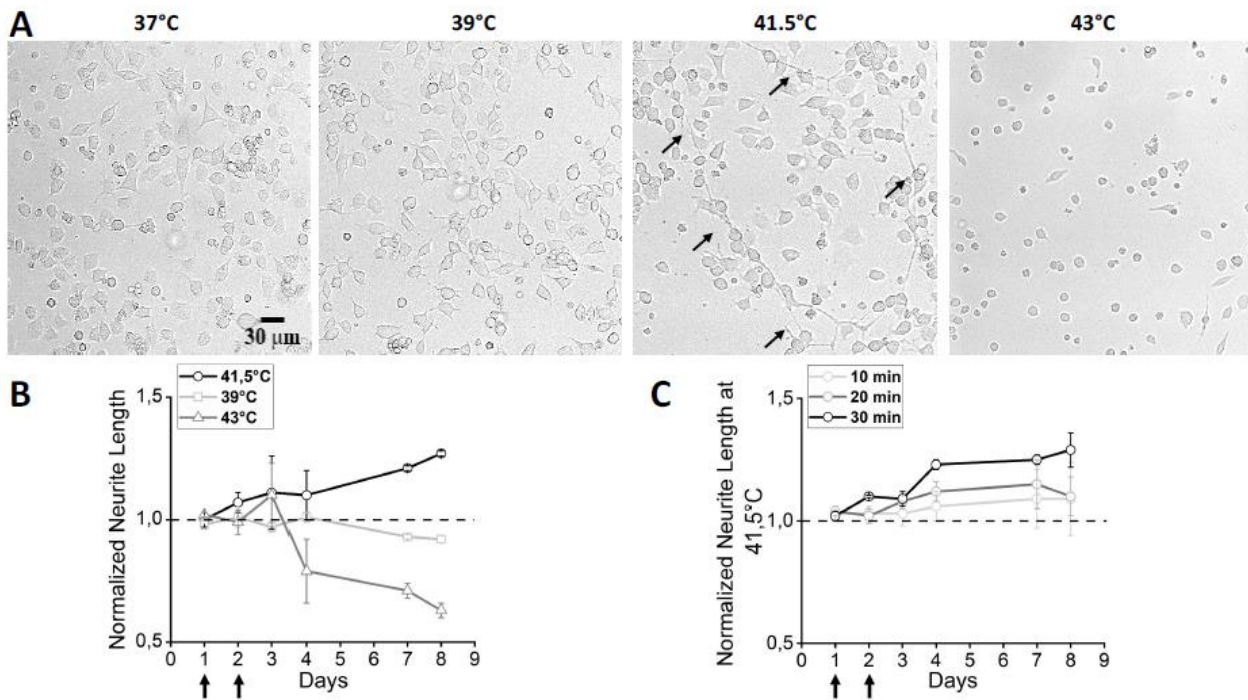
12. Figures and legends

Figure 1: Morphological properties of F-11 cells exposed to bulk heating. A) Representative images of cells at day 8, after exposure to bulk heating for 30 minutes at different temperatures. At 39°C, cells did not show significant differences with control cells (37°C), whereas, at 41,5 °C, an increase in neurite length (black arrows) was evident. Temperatures higher than 41,5°C (43°C) had detrimental effect on cell viability. B) Neurite length normalized to the value of the control group on one day after seeding. The different symbols refer to the different temperatures applied for 30 minutes on day 1 and day 2 after seeding (indicated by black arrows). The temperature of 39°C (squares) did not induce any effect on cell morphology compared to the control. In 41,5°C samples (circles) neurites were significantly longer versus the control, starting from day 3 (p <0,001, Mann-Whitney Test). The temperature of 43°C (triangles) seemed to induce cell stress particularly from day 4. C) Normalized neurite length of heated F-11 cells (41,5°C) at different times of exposure. 10 minutes of exposure at 41,5°C did not induce any effect on cell morphology compared to the control. Cells maintained at 41,5°C for 20 minutes showed neurites significantly longer versus the control only on day 2 (p=0,01, Mann-Whitney Test) and 4 (p<0,001, Mann-Whitney Test). Cells maintained

at 41,5°C for 30 minutes showed neurites significantly longer compared to the control starting from day 2 and for all the other days of the experiment (p<0,001, Mann-Whitney Test).
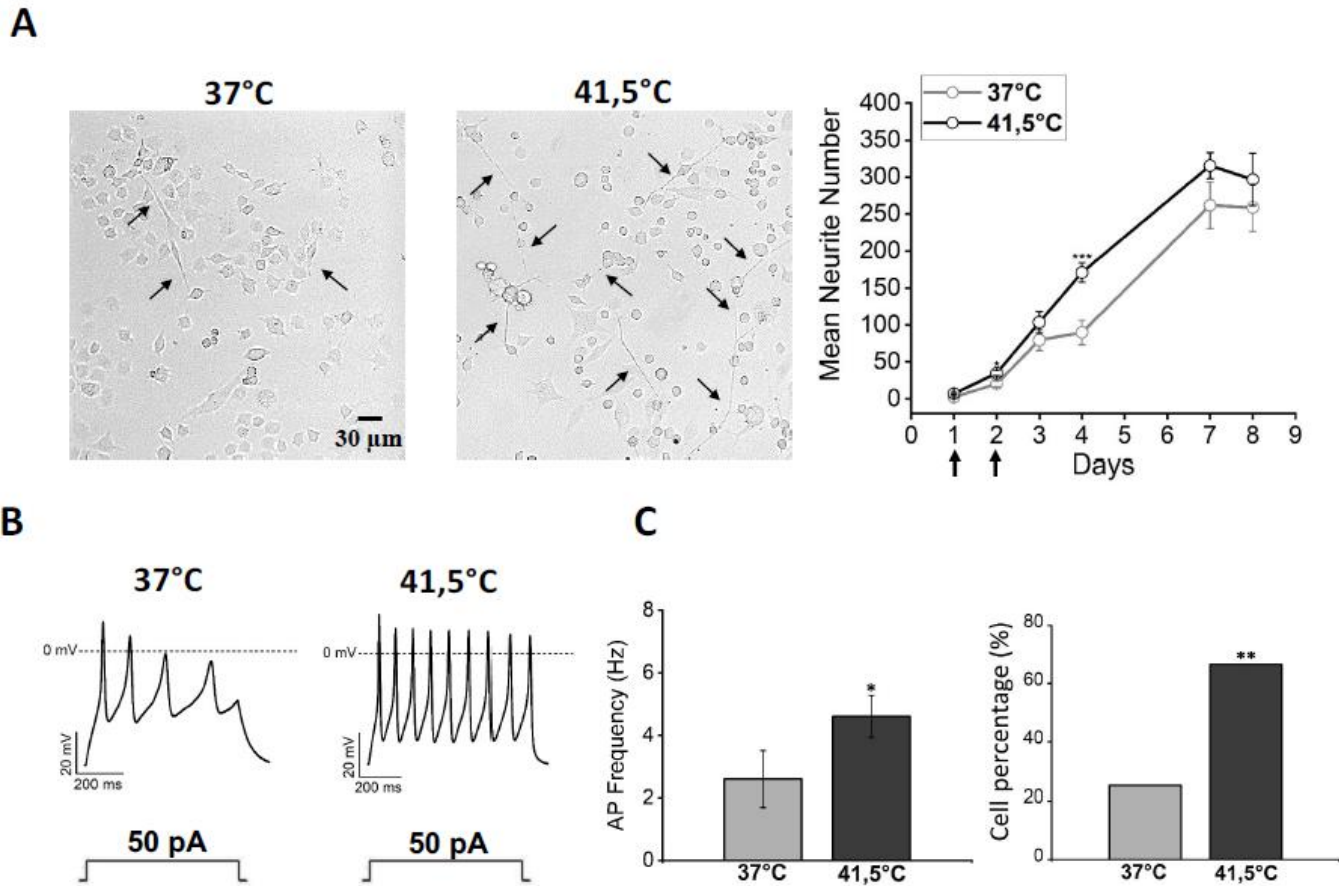

Figure 2: Morphological and electrophysiological properties of F-11 cells thermally stimulated at 41,5°C for 30 minutes. A) Cells heated at 41,5°C on day 1 and day 2 after seeding showed more numerous and significantly longer neurites (black arrows in the picture) compared to control cells maintained at 37°C, and B) showed the ability to discharge spontaneous or induced action potentials at a higher frequency compared to cells maintained at 37°C (for 41,5°C samples: 4,6 ± 0,7 Hz, n=22; for 37°C samples: 2,6 ± 0,9 Hz, n=15; p<0,05, Mann-Whitney Test). C) Moreover, 41,5°C samples had a higher percentage of cells with spontaneous activity compared to the control, indicating that thermally stimulated cultures had higher probability to develop small neuronal networks (for 41,5°C samples: 67%, n=16/24; for 37°C samples: 25%, n=4/16, p<0,001, Chi-Square Test).
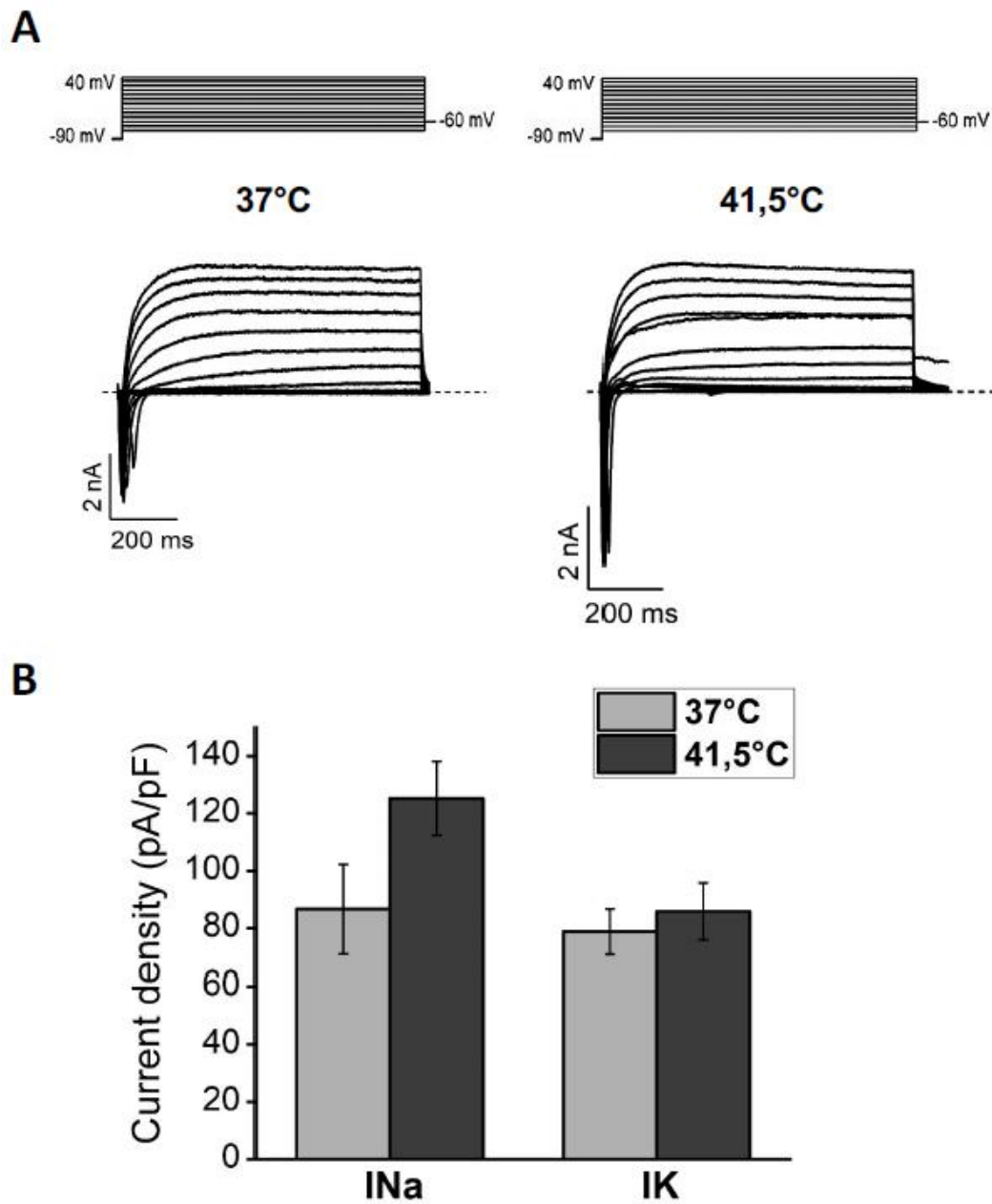
Figure 3: Functional analysis of F-11 cell electrophysiological properties by the patch-clamp technique on days 7 and 8 showed a more differentiated profile for heated cells versus 37°C cells. A) Representative sodium and potassium current traces obtained by the protocol indicated above and described in the Material and Methods section. B) Current density bar graphs; heated cultures showed a trend to express higher sodium and potassium current densities compared to the control (for 41,5 °C samples: I_{Na}, 125 ± 13 pA/pF and I_K, 86 ± 10 pA/pF, n=23; for 37°C samples: I_{Na}, 87 ± 16 pA/pF and I_K, 79 ± 8 pA/pF, n=15; for I_{Na} p=0,11, Mann-Whitney Test, for I_K p=0,94, Mann-Whitney Test).
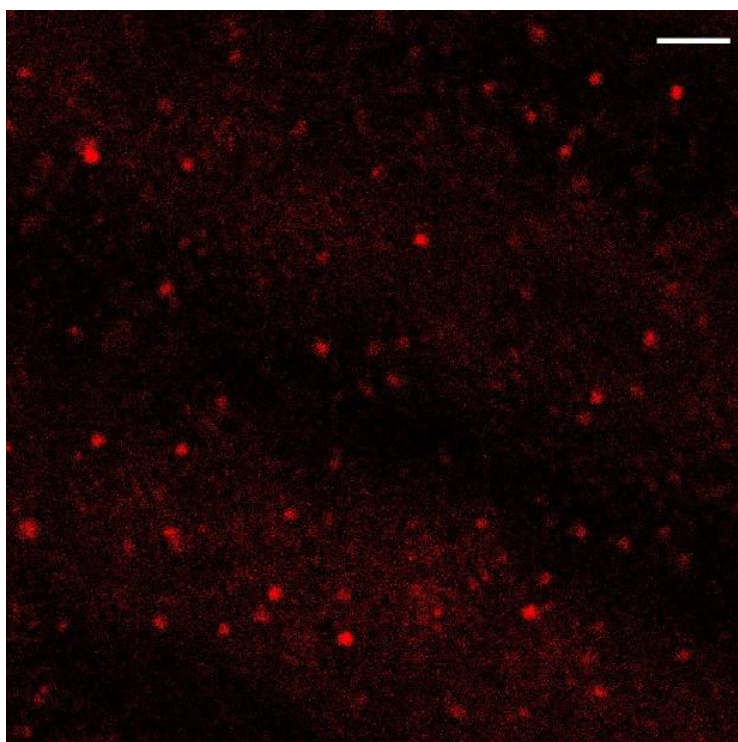
Figure 4: A 30 μm x 30 μm field of view of a selected plane in a z-scan acquisition of the PBNP-PVA smart layer (the bar corresponds to 30 μm). The red spots represent the reflection signal of the PBNPs upon 633 nm excitation.
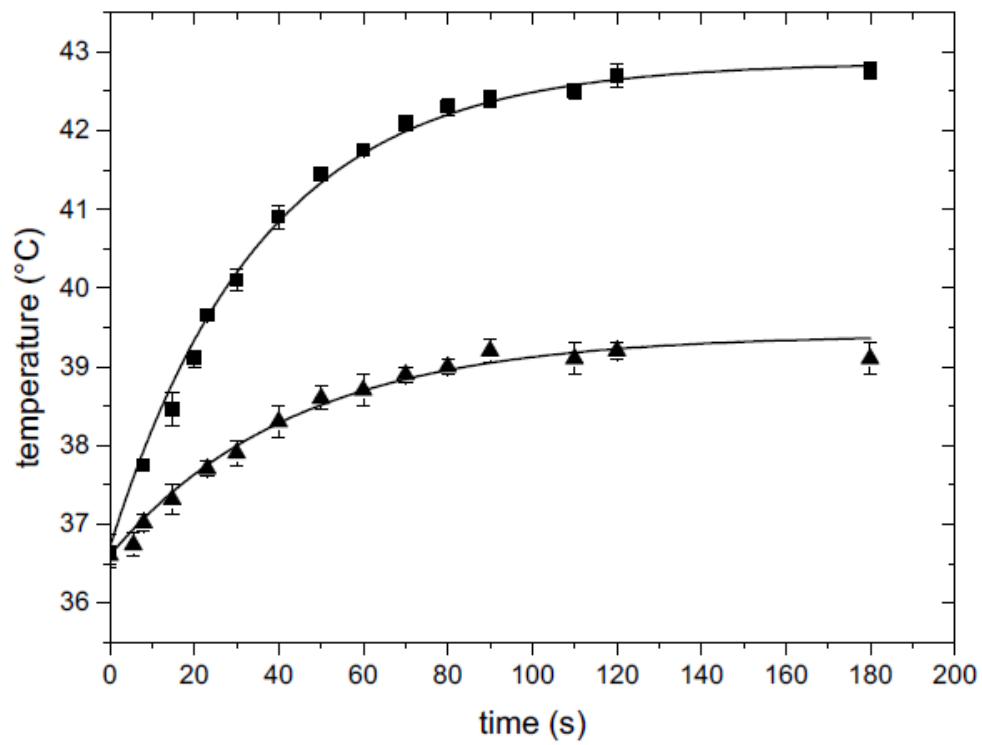
Figure 5: Temperature increase versus irradiation time as measured by a needle thermocouple directly inserted in the Petri dish with 2 ml of solution. Squares I=0.15 W/cm², triangles I=0.07 W/cm².
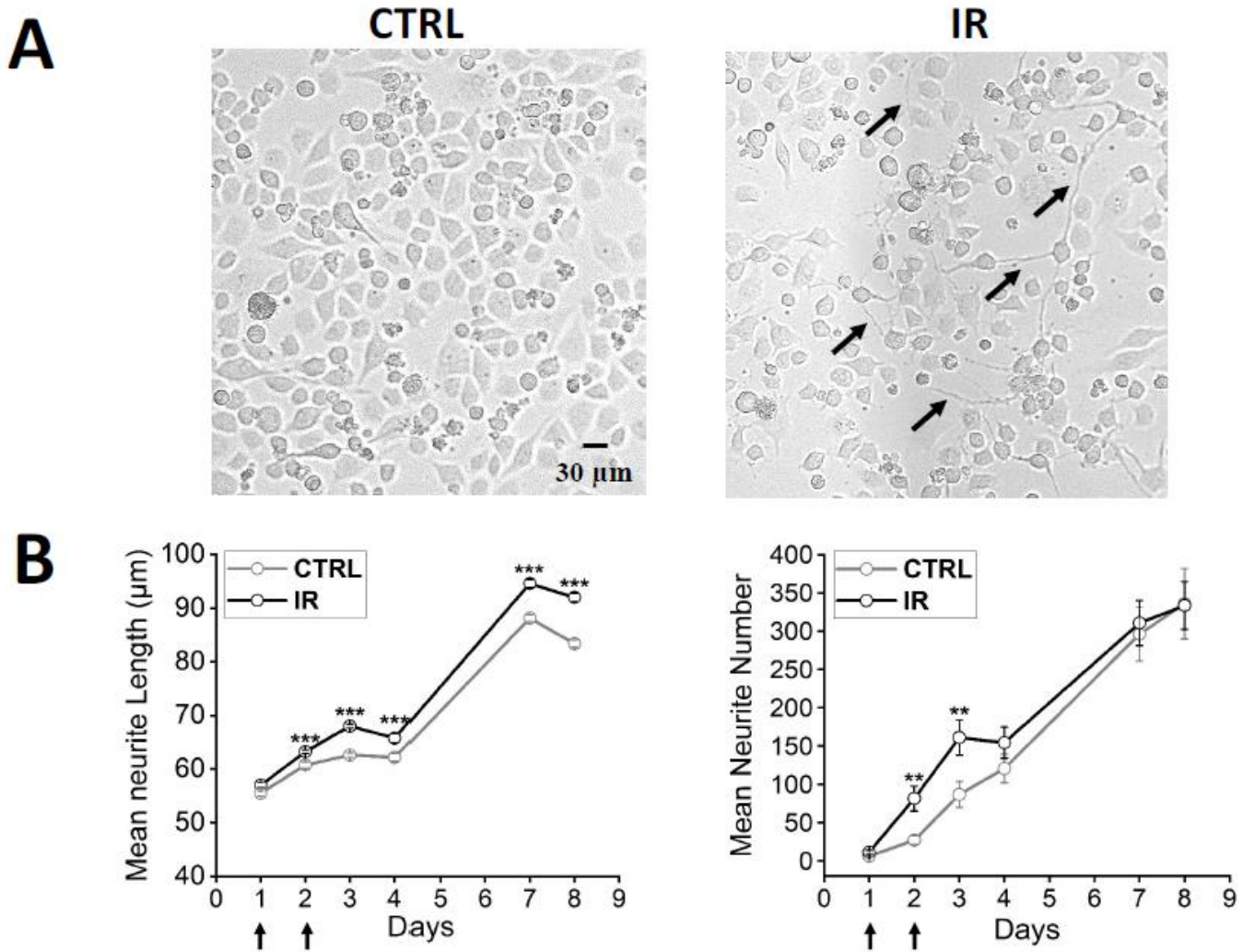
Figure 6: Morphological properties of irradiated F-11 cells. A) Representative images show longer and more numerous neurites in cultures irradiated at 41,5°C (IR) than in cultures maintained at 37°C (CTRL). B) Neurite length of cells irradiated at 41,5°C on day 1 and day 2 after seeding (indicated by black arrows), analyzed from day 1 to day 8, was significantly longer than the control starting from day 2 (p<0,001, Mann-Whitney Test). Moreover, in the irradiated cultures the number of neurites increased starting from day 2, with a significant difference at day 2 and 3 (p<0,01 and p≤0,01, respectively, Mann-Whitney Test).
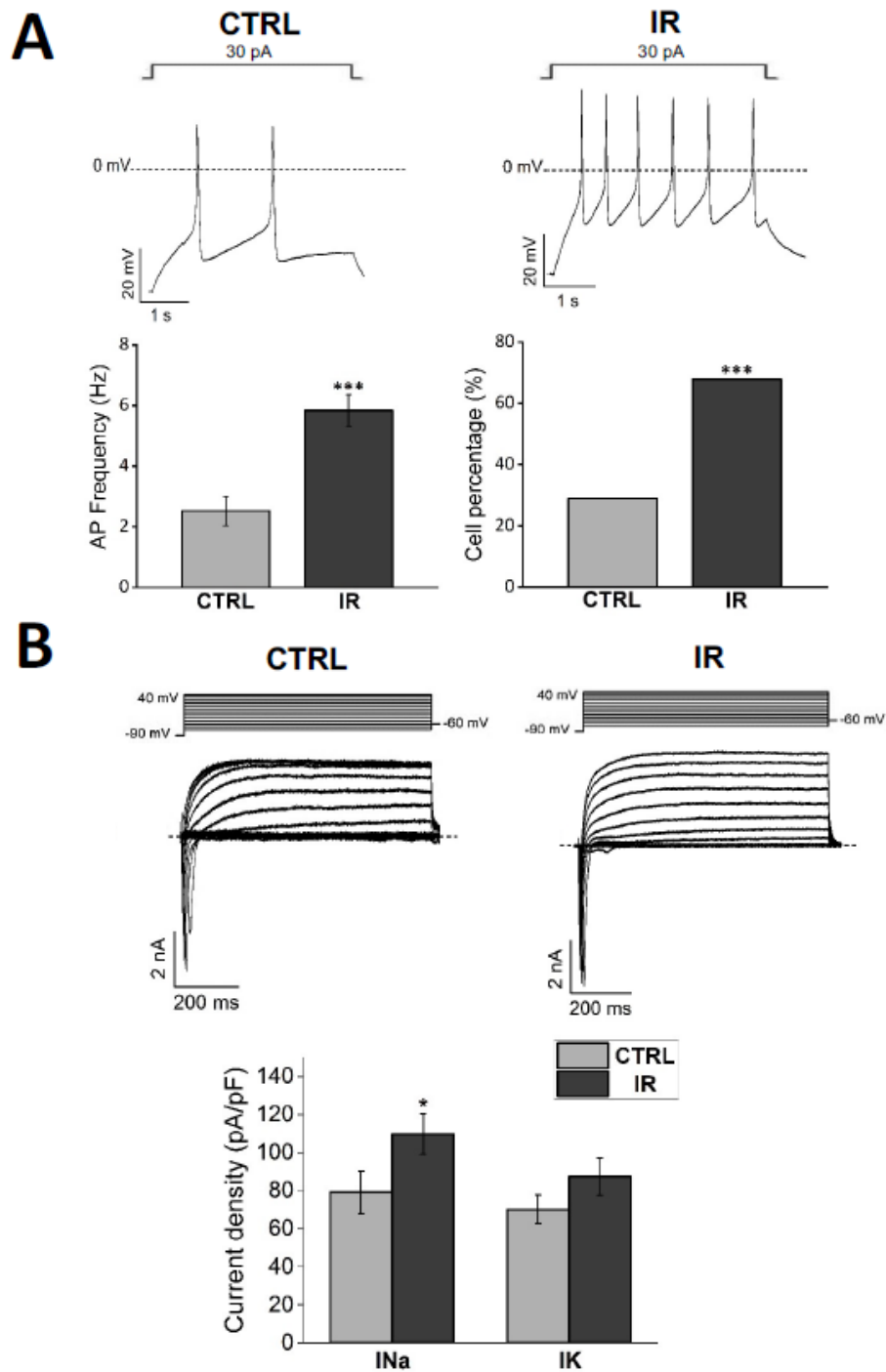
Figure 7: Functional analysis of F-11 cell electrophysiological properties by the patch-clamp technique on days 7 and 8 confirmed a more differentiated profile for stimulated cells (IR) versus 37°C (CTRL). A) Irradiated cultures had higher action potential firing frequency (for irradiated samples: 5,9 ± 0,5 Hz, n=36; for control samples: 2,5±0,5 Hz, n=36; p<0,001, Mann-Whitney Test) and a higher percentage of cells with spontaneous activity compared to the control (for irradiated samples: 68%, n=25/37; for control samples: 19%, n=7/36; p<0,001, Chi-Square Test). B) Stimulated cultures showed a higher sodium current density and a trend to had higher potassium

current density compared to the control (for irradiated samples: I_{Na}, 110 ± 11 pA/pF, and I_K, 87 ± 10 pA/pF, n=32; for control samples: I_{Na}, 80 ± 11 pA/pF and I_K, 70 ± 7 pA/pF, n=31; for I_{Na} p≤0,05, One-Way ANOVA Test, for I_K p=0,31, Mann-Whitney Test).
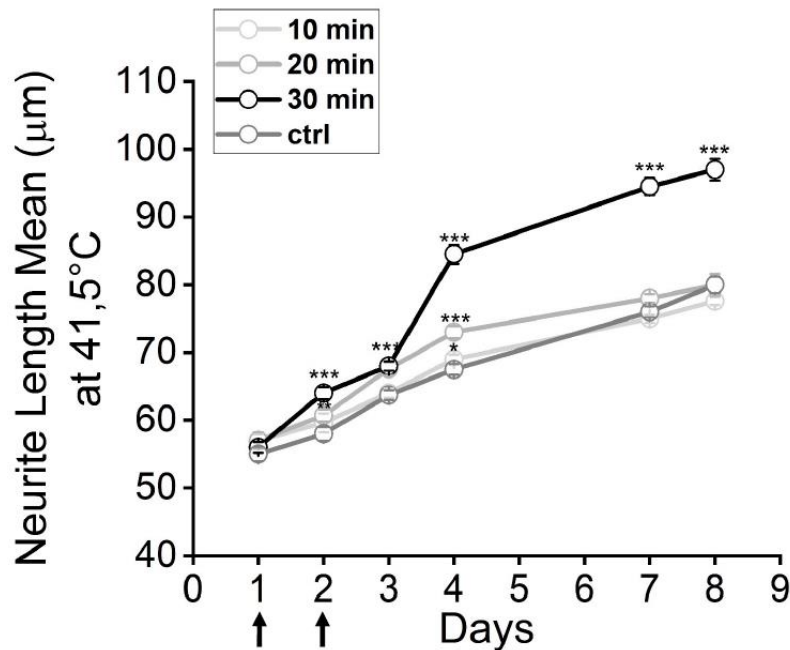
Supplementary Figure 1: Neurite length of heated F-11 cells (41,5°C) on day 1 and day 2 after seeding (black arrows) at different times of exposure: 10 minutes did not induce any effect on cell morphology compared to the control. Cells maintained at 41,5°C for 20 minutes showed neurites significantly longer versus the control only on day 2 (p=0,01, Mann-Whitney Test) and 4 (p <0,001, Mann-Whitney Test). Cells maintained at 41,5°C for 30 minutes showed neurites significantly longer compared to the control starting from day 2 (p<0,001, Mann-Whitney Test).
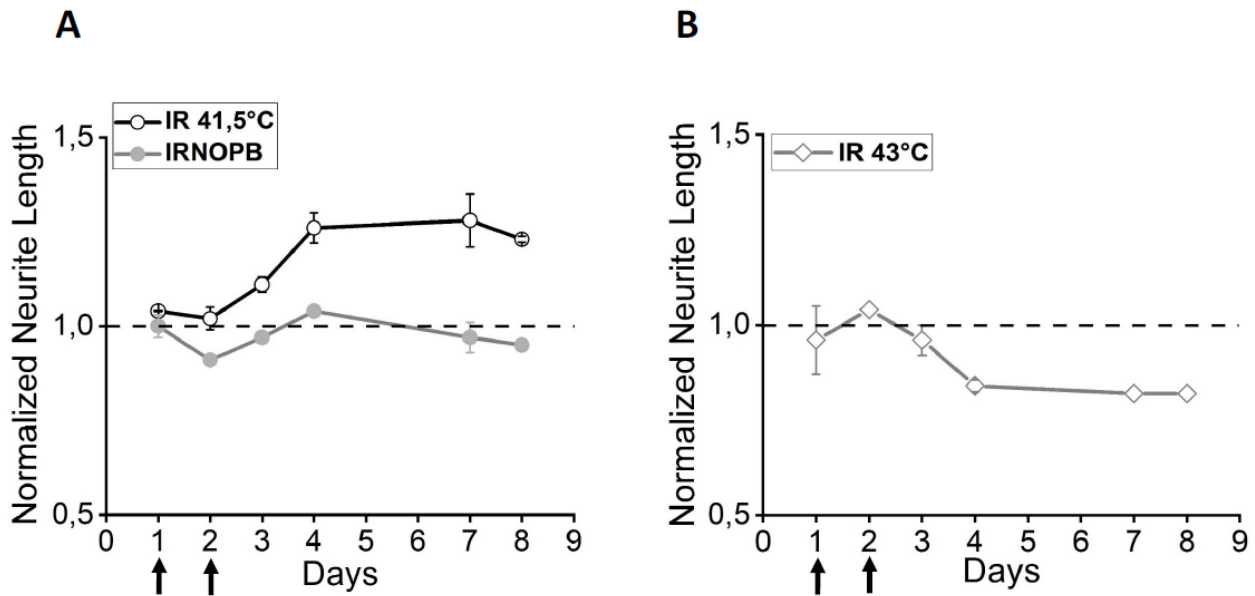
Supplementary Figure 2: A) Morphological properties of irradiated F-11 cells on day 1 and day 2 after seeding (black arrows) with and without PBNPs. Mean neurite length was significantly longer (p<0,001) in irradiated samples with PBNPs compared to both cells irradiated without PBNPs and control. Moreover, cells irradiated without PBNPs showed a trend similar to the control for all the days of the experiment. B) Morphological properties of irradiated F-11 cells at 43°C. Irradiated samples at 43°C showed shorter neurites and seemed to be more stressed compared to the control, which had a neurite length mean significantly longer starting from day 3 (p<0,001, Mann-Whitney Test), as seen in bulk heating experiments.

	Bulk Heating 41,5°C				Thermal Stimulation by IR at 41,5°C			
	37°C	S.E.	41,5°C	S.E.	CTRL	S.E.	IR	S.E.
Day 7-8	$4,98 \times 10^{-8}$	$1,28 \times 10^{-8}$	$4,86 \times 10^{-8}$	$1,16 \times 10^{-8}$	$9,9 \times 10^{-8}$	$1,14 \times 10^{-8}$	17×10^{-8}	$2,18 \times 10^{-8}$

Table 1: Lactate-dehydrogenase activity measured on bulk heated and thermally stimulated cells versus control samples. Results showed that stimulation at 41,5°C did not impair cell viability in 41,5°C cells (p>0,05, One-Way ANOVA Test, n=8 for each condition).

CHAPTER 5: Ongoing experiments

The promising results obtained both from bulk heating and irradiation experiments have brought out the need to investigate more in detail the mechanisms which sustain the acquisition of mature neuronal properties.

For this reason, in this chapter, ongoing experiments are reported, which principally concern:

- analysis of Ca^{2+} signals, to determine the involvement of temperature-sensitive channels;

- recordings of the electrophysiological properties on 12 days, to verify the maintenance of differentiation over a longer period;

- replication of the experiments in culture conditions which are standard for F-11 cell maintenance and proliferation.

1. Results

1.1. Calcium signals

Intracellular calcium variations were analyzed as fluorescence signals. Cells were seeded in 96-well plate at 3000 cells/well in 1% FBS medium. Heating was performed on day 1 and 2 following the same previous protocol. Then, on day 7, fluorescence was measured by incubating cells in 4 μM FLUO-4AM. After 1 hour, cells were washed with 100 μl of standard extracellular solution. The fluorescence was measured by the FLUOStar instrument (FLUOstar Omega Filter-based multi-mode microplate reader, BMG Labtech, Ortenberg, Germany) for 39 seconds in control and during the injection of 3 μM Capsaicin (Sigma-Aldrich, St. Louis, MO, USA). To verify if fluorescence variation during Capsaicin injection could be due to the expression of TRPV1 channels, cells were preincubated with the antagonist Capsazepine 10 μM (Sigma-Aldrich, St. Louis, MO, USA) for 10 and 20 minutes before the acquisition. TRPV1 channels are activated by capsaicin and by heat

above 40°C. Capsaicin evoked an increase in fluorescence, which represented a Ca^{2+} signal, and this signal was higher in heated cells than in control. When heated cells were preincubated with 10 μM Capsazepine, the calcium signal decreased, especially after 20 minutes of preincubation, suggesting that heated cells could present a higher expression of TRPV1 channels.
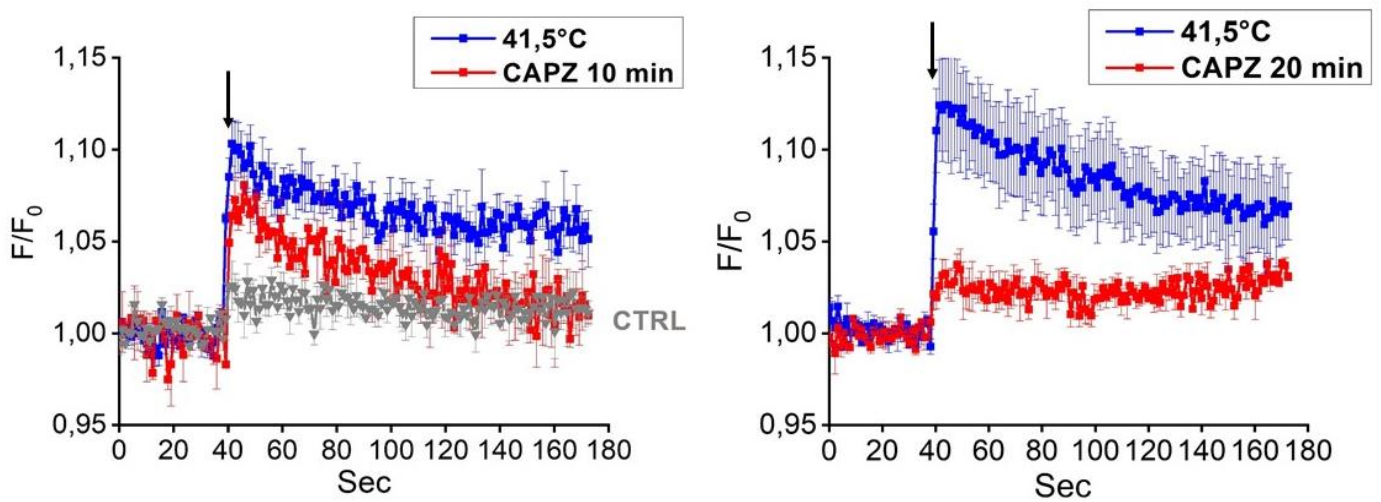

Figure 1: Intracellular Ca^{2+} responses acquired from heated F-11 cells on day 7. Traces illustrate average intracellular Ca^{2+} increases from different wells. Capsaicin could evoke a signal which was higher in heated cells compared to the control. When heated cells were preincubated with Capsazepine, the Ca^{2+} signal decreased especially after 20 minutes of preincubation. These data suggest that Ca^{2+} signals acquired in 41,5°C samples could be due to a higher expression of TRPV1 channels associated to thermal stimulation.

1.2. Long-term analysis of heat-induced differentiation

To analyse the effects of thermal stimulation at long term, F-11 cells were exposed to heating by the same procedure previously described, and electrophysiological properties were investigated on day 12. To verify if the markers/features of differentiation observed on day 7 could be maintained for a longer period, cells were heated on day 1 and 2 after seeding and maintained in culture for 12 days in incubator. The electrophysiological investigation showed that the resting membrane potential, Na$^+$ current density, the action potential firing frequency and the spontaneous activity were not significantly changed compared to heated cultures investigated on day 7, suggesting that cells could maintain the differentiation phenotype acquired on day 7 for a longer period.
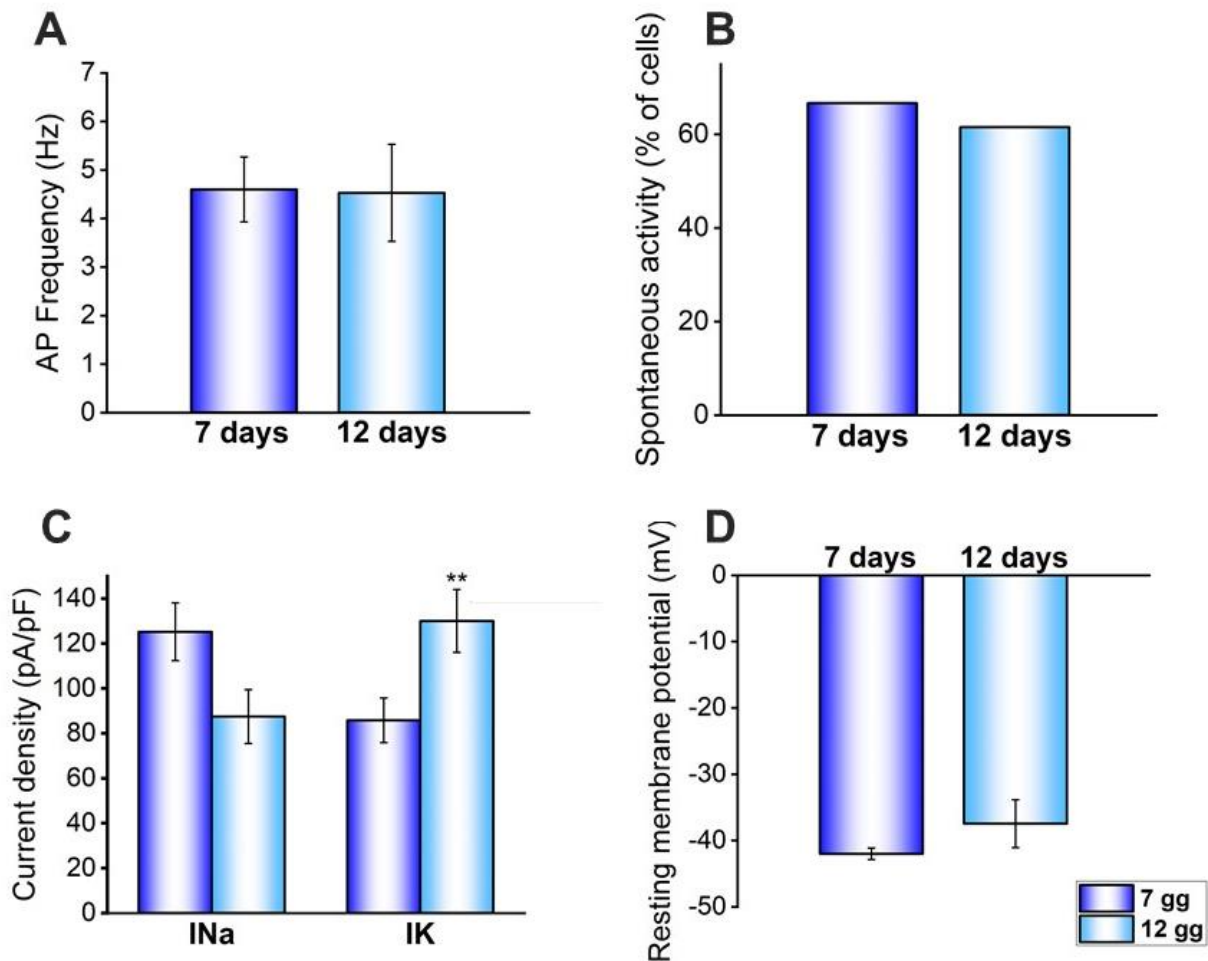
Figure 2: Electrophysiological properties of heated F-11 cells investigated on day 12 and compared to day 7. The action potential firing frequency (A) (for 12 days cells: 4,5 ± 1 Hz, n= 13; for 7 days cells: 4,6 ± 0,7 Hz, n= 24; p=0,9, One-Way ANOVA Test) and the percentage of cells with spontaneous activity (B) (for 12 days cells: 61,5%, n=13; for 7 days cells: 66,7%, n=24; p=0,5, Chi-Square Test) are not significantly different in cultures maintained for 12 days compared to samples investigated on day 7. Moreover, cells maintained in culture for 12 days showed similar Na^+ current density and a significantly higher K^+ current density compared to cells investigated on day 7 (C) (for 12 days cells: I_{Na}, 87,5 ± 12 pA/pF and I_K, 130 ± 14 pA/pF, n=12; for 7 days cells: I_{Na}, 125 ± 13 pA/pF and I_K, 86 ± 10 pA/pF, n=24; for I_{Na} p=0,06, Mann-Whitney Test, for I_K p=0,005, Mann-Whitney Test). The resting membrane potential of cells maintained for 12 days in culture also showed similarity with cells analysed on day 7 (D) (for 12 days cells: -37 ± 4 mV, n=13; for 7 days cells: -42 ± 1, n= 24; p=0,11, One-Way ANOVA Test). These data suggest that the differentiated phenotype acquired on day 7 in heated samples could be maintained for longer period.

1.3. Thermal stimulation on proliferating F-11 cells

In order to verify if differentiation could be ascribed to heating on its own, cells were seeded in a proliferative medium containing Dulbecco's modified Eagle's medium, 2 mM glutamine and 10% fetal bovine serum. Fresh medium was added into the dishes twice per week to prevent cell starvation. On the first and second day after seeding, cells were heated in an incubator set at 41,5°C without CO_2 for 30 minutes, and on the days 7 and 8 electrophysiological analysis were performed to investigate the eventual functional differentiation. Cells seeded at the same density and in the same medium composition, maintained at 37°C, were used as a control. After heating, cells were replaced in an incubator at 37°. Heated cultures showed a higher action potential firing frequency and a higher percentage of cells with spontaneous activity compared to control cultures. Moreover, they had higher Na^+ and K^+ current densities and their resting membrane potential was more hyperpolarized compared to the control. These results further confirm

that heating could induce neuronal differentiation, even in conditions permissive for proliferation.
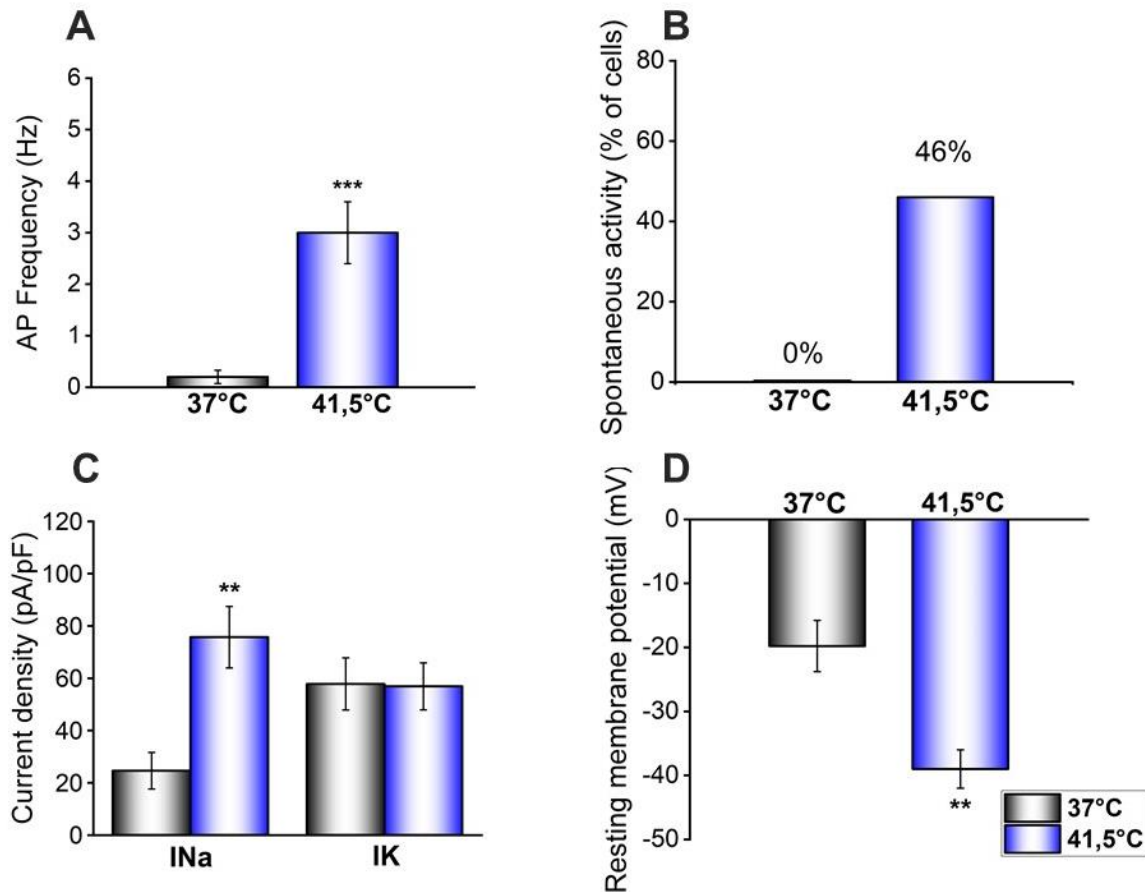

Figure 3: F-11 cells incubated in a standard medium (10% FBS) acquired a more differentiated profile when maintained at 41,5°C. Heated cells showed a significant higher action potential firing frequency (A) (for 41,5°C samples: 3 ± 0,6 Hz, n= 13; for 37°C samples: 0,2 ± 0,13, n= 10; p<0,001, Mann-Whitney Test) and a higher percentage of cells with spontaneous activity (B) (for 41,5°C samples: 46%, n= 13; for 37°C samples: 0%, n= 10, p=0,01, Chi-Square Test) compared to the control. Moreover, heated samples had a significantly higher Na^+ current densities compared to 37°C samples (C) (for 41,5°C samples: I_{Na}, 76 ± 12 pA/pF and I_K, 57 ± 9 pA/pF, n= 13; for 37°C: I_{Na}, 25 ± 7 pA/pF and I_K, 58 ± 10 pA/pF, n= 10; for I_{Na} p=0,005, Mann-Whitney Test, for I_K p=0,9, One-Way ANOVA Test). Cells maintained in 10% FBS medium showed a resting membrane potential more hyperpolarized compared to the control (D) (for 41,5°C samples: -39 ± 3 mV, n=14; for 37°C samples: -19 ± 4, n= 10; p=0,002, One-Way ANOVA Test).

CONCLUSIONS, OUTLOOKS AND FUTURE PERSPECTIVES

Peripheral nerve injuries represent one of the most important problems in public health and occur in up to 3% of all patients admitted in trauma centres. As the neural tissue has a limited regenerative ability, it needs supportive technologies and approaches for its repair. Among the different techniques developed for this purpose, surgery is still the most common intervention for injured patients, although several approaches have been designed in the last years to be placed by side of surgery or as an alternative to it.

Surgical approaches involve nerve grafting and conduits, direct nerve repair, nerve transfer, fibrin glue and cell-based therapy. Although these approaches can be useful for treating these injuries, they have many drawbacks. Nerve grafts and nerve conduits have the risk of site morbidity, loss of nerve function, neuroma formation and are expensive and difficult to perform. Direct nerve repair and nerve transfer could lead to a non-correct match of the nerve after the suture and to a loss of nerve function. The use of fibrin glue includes the risk of infection in patients, whereas cell-based therapy could lead to toxicity and it is still an invasive approach.

Non-surgical approaches include medications, such as corticosteroids, analgesics or opioids, which often calm the pain but cannot accelerate nerve regeneration or functional recovery; or phytochemical agents, like quercetin, curcumin or soy bean fermentation extracts, which could have neuroprotective and antinflammatory effects but are still under study to verify their effectiveness in functional recovery. Another approach is the electrical stimulation, that can be used as a remote application or through implants, but is limited by the risk of infection, the risk of losing effectiveness of the stimulator and the cost of additional implantation after battery failure.

Optogenetics is also a promising technique, but is often invasive, the opsin expression in the tissue is spatially heterogeneous, it could lead to accumulation of toxic products in the tissue and there are risks of immunogenicity due to the viral particles used. In the Infrared stimulation therapy (INS), the laser beam could be refracted or absorbed by the fluids and

the multiple tissue layers in the body, and for this reason a high intensity of the laser is often required.

Heating has proved to be a promising technique to induce cell differentiation, but it could lead to a risk of burn and is difficult to set-up in view of an *in vivo* treatment.

In this work, a novel method to induce a targeted and scalable heating was established, which involves the use of a near infrared laser and specific nanoparticles, safe and versatile, that can convert the light of the laser into heat. This combination of tools allows to avoid some drawbacks of the other techniques such as invasiveness, cytotoxicity, site morbidity and the loss of penetration depth of the laser beam, which can be used at a low intensity with a high efficacy, preventing also burns or scars. This method could induce morphological and functional neuronal differentiation *in vitro*, and it might be promising for nerve regeneration after injury. Moreover, it might be used both for biomedical research, as a new nerve regeneration treatment, and at industrial level, as a novel tool for basic research (i.e., 3D-printed Prussian Blue nanoparticle "smart" dishes).

This new approach has clearly some limits that need to be overcome in the perspective of its future application *in vivo*. First, the method should be applied on different *in vitro* models, to verify if the effects are reproducible/repeatable on different types of cells other than F-11 cell line. In this regard, neural stem cells and fibroblasts, that play a fundamental role in nerve regeneration, in the central and in the peripheral nervous system, would be used to verify if this treatment allows neuronal behavior modifications or differentiation also in these cultures. Moreover, a co-culture with glial cells could lead to more complete and interesting data, simulating the complex environment in which neurons lie.

Concerning the biomaterials, the combination of a biocompatible and easy-to-produce material, such as PVA, with safe and FDA-approved nanoparticles, like PBNPs, is a versatile and reliable way to induce a targeted thermal stimulation from the outer surface,

but, in the actual configuration, we could try also other types of nanoparticles such as GNSTs, or other biomaterials such as chitosan.

Moreover, tests related to the penetration depth and the temperature within the nerve should be done in order to verify if the temperature applied in the culture media could be maintained also through the tissue layers or if it is necessary to modify the parameters. To reach this goal, a fundamental step would be the validation of this technique in animal models. This would allow us to verify the penetration depth and temperature parameters and to confirm this approach as a novel therapeutic method to be employed in the biomedical field. The next future studies will also include gene expression analysis and metabolic assays, to further investigate the functional expression of receptors in the cell membrane; moreover, we have to complete the ongoing studies on proliferative medium and on Ca^{2+} signals.

Taken together, these experiments could lead to an exhaustive characterization of this new technique, opening the possibility to apply it to treat nerve lesions and to allow nerve functional recovery in injured patients.

ACKNOWLEDGEMENTS

PUBLISHED PAPERS ON OTHER PROJECTS

Bianchessi, D.; Ibba, M.C.; Saletti, V.; **Blasa, S**.; Langella, T.; Paterra, R.; Cagnoli, G.A.; Melloni, G.; Scuvera, G.; Natacci, F.; Cesaretti, C.; Finocchiaro, G.; Eoli, M. Simultaneous Detection of NF1, SPRED1, LZTR1, and NF2 Gene Mutations by Targeted NGS in an Italian Cohort of Suspected NF1 Patients. Genes 2020, 11, 671. https://doi.org/10.3390/genes11060671

Article

Simultaneous Detection of *NF1*, *SPRED1*, *LZTR1*, and *NF2* Gene Mutations by Targeted NGS in an Italian Cohort of Suspected NF1 Patients

Donatella Bianchessi [1,†] ![ORCID]**, Maria Cristina Ibba** [1,†]**, Veronica Saletti** [2]**, Stefania Blasa** [1,3] ![ORCID]**, Tiziana Langella** [1,4]**, Rosina Paterra** [1]**, Giulia Anna Cagnoli** [5]**, Giulia Melloni** [2]**, Giulietta Scuvera** [6]**, Federica Natacci** [5]**, Claudia Cesaretti** [5]**, Gaetano Finocchiaro** [1] **and Marica Eoli** [1,*] ![ORCID]

[1] Molecular Neuro-Oncology Unit, Fondazione IRCCS Istituto Neurologico Carlo Besta, via Celoria 11, 20133 Milan, Italy; donata.bianchessi@istituto-besta.it (D.B.); mariacristina.ibba@istituto-besta.it (M.C.I.); s.blasa@campus.unimib.it (S.B.); tiziana.langella89@gmail.com (T.L.); rosina.paterra@istituto-besta.it (R.P.); gaetano.finocchiaro@istituto-besta.it (G.F.)

[2] Developmental Neurology Unit, Fondazione IRCCS Istituto Neurologico Carlo Besta, via Celoria 11, 20133 Milan, Italy; veronica.saletti@istituto-besta.it (V.S.); giulia.melloni@istituto-besta.it (G.M.)

[3] Department of Biotechnology and Biosciences, University of Milano-Bicocca, Piazza dell'Ateneo Nuovo, 1, 20126 Milan, Italy

[4] Molecular Immunology Unit, Department of Research, Fondazione IRCCS Istituto Nazionale dei Tumori, Via Venezian, 20133 Milan, Italy

[5] Medical Genetics Unit, Woman-Child-Newborn Department, Fondazione IRCCS Ca' Granda-Ospedale Maggiore Policlinico, via Francesco Sforza 28, 20122 Milan, Italy; giulia.cagnoli@policlinico.mi.it (G.A.C.); federica.natacci@policlinico.mi.it (F.N.); claudia.cesaretti@policlinico.mi.it (C.C.)

[6] Pediatric Highly Intensive Care Unit, Università degli Studi di Milano, Fondazione IRCCS Ca' Granda Ospedale Maggiore Policlinico, via Francesco Sforza 28, 20122 Milan, Italy; giulietta.scuvera@policlinico.mi.it

* Correspondence: marica.eoli@istituto-besta.it

† These authors contributed equally to this work.

![check for updates]

Abstract: Neurofibromatosis type 1 (NF1) displays overlapping phenotypes with other neurocutaneous diseases such as Legius Syndrome. Here, we present results obtained using a next generation sequencing (NGS) panel including *NF1*, *NF2*, *SPRED1*, *SMARCB1*, and *LZTR1* genes on Ion Torrent. Together with NGS, the Multiplex Ligation-Dependent Probe Amplification Analysis (MLPA) method was performed to rule out large deletions/duplications in *NF1* gene; we validated the MLPA/NGS approach using Sanger sequencing on DNA or RNA of both positive and negative samples. In our cohort, a pathogenic variant was found in 175 patients; the pathogenic variant was observed in *NF1* gene in 168 cases. A *SPRED1* pathogenic variant was also found in one child and in a one year old boy, both *NF2* and *LZTR1* pathogenic variants were observed; in addition, we identified five *LZTR1* pathogenic variants in three children and two adults. Six *NF1* pathogenic variants, that the NGS analysis failed to identify, were detected on RNA by Sanger. NGS allows the identification of novel mutations in five genes in the same sequencing run, permitting unambiguous recognition of disorders with overlapping phenotypes with NF1 and facilitating genetic counseling and a personalized follow-up.

Keywords: neurofibromatosis type 1; targeted next generation sequencing (NGS); *NF1*, *SPRED1*, *LZTR1*, *NF2* genes pathogenic variants; schwannomatosis

1. Introduction

Neurofibromatosis type 1 (NF1), an autosomal dominant disorder, is the most frequent tumor predisposition syndrome [1].

The condition is caused by mutations in the neurofibromin gene (17q11.2.5-7) encoding a negative regulator of Ras guanosine triphosphate (GTPase) proteins and acting as a tumor suppressor gene. Mutation detection in the *NF1* gene is challenging, due to the large size of the gene (>350 kb), the presence of pseudogenes, the lack of hot spots, and the high mutation rate that is responsible for 50% of all pathogenic variants being de novo [1,2].

Point mutations, including nonsense, missense, frameshift, and splicing mutations, are the most frequent alterations identified in *NF1* (around 80–90%) [3,4]. Only 5% of NF1 patients have deletions of the entire *NF1* gene including contiguous genes (1–1.4 Mb) [4,5]. Insertion, duplication, and copy number variations (CNV) are rarely reported in the literature [6]. In the Leiden Open Variation Database-NF1, over two thousand unique germline *NF1* variants [7] are reported. Several studies using a comprehensive approach that includes RNA analysis coupled with Multiplex Ligation-Dependent Probe Amplification Analysis (MLPA) reported a germline mutation rate in 83–95% of clinically confirmed cases [8–10].

The diagnosis of NF1 was based on the clinical criteria defined in a National Institutes of Health (NIH) conference in 1988 [11] requiring the presence of at least two specific features of the disease. In most cases, a definitive clinical diagnosis can be performed. However, disease signs are age-dependent and the full clinical manifestation usually appears at 8 years of age. Furthermore, in 2007 a clinically overlapping disorder, Legius Syndrome, characterized by the presence of multiple café au lait spots (CALS), freckling and macrocephalia, was described [12]. In a large database of individuals that met NIH criteria for NF1 diagnosis 1.9% had a molecular diagnosis of Legius [13] and 8% of cases aged 0–20 years with CAL but without non-pigmentary criteria for NF1 had *SPRED1* mutations [8].

Spinal Neurofibromatosis (SNF), a distinct clinical entity of NF1, is characterized by bilateral neurofibromas involving all spinal roots and a few, if any, cutaneous manifestations [14]. Most of those patients received a delayed NF1 diagnosis, because the NIH diagnostic criteria were unfulfilled. In addition, a *SOS1* mutation was identified [15] in two familial cases with previous clinical diagnosis of NF1 and multiple spinal nerve enlargements resembling plexiform neurofibromas. Individuals with constitutional mismatch repair (MMR) deficiency, a rare tumor predisposing syndrome caused by biallelic mutations in one of *MMR* genes, display features reminiscent of NF1 [16].

Therefore, the recognition of disorders with overlapping clinical and radiological phenotypes but with different prognoses, emphasize the importance of molecular diagnosis.

Targeted Next Generation Sequencing (NGS) is now applied to the fast and unambiguous diagnosis of NF1, schwannomatosis or Legius Syndrome. In the present study, we validated an NGS approach coupled with MLPA, analyzing prospectively 250 consecutive patients with suspected NF1.

2. Materials and Methods

2.1. Patient Population

Two-hundred fifty consecutive patients, referred to our institution from several Italian centers for suspected NF1 from 1 July 2017 to 30 June 2018, were included in the study. The median age was 15.5 years (3 months–74 years), 132 were pediatric (<18 years) and 118 adult cases; females and males were equally represented. One-hundred eighty-four were sporadic patients and 66 familial cases. One-hundred seventy-one fulfilled NIH criteria (68%), 82/184 sporadic subjects had just pigmentary criteria (i.e., CAL with or without freckling and no other NF1 features,) and age < 20 years. Ninety-one percent of patients manifesting only one clinical feature of NF1 (79 cases) were children, 65% were under 8 years. All patients or authorized relatives gave informed consent prior to genetic analysis. The investigations were carried out in accordance with the principles laid down in the 2013 revision of

the Declaration of Helsinki. This retrospective study was approved by the Fondazione IRCCS Istituto Neurologico Carlo Besta Ethical Committee and Scientific Board (N°72-2020).

2.2. DNA and RNA Extraction and Retro-Transcription

As already described by Bianchessi [17], genomic DNA (gDNA) was isolated from blood samples in ethylenediamine tetraacetic acid (EDTA) using a Gentra Puregene® Blood Core Kit B (Qiagen, Venlo, The Netherlands; Carlsband, CA, USA).

RNA samples were collected in Tempus™ Blood RNA Tubes (Life Technologies, Carlsbad, CA, USA) and extracted with a Tempus™ Spin RNA Isolation Kit within 5 days. DNase treatment with Absolute RNA Wash Solution was performed for all samples during the RNA extraction protocol. RNA samples were reverse-transcribed using 50 units of High-Capacity cDNA Reverse Transcription mix (Life Technologies) and 20 units of RNAse inhibitor (Ambion, Austin, TX, USA). β-2-Microglobulin amplification was used as a quality control for retro-transcription.

2.3. Multiplex Ligation-Dependent Probe Amplification Analysis (MLPA)

Patients' DNA was analyzed by MLPA with NF1 MLPA salsa P081 and P082 (MRC Holland, Amsterdam, The Netherlands). P081/P082 salsa kit identified single- and multi-exon deletion/duplications inside the *NF1* gene. The amplification products were covering all 58 exons of the *NF1* gene. P081/P082 positive patients for the entire *NF1* deletion were screened also with MLPA P122 salsa kit. Results obtained by ABI Prism 3130 Genetic Analyzer (Life Technologies) were analyzed with the Coffalyser.Net Software (MRC Holland, Amsterdam, The Netherlands).

Patients positive for deletion or duplication were excluded from NGS analysis.

2.4. NGS Sequencing

Library preparation was carried out using the Ion AmpliSeq Library Kit 2.0 (Life Technologies). Thirty ng of gDNA were added to multiplex primer pools to amplify target genomic regions. Primers were partially digested using a FuPa reagent, and the sequencing adapters were ligated to the amplicons. The library was purified using the Agencourt AMPure XP reagent (Beckmann Coulter, CA, USA). Concentrations and quality of purified libraries, as well as size of the amplicon, were determined using Qubit® 2.0 (Life Technologies) and Agilent 2100 Bioanalyzer® (Agilent Technologies, Inc., Santa Clara, CA, USA) with Agilent® High Sensitivity DNA kit (Agilent Technologies, Inc. Santa Clara, CA, USA). Template preparation was performed with Ion PGM™ Hi-Q™ OT2 Kit (Cat. no. A27739) (Thermo Fisher Scientific, Waltham, MA, CA, USA) on Ion One Touch instrument using the emulsion PCR method.

Unlinked beads were removed from the solution during the semi-automated enrichment process on Ion One Touch ES instrument (Life Technologies).

Libraries were pooled equimolar and after adding the sequencing primer and DNA polymerase, the fully prepared Ion Sphere Particle (ISP) beads were loaded into an Ion 318 sequencing chip and the sequencing runs were performed using the Ion PGM™ Hi-Q™ Sequencing Kit (Life Technologies) with 500 flows.

The multigenic panel was designed using Ampliseq Designer (Life Technologies) and included all exons and 3′/5′-UTR of the *NF1*, *LZTR1*, *NF2*, *SMARCB1*, and *SPRED1* genes.

The average coverage was 96% and the target regions were sequenced at a 130× depth.

2.5. Data Analysis

Data of runs were processed using the Ion Torrent Suite 5.0 VariantCaller 5.0, Coverage Analysis 5.0 (Life Technologies) and the Ion Reporter (Life Technologies).

The TMAP algorithm was used to align the reads to the hg19 human reference genome, and the variant caller plug-in was selected to run the search for germ line variants in the targeted regions.

To visualize the status of each read alignment and variant interpretation the Integrative Genomic Viewer version 2.3 (IGV) (Broad Institute and the Regents of the University of California) was used.

We removed all the common variants (Minor Allele Frequency, MAF > 1%) reported in the following public databases: *1000 Genomes Project*.

The effect on genes and proteins of the mutations identified were predicted based on Mutation Taster HGMD (Human Genome Mutation Database–Institute of Medical Genetics, Cardiff, Wales, UK; and LOVD [18] databases were interrogated to verify if the mutation was novel.

Novel variants with amino acid changes were further examined for their disease-causing potential using PolyPhen-2 [19]. The possible effects on mRNA (canonical and not canonical splicing mutation) were evaluated with Splice site Prediction by neural network [20], the Human Splicing Finder [21] and ESE Finder tools [22,23].

2.6. Sanger Sequencing

Called and deleterious variants identified with NGS Ion Torrent were confirmed by Sanger Sequencing. PCR reactions were performed using Taq Gold Polymerase® (Life Technologies, Foster City, CA, USA). The size of PCR products was verified by electrophoresis on a 2% agarose gel. The PCR products were purified using ExoSAP-IT® (USB Corporation, Cleveland, OH, USA) according to the manufacturer's protocol and were sequenced in both directions using the BigDye terminator sequencing kit v1.1 (Life Technologies) on ABI 3130 Genetic Analyzer (Life Technologies).

Sequencing analysis on Sanger using the BigDye terminator sequencing kit v3.1 (Life Technologies) was performed on negative *NF1* NGS samples using cDNA that was amplified in 23 overlapping fragments from 400 to 560 bp.

2.7. Submission of Genomic Variations

All novel pathogenic variants identified in *NF1*, *NF2*, *SPRED1* and *LZTR1* genes have been deposited in the "Leiden open (source) variation database" (LOVD) public database [18].

3. Results

A comprehensive analysis of *NF1*, *NF2*, *SPRED1*, *SMARCB1*, and *LZTR1* genes was performed on a total of 250 consecutive cases with suspected NF1 using the NGS panel. Before NGS, MLPA method was performed to rule out large deletions/duplications in the *NF1* gene. Screening results are summarized in Figure 1.

Our approach allowed the identification of a pathogenic variant in 175 patients: 168 in *NF1*, 1 in *SPRED1*, 6 in *LZTR1* and 1 in *NF2* genes, two variants were present in the same patient and six benign variations (5 in *NF1* and 1 in *LZTR1* genes).

3.1. Detection of NF1 Pathogenic Variants

Using NGS coupled with MLPA and cDNA Sanger sequencing, we identified pathogenic *NF1* variants in 168/250 unrelated patients submitted for NF1 clinical genetic testing to the Neurological Institute C. Besta (Figure 1). 138 mutations were detected among the 171 fulfilling NIH criteria for NF1 diagnosis (detection rate 81%), while 30 pathogenic *NF1* variants were detected (21 by NGS and 7 by MLPA) in 79 cases not fulfilling NIH clinical criteria (37.9%). Furthermore, 39 of 82 sporadic subjects with CAL and only pigmentary criteria for NF1 (age < 20 years) had *NF1* pathogenic variants (47%), 3 had *LZTR1* pathogenic variants (3.6%); in one of them a *NF2* pathogenic variant (1.1%) was also present.
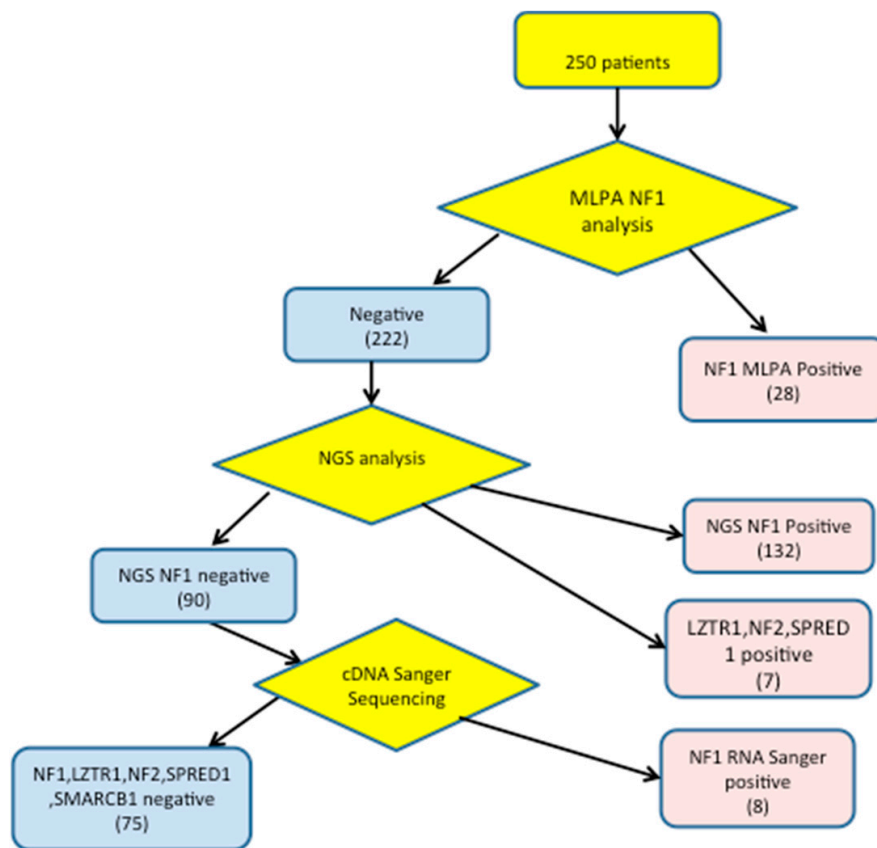
Figure 1. Molecular screening flow chart for patients with suspected NF1.

Fifty-two of 160 pathogenic variants (31%) (40 detected by NGS and 12 by MLPA) were novel, i.e., not present in HGMD and LOVD databases. Novel pathogenic variants were deposited in the LOVD database [18] and described according to recommendations of the Human Genome Structural Variant (HGSV) consortium.

The 52 novel pathogenic variants are reported in Table 1.

Figure 2. Distributions of the *NF1* single small pathogenic variants identified for each exon.

Table 1. New *NF1* and *LZTR1* pathogenic variants observed.

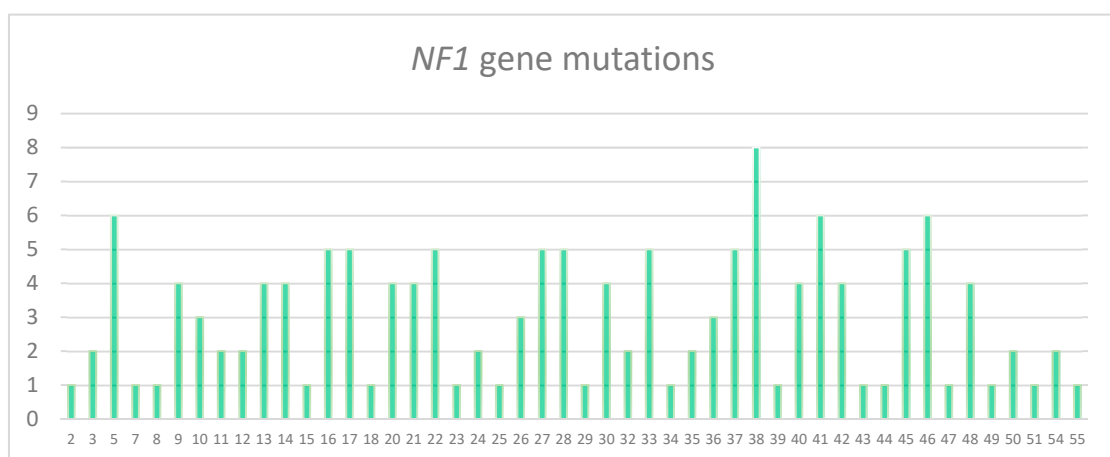| Variant On Genome/DBID.	DNA Change	RNA Change	Protein Change
NF1_002811	c.980delT	r.980delu	p.Leu327Argfs*49
NF1_002809	c.269T>G	r.269u>g	p.Leu90Arg
NF1_000806	c.6755A>G	r.6642_6756del115	p.Phe2215fs
NF1_002823	c.6770dupG	r.6770dupg	p.Cys2257Trpfs*6
NF1_002817	c.3574G>T	r.3574g>u	p.Glu1192*
NF1_002812	c.1170delC	r.1170delc	p.Asn390Lysfs*22
NF1_002816	c.2026_2027insT	r.2026_2027insu	p.Thr676fs
NF1_002810	c.586+2 T>G	r.480_586del107	p.Leu161fs
NF1_002819	c.4653delT	r.4653delu	p.Phe1551Leufs*2
NF1_001963	c.5870T>C	r.5870u>c	p.Leu1957Pro
NF1_002826	c.7907+1 _7907+4 delGTAA	r.7807_7907del101	p.Thr2604*
NF1_002818	c.3703C>T	r.3703c>u	p.Gln1235*
NF1_002815	c.1541_1542delAG	r.1541_1542delag	p.Gln514Argfs*43
NF1_002813	c.1185+2delT	r.1063_1185del123	p.Asn355_Lys395del
NF1_002821	c.5199_5205delTATTAAA	r.5199_5205deluauuaaa	p.Ile1734Leufs*8
NF1_002822	c.6756+11 C>T	r.6642_6756del115	p.Phe2215Hisfs*6
NF1_002822	c.6756+11 C>T	r.6642_6756del115	p.Phe2215Hisfs*6
NF1_002824	c.7345_7346delAA	r.7345_7346delaa	p.Asn2449Cysfs*12
NF1_002814	c.1393-3 delTA	r.1393_1527del135	p.Ser465_Cys509del
NF1_002825	c.7433dupG	r.7433dupg	p.Ser2479fs
NF1_002820	c.4773-2A>C	r.4773_5065del293	p.Phe1592Leufs*7
NF1_002834	c.6326_6329delTTCA	r.6326_6329deluuca	p.Ile2109Thrfs*19
NF1_002832	c.4701_4708delAACGTTAA	r.4701_4708delAaacguuaa	p.Thr1568Tyrfs*30
NF1_002827	c.288+1137C>T	r.288_289ins288+1019_288+1136 ins118	p.Gly96Glu97ins39+fs*10
NF1_002829	c.3197+2T>A	r.3114_3197del84	p.Arg1038_Thr1066del
NF1_002828	c.2810T>A	r.2810u>a	p.Leu937*
NF1_002831	c.4684G>T	r.4684g>u	p.Glu1562*
NF1_002830	c.3314+1G>C	r.3275_3314del40	p.Gly1092Aspfs*7
NF1_002833	c.5425delC	r.5425delc	p.Arg1809Alafs*33
NF1_002301	c.2915T>C	r.2915u>c	p.Leu972Pro
NF1_002841	c.5513_5514delTA	r.5513_5514delua	p.Leu1838Serfs*2
NF1_002836	c.1280delC	r.1280delc	p.Pro427Leufs*46
NF1_002838	c.3564_3565delACinsTGA	r.3564_3565delacinsuga	p.Gln1188Hisfs*7
NF1_002840	c.4719_4720dupAC	r.4719_4720dupac	p.Gln1574fs
NF1_002842	c.5989A>C	r.5989a>c	p.Ser1997Arg
NF1_002837	c.3315-8 T>G	r.3315_3496del182	p.Thr1106Leufs*28
NF1_002844	c.7921dupG	r.7921dupg	p.Asp2641fs
NF1_002301	c.2915T>C	r.2915u>c	p.Leu972Pro
NF1_002839	c.3709-9T>A	r.3708_3709insuucucag	p.Asp1237Phefs*4
NF1_002835	c.1260+2 T>G	r.1260_1261insggaaguccaaaag	p.Ser421Glyfs*12
NF1_002843	c.6085G>T	r.6085_6364del280	p.Val2029Lysfs*7
NF1_002861	c.-383_(60+1_61-1)del	r.(?)	p.(?)
NF1_001695	c.(3708+1_3709-1)_(3974+1_3975-1)dup	r.(?)	p.(?)
NF1_002858	c.4435A>G	r.4368_4435del68	p.Phe1457*
NF1_002862	c.1944_1945delAGinsC	r.1944_1945delinsc	p.Glu648Aspfs*40
NF1_002858	c.1122_1125delTCTA	r.1122_1125delucua	p.Asp374Glufs*2
NF1_002858	c.6762_6783delTGAGAGTTGCTTAAAAGGACCT	r.6762_6783del22	p.Glu2255Thrfs*8
NF1_002860	c.1463_1466dupGCTA	r.1463_1466dupgcua	p.Tyr489*
NF1_002859	c.7151_7161delTTGTTGCAAGA	r.7151_7161del	p.Ile2384Asnfs*13
NF1_002858	c.4435A>G	r.4368_4435del68	p.Phe1457*
NF1_002864	c.6005T>A	r.6005u>a	p.Leu2002*
NF1_002863	c.7000-?_8314+?del	r.7000_8314del1314	p.Ser2334Glufs*59
LZTR1_000102	c.844C>T	r.844c>u	p.Gln282*
LZTR1_000103	c.154delC	r.154delc	p.His52Ilefs*49
LZTR1_000041	c.1394C>T	r.1394c>u	p.Ala465Val
LZTR1_000104	c.161G>A	r.161g>a	p.Trp54*

No hot spot region for pathogenic variants was identified in the *NF1* gene (Figure 2).

Four subtypes of gross *NF1* gene deletions have been described that differ in terms of the deletion size and the positions of their respective breakpoints: type 1, type 2, type 3, and atypical *NF1* deletions [3]. Type-1 microdeletion is characterized by breakpoints located within the low copy number repeats *NF1-REPa* and *NF1-REPc* and involves the *NF1* gene and contiguous genes *SUZ12P*, *CRLF3*, *ATAD5, ADAP2*, *RNF135*, *UTP6*, *SUZ12* and *LRRC37B*; while atypical *NF1* microdeletions have non-recurring breakpoints [13].

MLPA analysis of the *NF1* gene identified 28/168 pathogenic variations: four type 1 microdeletions, two atypical microdeletions, seven intragenic deletions and two intragenic duplication. In addition MLPA revealed also six splicing pathogenic variants, two nonsense and five frameshift pathogenic variants that were located in the probe binding sequence.

3.2. Characterization of the Pathogenic Variants Detected by NGS

We observed the following types of pathogenic variants: frameshift (31% 41/132), in frame deletions (2.2% 3/132), splicing (27% 36/132), missense (16% 22/132) and nonsense (23% 30/132) pathogenic variants). Overall, 115 (87%) pathogenic variants were "private" (only observed in one unrelated patient/family). The remaining pathogenic variants were found more than once.

NGS analysis also allowed to detect five benign variations of the *NF1* gene in three subjects. The first one was missense variation c.4768 C>T (*p*. Arg1590Trp) also observed in the father and the brother who did not show signs of the disease. Another missense benign variant was c.3734 C>G (*p*.Thr1245Ser) inherited from the father and the paternal grandmother who did not show clinical phenotype. In the same subject the variant c.861 C>T (*p*.Asp287Asp) (described as polymorphism; the variation c.2326-25 C>G and the variation c.7394 + 61 A>C, all resulted by in silico prediction analysis with "Mutation Taster" as benign.

All *NF1* variants identified by NGS were confirmed by Sanger DNA sequencing.

All the *NF1* NGS negative cases ($n° = 90$) were tested using cDNA Sanger sequencing. The NGS analysis failed to identify six types of pathogenic variant in eight patients that were detected on RNA by Sanger: these pathogenic variants are reported on Table 2. Four were frameshift and two were splicing.

Table 2. *NF1* pathogenic variants not observed by NGS and detected on RNA by Sanger.

Mutation Type	Location	$n°$pts
c.288 + 1138 C>T	Intron 3	1
c.499_502 del TGTT	Exon 5	3
c.1021_1022 del GT	Exon 9	1
c.2033 dupC	Exon 18	1
c.4224_4225 del AA insT	Exon 32	1
c.7907 + 791 C>G	Intron 54	1

By NGS, a *SPRED1* pathogenic variant that was previously described, [12] (c.349 C>T causing a premature stop codon), was observed in a five year old child, with macrocephaly, diffuse Cal spots, freckling, no neurofibroma, no Lisch nodule neither coroideal amartoma; the father had the same clinical phenotype. Legius Syndrome was diagnosed in both.

Furthermore, a *NF2* missense pathogenic variant already reported [24] c.397 T>C, p.Cys133Arg and a de novo *LZTR1* nonsense alteration c.844 C>T, *p*.Gln282* were both found in a one year old child with only eight Cal spots.

The de novo frameshift *LZTR1* pathogenic variant: c.154_154 delC, p.His52lle Fs*49 was observed in a 12 years old girl with only 15 Cal spots and her father with multiple Schwannomas; the de novo missense pathogenic variant c.1394 C>T, Ala465Val was detected in a six years old boy with diffuse freckling, pectum excavatum, scleral nevi. Further genetic analysis showed the heteroziygous

pathogenic variant c.1403 C>T in PTPN11 gene allowing Leopard Syndrome to be diagnosed. The already described missense pathogenic variant: c.1394 C>A, Ala465Glu missense-in a 6 years girl with only ten Cal spots (see Table 1).

In a 55 years old female, the de novo nonsense pathogenic variant *LZTR1* c.161 G>A was detected, the patient showed only two Cal spots, multiple subcutaneous nodules in limbs and trunk, and neither Lisch nodule nor coroideal amartomas. At cervical MRI an intramedullary alteration in T2 weighted imagines was present.

The de novo intronic splicing *LTZTR1* pathogenic variant: c.264-3 A>G, r.264_320del57, p.Lys89Arg107del was detected in a 25 years old male with two Cal spots, subcutaneous nodules, retroperitoneal nodules, D12-L1 nodules, neither Lisch nodule nor coroideal amartoma. After genetic testing, the diagnosis of schwannomatosis was confirmed according to current diagnostic criteria, when one subcutaneous nodule and the D12 nodule were examined respectively. The histopathological diagnosis was Schwannoma for both.

A synonymous single base *LZTR1* variation c.1530 C>T r.1530 C>U, p.His510His likely not pathogenic was observed in a 55 year old man, one Cal spot, one angiolipoma, multiple paraspinal nodules at lumbar spine involving also left iliopsoas, and neither Lisch nodule nor coroideal amartoma.

No variations were observed in the *SMARCB1* gene.

4. Discussion

NF1 pathogenic variants can be detected through several different techniques.

To date, the application of NGS method for the molecular diagnosis of NF1 has been reported in six studies. Different NGS platforms have been used, some studies were focused only on the *NF1* gene [25,26], while others included also genes such as *SPRED1* [27,28] *BRAF*, *p53* [29]. Apart from Pasmant [27], in all studies targeted NGS was combined with MLPA to rule out large deletions/duplications in *NF1* gene.

Using NGS coupled with MLPA, our detection rate, for *NF1* pathogenic variants (77%) is similar to that reported (76%) in Turkish patients [30] and lower than that found in other reports ranging from 88% to 96% [25–27]. The discrepancies can reflect disparities in the inclusion criteria of the patients studied. We and [30] tested all consecutive patients referred for suspected neurofibromatosis type 1 to our laboratories over a certain interval time without any selection of the cases.

NGS is a complex technology, requiring validation efforts. Various variables related to laboratory procedures and bioinformatics analysis can influence the accuracy of the results.

For clinicians it is important to test accuracy and to understand the potential limitations of the sequencing technologies employed.

Unfortunately all the negative cases were tested using DNA and/or cDNA Sanger sequencing only in another study [27].

No *NF1* unidentified pathogenic variant was found in the French study [26], while we observed eight cases in which both MLPA and NGS failed to identify the pathogenic variants. In two cases these pathogenic variants were intronic (c.288 + 1138 C>T; c.7907 + 791 C>G) therefore not covered in our panel, two pathogenic variants were inserted just before repeated C or A sequences (c.2033 dupC, c.4224_4225 del AA insT) that can interfere with probe ligation. Furthermore, it is already known that NGS approaches may present limitations in detection of insertion/deletion. The most frequently undetected pathogenic variant was in exon five: a tetranucleotide tandem repeat (TGTTTGTT) comprising nucleotides 495–502 that can prevent efficient ligation of MLPA and NGS probes is present in this exon [31].

In addition, Calì [26] reported that NGS analysis failed to identify a pathogenic variant on the same exon that was detected on DNA by Sanger.

However, using MLPA followed by NGS and cDNA amplification and sequencing we have been able to find the disease-causing lesion in 138/171 (81%) of our patients fulfilling NIH criteria for NF1 diagnosis. Based on our results, we suggest performing cDNA analysis by Sanger sequencing in all patients satisfying diagnostic criteria with negative NGS/MLPA testing for NF1.

Among the 28 patients fulfilling NF1 NH criteria with no *NF1*, *SPRED1* and *LZTR1* pathogenic variant, five patients were affected by a sporadic segmental NF1. The typical features of NF1 were restricted to one part of the body and both parents were unaffected [32]. This distinct form of NF1 has an estimated prevalence equal to 0.002% in the general population [32,33], 10–20 times lower than the frequency of generalized NF1. In those case *NF1* pathogenic variant can be present in a very low percentage of blood cells [32,34,35] and therefore not detectable by NGS at a 130X depth.

Moreover, three negative patients had a spinal form of NF1 and recently Santoro [15] has reported p.Ser548Arg missense pathogenic variant in *SOS1* gene in a patient with bilateral cervical and lumbar spinal lesions resembling plexiform neurofibromas and features suggestive of NF1. We therefore cannot exclude that these three patients bear a causative pathogenic variant of *SOS1* or in other genes not tested with this panel.

The possible occurrence of pathogenic variants in "deep" intronic regions, reported in NF1 cases [36], could be at the basis of the clinical NF1 diagnosis in 14 of the negative patients, who showed a mild sporadic form of NF1 including Cal and freckling, and six others who showed a typical NF1 familial form.

Because of the overlapping phenotype of Legius Syndrome with *NF1*, the *SPRED1* gene was included in our panel. The exact prevalence of this syndrome is still unknown, using NGS we observed one *SPRED1* pathogenic variant in one case out of 171 (0.58%) patients fulfilling diagnostic criteria for NF1. In other studies this percentage ranged from 1.9% [13] to 4% [27]. Recently the co-occurrence of pathogenic variants in the *NF1* and *SPRED1* genes was observed using NGS in one family with NF1 and Legius Syndrome [37]. One sibling with typical features of NF1 with microdeletion type 1 inherited a complete deletion of the *NF1* gene from her mother and carried a variant of unknown significance in the *SPRED1* gene ac.944C>T, p.(Pro315Leu).

Previously, one more case of co-occurrence of NF1 and Legius Syndrome in the same family (with confirmed pathogenic variants in the *NF1* and *SPRED1* genes) was reported [13]. Those findings highlight the relevance of the simultaneous detection of *NF1* and *SPRED1* in genetic testing and the complexity of molecular diagnosis in patients suspected NF1.

Schwannomatosis (SCHW) is a rare disease predisposing to multiple peripheral neurologic tumors development with an incidence approximately of one in 69,000, even if the true incidence could be higher due to the difficulties in case ascertainment. To date two causative genes for schwannomatosis, *SMACRB1* and *LZTR1*, were identified [38,39]. Approximately, one third of patients with Schwannomatosis are carriers of a germline pathogenic variant in *LZTR1* (Leucin Zipper Transcription Regulator 1).

The clinical features of the disease are still poorly described, especially when *LZTR1* is mutated. Most patients developed symptoms in the second or third decade of life but the diagnosis is usually delayed for several years. The most common presenting features is asymtomatic mass or diffuse or localized pain. Until recently, the presence of vestibular schwannoma excluded a diagnosis of schwannomatosis but patients with *SMARCB1* and *LZTR1* pathogenic variants that met neurofibromatosis type 2 (NF2) criteria have been described [40,41]. However, recently, pathogenic variants in *LZTR1* have also been involved in a small proportion of patients with Noonan syndrome, a rare neurodevelopmental syndrome [42] either in a dominant or in a recessive fashion of transmission; it has been postulated that dominant negative missense variant cause the dominant form and hypomorphic in trans with loss-of-function variants are at the base of the recessive one. Moreover, a recurrent mixed glioma tumor of oligoastrocytoma type was described in such a patient [43] and coexistence of schwannomatosis and glioblastoma in two families [44].

Very recently the role of LZTR1 as a negative RAS modulator has been demonstrated, since different classes of *LZTR1* mutations are predicted to interfere with ubiquitination and degradation of substrates that act as a positive modulator of the RAS-MAPK pathway [45].

Even if the presence of cutaneous Cal spots is included among clinical signs in Rasopathies, until now they are not considered a typical sign of schwannomatosis due to LZTR1 pathogenic variants.

In our patients, the presence of Cal spots and the young age have led to the suspicion of NF1. The exams which followed confirmed the diagnosis of SCHW in the two adult patients according to actual diagnostic criteria. The other patients were too young at present to confirm NF2 and SCHW diagnosis.

However, the observation of more than 6 Cals in young patients bearing a pathogenic variant in *LZTR1* or *NF2* genes is interesting, and deserves to be explored in further studies.

Because of the clinical overlap of NF1 and other phenotypes, the variability of the disease, with age-dependent signs and symptoms, in many cases it is difficult to diagnose the disease based on clinical features only.

NGS allows the identification of novel mutations in five genes in the same sequencing run, allowing unambiguous recognition of disorders. It is, therefore, particularly useful to identify genetic pathogenic variant in patients with few symptoms, allowing an appropriate genetic counseling and a personalized follow-up.

Conflicts of Interest: The authors declare no conflicts of interest.

References

1. Cawthon, R.M.; Weiss, R.; Xu, G.F.; Viskochil, D.; Culver, M.; Stevens, J.; Robertson, M.; Dunn, D.; Gesteland, R.; O'Connell, P. A major segment of the neurofibromatosis type 1 gene: cDNA sequence, genomic structure, and point mutations. *Cell* **1990**, *62*, 193–201. [CrossRef]
2. Huson, S.M. The Neurofibromatoses: Classification, Clinical Features and Genetic Councelling. In *Neurofibromatoses*; Kaufmann, D., Ed.; Karger Publishers: Basel, Switzerland, 2008; pp. 1–20.
3. Messiaen, L.M.; Callens, T.; Mortier, G.; Beysen, D.; Vandenbroucke, I.; van Roy, N.; Speleman, F.; Paepe, A.D. Exhaustive mutation analysis of the *NF1* gene allows identification of 95% of mutations and reveals a high frequency of unusual splicing defects. *Hum. Mutat.* **2000**, *15*, 541–555. [CrossRef]
4. Wimmer, K.; Roca, X.; Beiglbock, H.; Callens, T.; Etzler, J.; Rao, A.R.; Krainer, A.R.; Fonatsch, C.; Messiaen, L. Extensive in silico analysis of NF1 splicing defects uncovers determinants for splicing outcome upon 5' splice-site disruption. *Hum. Mutat.* **2007**, *28*, 599–612. [CrossRef] [PubMed]
5. Kluwe, L.; Siebert, R.; Gesk, S.; Friedrich, R.E.; Tinschert, S.; Kehrer-Sawatzki, H.; Mautner, V.F. Screening 500 unselected neurofibromatosis 1 patients for deletions of the *NF1* gene. *Hum. Mutat.* **2004**, *23*, 111–116. [CrossRef]
6. Kehrer-Sawatzki, H.; Bengesser, K.; Callens, T.; Mikhail, F.; Fu, C.; Hillmer, M.; Walker, M.E.; Saal, H.M.; Lacassie, Y.; Cooper, D.N.; et al. Identification of large NF1 duplications reciprocal to NAHR-mediated type-1 *NF1* deletions. *Hum. Mut.* **2014**, *35*, 1469–1475. [CrossRef]
7. Van Minkelen, R.; van Bever, Y.; Kromosoeto, J.N.R.; Withagen-Hermans, C.J.; Nieuwlaat, A.; Halley, D.J.J.; van den Ouweland, A.M.W. A clinical and genetic overview of 18 years neurofibromatosis type 1 molecular diagnostics in the Netherlands. *Clin. Genet.* **2014**, *85*, 318–327. [CrossRef]
8. Evans, D.G.; Bowers, N.; Burkitt-Wright, E.; Miles, E.; Garg, S.; Scott-Kitching, V.; Penman-Splitt, M.; Dobbie, A.; Howard, E.; Ealing, J.; et al. Comprehensive RNA analysis of the *NF1* gene in classically affected NF1 affected individuals meeting NIH criteria has high sensitivity and mutation negative testing is reassuring in isolated cases with pigmentary features only. *EBioMedicine* **2016**, *7*, 212–220. [CrossRef]
9. Hutter, S.; Piro, R.M.; Waszak, S.M.; Kehrer-Sawatzki, H.; Friedrich, R.E.; Lassaletta, A.; Witt, O.; Korbel, J.O.; Lichter, P.; Schuhmann, M.U.; et al. No correlation between *NF1* mutation position and risk of optic pathway glioma in 77 unrelated NF1 patients. *Hum. Genet.* **2016**, *135*, 469–475. [CrossRef]

10. Thomas, L.; Spurlock, G.; Eudall, C.; Thomas, N.S.; Mort, M.; Hamby, S.E.; Chuzhanova, N.; Brems, H.; Legius, E.; Cooper, D.N.; et al. Exploring the somatic *NF1* mutational spectrum associated with NF1 cutaneous neurofibromas. *Eur. J. Hum. Genet.* **2012**, *20*, 411–419. [CrossRef]

11. National Institutes of Health Consensus Development Panel. Neurofibromatosis: Conference Statement. *Arch. Neurol.* **1988**, *45*, 575–578. [CrossRef]

12. Brems, H.; Chmara, M.; Sahbatou, M.; Denayer, E.; Taniguchi, K.; Kato, R.; Somers, R.; Messiaen, L.; de Schepper, S.; Fryns, J.P.; et al. Germline loss-of-function mutations in SPRED1 cause a neurofibromatosis1-like phenotype. *Nat. Genet.* **2007**, *39*, 1120–1126. [CrossRef] [PubMed]

13. Messiaen, L.; Yao, S.; Brems, H.; Callens, T.; Sathienkijkanchai, A.; Denayer, E.; Spencer, E.; Arn, P.; Babovic-Vuksanovic, D.; Bay, C.; et al. Clinical and mutational spectrum of neurofibromatosis type 1-like syndrome. *JAMA* **2009**, *302*, 2111–2118. [CrossRef] [PubMed]

14. Ruggieri, M.; Polizzi, A.; Spalice, A.; Salpietro, V.; Caltabiano, R.; D'Orazi, V.; Pavone, P.; Pirrone, C.; Magro, G.; Platania, N.; et al. The natural history of spinal neurofibromatosis: A critical review of clinical and genetic features. *Clin. Genet.* **2015**, *87*, 401–410. [CrossRef] [PubMed]

15. Santoro, C.; Giugliano, T.; Melone, M.A.B.; Cirillo, M.; Schettino, C.; Bernardo, P.; Cirillo, G.; Perrotta, S.; Piluso, G. Multiple spinal nerve enlargement and SOS1 mutation: Further evidence of overlap between neurofibromatosis type 1 and Noonan phenotype. *Clin. Genet.* **2018**, *93*, 138–143. [CrossRef] [PubMed]

16. Wimmer, K.; Rosenbaum, T.; Messiaen, L. Connection between constitutional mismatch repair deficiency 2 syndrome and Neurofibromatosis type 1. *Clin. Genet.* **2017**, *91*, 507–519. [CrossRef]

17. Bianchessi, D.; Morosini, S.; Saletti, V.; Ibba, M.C.; Natacci, F.; Esposito, S.; Cesaretti, C.; Riva, D.; Finocchiaro, G.; Eoli, M. 126 novel mutations in Italian patients with neurofibromatosis type 1. *Mol. Genet. Genom. Med.* **2015**, *3*, 513–525. [CrossRef]

18. Fokkema, I.F.A.C.; Taschner, P.E.M.; Schaafsma, G.C.P.; Celli, J.; Laros, J.F.J.; Dunnen, J.T.d. LOVD v.2.0: The next generation in gene variant databases. *Hum. Mutat.* **2011**, *32*, 557–563. [CrossRef]

19. Adzhubei, I.A.; Schmidt, S.; Peshkin, L.; Ramensky, V.; Gerasimova, A.; Bork, P.; Kondrashov, A.S.; Sunyaev, S.R. A method and server for predicting damaging missense mutations. *Nat. Methods* **2010**, *7*, 248–249. [CrossRef]

20. Reese, M.G.; Eeckman, F.H.; Kulp, D.; Haussler, D. Improved Splice Site Detection in Genie. *J. Comput. Biol.* **1997**, *4*, 311–323. [CrossRef]

21. Desmet, F.O.; Hamroun, D.; Lalande, M.; Collod-Béroud, G.; Claustres, M.; Béroud, C. Human SplicingFinder: An online bioinformatics tool to predict splicing signals. *Nucleic Acids Res.* **2009**, *37*, e67. [CrossRef]

22. Cartegni, L.; Wang, J.; Zhu, Z.; Zhang, M.Q.; Krainer, A.R. ESEfinder: A web resource to identify exonic splicing enhancers. *Nucleic Acids Res.* **2003**, *31*, 3568–3571. [CrossRef]

23. Smith, P.J.; Zhang, C.; Wang, J.; Chew, S.L.; Zhang, M.Q.; Krainer, A.R. An increased specificity score matrix for the prediction of SF2/ASF-specific exonic splicing enhancers. *Hum. Mol. Genet.* **2006**, *15*, 2490–2508. [CrossRef]

24. Seong, M.W.; Yeo, I.K.; Cho, S.I.; Park, C.K.; Kim, S.K.; Paek, S.H.; Kim, D.G.; Jung, H.W.; Park, H.; Kim, S.Y.; et al. Molecular characterization of the NF2 gene in Korean patients with neurofibromatosis type 2: A report of four novel mutations. *Korean J. Lab. Med.* **2010**, *30*, 190–194. [CrossRef]

25. Tsipi, M.; Poulou, M.; Fylaktou, I.; Kosma, K.; Tsoutsou, E.; Pons, M.R.; Kokkinou, E.; Kitsiou-Tzeli, S.; Fryssira, H.; Tzetis, M. Phenotypic expression of a spectrum of Neurofibromatosis Type 1 (NF1) mutations identified through NGS and MLPA. *J. Neurol. Sci.* **2018**, *395*, 95–105. [CrossRef]

26. Calì, F.; Chiavetta, V.; Ruggeri, G.; Piccione, M.; Selicorni, A.; Palazzo, D.; Bonsignore, M.; Cereda, A.; Elia, M.; Failla, P.; et al. Mutation spectrum of NF1 gene in Italian patients with neurofibromatosis type 1 using Ion Torrent PGM™ platform. *Eur. J. Med. Genet.* **2017**, *60*, 93–99. [CrossRef] [PubMed]

27. Pasmant, E.; Parfait, B.; Luscan, A.; Goussard, P.; Briand-Suleau, A.; Laurendeau, I.; Fouveaut, C.; Leroy, C.; Montadert, A.; Wolkenstein, P.; et al. Neurofibromatosis type 1 molecular diagnosis: What can NGS do for you when you have a large gene with loss of function mutations? *Eur. J. Hum. Genet.* **2015**, *23*, 596–601. [CrossRef]

28. Giugliano, T.; Santoro, C.; Torella, A.; del Vecchio, F.; Grandone, B.A.; Onore, M.E.; Melone, M.R.B.; Straccia, G.; Melis, D.; Piccolo, V. Clinical and Genetic Findings in Children with Neurofibromatosis Type 1, Legius Syndrome, and Other Related Neurocutaneous Disorders. *Genes* **2019**, *10*, 580. [CrossRef] [PubMed]

29.　Wu-Chou, Y.H.; Hung, T.C.; Lin, Y.T.; Cheng, H.W.; Lin, H.W.; Lin, C.H.; Yu, C.C.; Chen, K.T.; Yeh, T.H.; Chen, Y.R. Genetic diagnosis of neurofibromatosis type 1: Targeted next- generation sequencing with Multiple Ligation-Dependent Probe Amplification analysis. *J. Biomed. Sci.* **2018**, *25*, 72. [CrossRef] [PubMed]

30.　Ulusal, S.D.; Gürkan, H.; Atlı, E.; Özal, S.A.; Çiftdemir, M.; Tozkır, H.; Karal, Y.; Gü lü, H.; Eker, D.; Görker, I. Genetic analyses of the NF1 gene in Turkish neurofibromatosis type 1 patients and definition of three novel variants. *BJMG* **2017**, *20*, 13–20. [PubMed]

31.　Toliat, M.R.; Erdogan, F.; Gewies, A.; Fahsold, R.; Buske, A.; Tinschert, S.; Nürnberg, P. Analysis of the NF1 gene by temperature gradient gel electrophoresisreveals a high incidence of mutations in exon 4b. *Electrophoresis* **2000**, *21*, 541–544. [CrossRef]

32.　Ruggieri, M.; Huson, S.M. The clinical and diagnostic implications of mosaicismin the neurofibromatoses. *Neurology* **2001**, *56*, 1433–1443. [CrossRef] [PubMed]

33.　Ogose, A.; Hotta, T.; Imaizumi, S.; Saito, H.; Homma, T.; Takahashi, H.E. Deepseated segmental neurofibromatosis without cafe au lait spots. *Skelet. Radiol.* **2000**, *29*, 543–547. [CrossRef] [PubMed]

34.　Biesecker, L.G.; Spinner, N.B. A genomic view of mosaicism and human disease. *Nat. Rev. Genet.* **2013**, *14*, 307–320. [CrossRef] [PubMed]

35.　Maertens, O.; de Schepper, S.; Vandesompele, B.; Heyns, I.; Janssens, S.; Speleman, F.; Legius, E.; Messiaen, L. Molecular dissection of isolated disease features in mosaic neurofibromatosis type 1. *Am. J. Hum. Genet.* **2007**, *81*, 243–251. [CrossRef]

36.　Griffiths, S.; Thompson, P.; Frayling, I.; Upadhyaya, M. Molecular diagnosis of neurofibromatosis type 1: 2 years experience. *Fam. Cancer* **2007**, *6*, 21–34. [CrossRef]

37.　Pacot, L.; Burin des Roziers, C.; Laurendeau, I.; Briand-Suleau, A.; Coustier, A.; Mayard, T.; Tlemsani, C.; Faivre, L.; Thomas, Q.; Rodriguez, T. One NF1 Mutation may Conceal Another. *Genes* **2019**, *10*, 633. [CrossRef]

38.　Plotkin, S.R.; Blakeley, J.O.; Evans, D.G.; Hanemann, C.O.; Hulsebos, T.J.; Hunter-Schaedle, K.; Kalpana, G.V.; Korf, B.; Messiaen, L.; Papi, L.; et al. Update from the 2011International Schwannomatosis Workshop: From genetics to diagnostic criteria. *Am. J. Med. Genet.* **2013**, *161*, 405–416. [CrossRef]

39.　Piotrowski, A.; Xie, J.; Liu, Y.F.; Poplawski, A.B.; Gomes, A.R.; Madanecki, P.; Fu, C.; Crowley, M.R.; Crossman, D.K.; Armstrong, L.; et al. Germline loss-of-function mutations in LZTR1 predispose to an inherited disorder of multiple schwannomas. *Nat. Genet.* **2014**, *46*, 182–187. [CrossRef]

40.　Smith, M.; Kulkarni, A.; Rustad, C.; Bowers, N.L.; Wallace, A.J.; Holder, S.E.; Heiberg, A.; Ramsden, R.T.; Evans, D.G. Vestibular schwannoma occur in schwannomatosis and should not be considered an exclusion criteria for clinical diagnosis. *Am. J. Med. Genet.* **2012**, *158*, 215–219. [CrossRef]

41.　Smith, M.J.; Bulman, M.; Gokhale, C.; Wallace, A.J.; King, A.T.; Lloyd, S.K.; Rutherford, S.A.; Hammerbeck-Ward, C.L.; Freeman, S.R.; Evans, D.G. Revisiting neurofibromatosis type 2 diagnostic criteria to exclude LZTR1 related schwannomatosis. *Neurology* **2017**, *88*, 87–92. [CrossRef]

42.　Yamamoto, G.L.; Aguena, M.; Gos, M.; Hung, C.; Pilch, S.; Fahiminiya, S.; Abramowicz, A.; Cristian, I.; Buscarilli, M.; Naslavsky, M.S.; et al. Rare variants in SOS2 and LZTR1 are associated with Noonan syndrome. *J. Med. Genet.* **2015**, *52*, 413–421. [CrossRef] [PubMed]

43.　Jacquinet, A.; Bonnard, A.; Capri, Y.; Martin, D.; Sadzot, B.; Bianchi, E.; Servais, L.; Sacré, J.P.; Cavé, H.; Verloes, A. Oligo-astrocytoma in LZTR1-related noonan syndrome. *Eur. J. Med. Genet.* **2019**, *18*, 30629–30633. [CrossRef] [PubMed]

44.　Deiller, A.C.; Van-Gilsa, J.; Zordana, C.; Tinata, J.; Loiseauc, H.; Fabred, T.; Dellecie, C.; Cohenf, J.; Vidaudf, M.; Parfaitf, M.; et al. Coexistence of schwannomatosis and glioblastoma in two families. *Eur. J. Med. Genet.* **2019**, *62*, 103680. [CrossRef]

45.　Motta, M.; Fidan, M.; Bellacchio, E.; Pantaleoni, F.; Schneider-Heieck, K.; Coppola, S.; Borck, G.; Salviati, L.; Zenker, M.; Cirstea, I.C.; et al. Dominant Noonan syndrome-causing LZTR1 mutations specifically affect the Kelch domain substrate-recognition surface and enhance RAS-MAPK signaling. *Hum. Mol. Genet.* **2019**, *28*, 1007–1022. [CrossRef] [PubMed]